

**MISSION TO MARS:
HOW TO GET PEOPLE THERE
AND BACK WITH NUCLEAR ENERGY**



**22.033 Final Design Report
Nuclear Engineering Department
Massachusetts Institute of Technology**

Spring 2003

Team Members:

**Vasek Dostal
Knut Gezelius
Jack Horng
John Koser
Joseph E. Palaia, IV
Eugene Shwageraus
Pete Yarsky**

Acknowledgements:

The team would like to thank Kalina Galabova and Nilchiani Roshanak for their valuable contributions to this project. The team would also like to extend thanks to the course advisor, Dr. Kadak, for his instruction and guidance in completing the assigned task.

Table of Contents

| | |
|---|-----|
| List of Figures..... | v |
| List of Tables | vii |
| Abstract..... | 1 |
| 1.0 Introduction..... | 3 |
| 2.0 Mars Exploration Mission Plan | 5 |
| 2.1 Introduction to Mission Plan..... | 5 |
| 2.2 Earth-Mars Transit Breakdown..... | 6 |
| 2.2.1 Hohmann Transfer | 7 |
| 2.2.2 Early Nuclear - Electric Propulsion Transfers | 7 |
| 2.2.3 Power and Propulsion System Return..... | 8 |
| 2.2.4 Nuclear Powered VASIMR Fast Crew Transfer | 8 |
| 2.3 Overview of Proposed Missions | 10 |
| 2.4 Mars Nuclear Powered Telecommunications Satellite..... | 11 |
| 2.5 Overview of Proposed Magnum Launch Vehicle..... | 14 |
| 2.6 Mars Sample Return and Technology Demonstrator Mission..... | 16 |
| 2.7 Transit Habitat Testing and Verification at the ISS..... | 20 |
| 2.8 Manned Missions..... | 21 |
| 2.8.1 Launch Opportunity 1 | 21 |
| 2.8.2 Launch Opportunity 2 | 28 |
| 2.8.3 Crew 1 Return and Launch Opportunity 3..... | 35 |
| 2.8.4 Crew 2 Return and Launch Opportunity 4..... | 38 |
| 2.9 Prospective on Continued Exploration and Conclusion | 40 |
| 2.10 Conclusion | 41 |
| 2.11 References for Mission Section | 41 |
| 3.0 Decision Methodology | 43 |
| 3.1 Overview..... | 43 |
| 3.2 Four-Step Methodology | 43 |
| 3.3 Application of MAUT..... | 45 |
| 3.4 Case Study on Surface Reactor..... | 47 |
| 3.5 Conclusion | 55 |
| 3.6 References..... | 55 |
| 4.0 Space Power System: | 57 |
| 4.1 Space Propulsion Options | 57 |
| 4.1.1 Introduction..... | 57 |
| 4.1.2 Choice of Propulsion System for Precursor Missions | 58 |
| 4.1.3 Manned Mission Propulsion System | 60 |
| 4.1.4 References..... | 61 |

| | | |
|--------|--|-----|
| 4.2 | Space Reactor Power System..... | 62 |
| 4.2.1 | Introduction..... | 62 |
| 4.2.2 | Spaced Nuclear Reactor Design..... | 63 |
| 4.2.3 | References..... | 78 |
| 4.3 | Thermo Photovoltaic (TPV) Primer..... | 79 |
| 4.3.1 | Overview..... | 79 |
| 4.3.2 | Introduction of TPV..... | 79 |
| 4.3.3 | The Chosen Material for TPV Cells..... | 82 |
| 4.3.4 | Structure of TPV Cells..... | 82 |
| 4.3.5 | Filter and Spectral Shaping..... | 83 |
| 4.3.6 | Layers..... | 83 |
| 4.3.7 | Photon Recirculation..... | 83 |
| 4.3.8 | Performance of TPV – Efficiency and Power Density..... | 84 |
| 4.3.9 | Space Power TPV Energy Conversion System..... | 84 |
| 4.3.10 | References..... | 85 |
| 4.4 | MSFR Thermal Hydraulics..... | 86 |
| 4.4.1 | Introduction..... | 86 |
| 4.4.2 | Analysis..... | 86 |
| 4.4.3 | Power Conversion System..... | 90 |
| 4.4.4 | References..... | 92 |
| 4.5 | Pump Selection for MSFR..... | 92 |
| 4.5.1 | Introduction..... | 92 |
| 4.5.2 | Comparison..... | 92 |
| 4.5.3 | References..... | 94 |
| 4.6 | Shielding of the MSFR..... | 94 |
| 4.6.1 | Introduction..... | 94 |
| 4.6.2 | Key Parameters..... | 94 |
| 4.6.3 | Design Options..... | 95 |
| 4.6.4 | Water Tank..... | 95 |
| 4.6.5 | Special Shield..... | 95 |
| 4.6.6 | Design Methodology..... | 96 |
| 4.6.7 | Physical Implementation..... | 98 |
| 4.6.8 | Limitations of Study..... | 98 |
| 4.6.9 | General Comments on Radiation in Space..... | 99 |
| 4.6.10 | References..... | 100 |
| 5.0 | Surface Power System:..... | 101 |
| 5.1 | Surface Power System Reactor (CECR)..... | 101 |
| 5.1.1 | Introduction..... | 101 |
| 5.1.2 | Design Goals..... | 101 |
| 5.1.3 | Design Methodology..... | 102 |
| 5.1.4 | Viable Alternatives..... | 108 |
| 5.1.5 | Assumptions..... | 109 |
| 5.1.6 | Core Design..... | 109 |
| 5.1.7 | Reflector Design..... | 117 |
| 5.1.8 | Reactivity Feedback and Transients..... | 119 |

| | | |
|--------|--|-----|
| 5.1.9 | Total Size and Mass | 120 |
| 5.1.10 | Integration and Operational Issues..... | 121 |
| 5.1.11 | Future Work and Design Evolution | 121 |
| 5.1.12 | References..... | 122 |
| 5.2 | CECR CO ₂ Brayton Cycle | 123 |
| 5.2.1 | Introduction..... | 123 |
| 5.2.2 | Analysis | 123 |
| 5.2.3 | Core Thermal Hydraulics..... | 127 |
| 5.2.4 | Investigated Concepts – Results | 129 |
| 5.2.5 | Conclusion | 133 |
| 5.2.6 | References..... | 134 |
| 5.3 | Shielding of the CECR..... | 134 |
| 5.3.1 | Introduction..... | 134 |
| 5.3.2 | Time – Distance – Shielding for Mars Explorers | 134 |
| 5.3.3 | Comparison with MITR..... | 135 |
| 5.3.4 | Martian Soil Composition..... | 136 |
| 5.3.5 | Required Thickness of Martian Soil Shield | 136 |
| 5.3.6 | Listing of Shielding Deployment Options | 138 |
| 5.3.7 | Environmental Constraints | 138 |
| 5.3.8 | Shield Option Selection Process | 139 |
| 5.3.9 | Assembling the Shield | 140 |
| 5.3.10 | Support Structure | 140 |
| 5.3.11 | Enhanced Shielding Options..... | 141 |
| 5.3.12 | References..... | 141 |
| 6.0 | Summary, Conclusions, and Future Work | 143 |
| 6.1 | Summary | 143 |
| 6.2 | Conclusions..... | 143 |
| 6.3 | Recommendations for Future Work..... | 143 |

List of Figures

| | | |
|---------|---|----|
| 2.2-1 | Closest Distances between Mars and Earth | 6 |
| 2.2.2-1 | Nuclear-Electric Propulsion Transfer for Precursor and Cargo Missions | 8 |
| 2.2.4-1 | VASIMR Fast Transfer and Mars Overshoot | 9 |
| 2.3-1 | Order of Proposed Mars Mission | 10 |
| 2.4-1 | Flow of Precursor Mission 1 (chart) | 12 |
| 2.4-2 | Flow of Precursor Mission 1 (diagram) | 13 |
| 2.4-3 | Three Telecommunications Satellites in Mars Orbit | 14 |
| 2.5-1 | Basic Configuration of Magnum Launch Vehicle | 15 |
| 2.5-2 | Magnum Payload (Capability to 407 km) | 15 |
| 2.5-3 | Magnum Launch Capabilities | 15 |
| 2.6-1 | Flow of Precursor Missions 2 and 3 | 17 |
| 2.6-2 | Flow of Precursor Mission 2, Stages 1-4 | 19 |
| 2.6-3 | Flow of Precursor Mission 2, Stage 5 | 19 |
| 2.6-4 | Flow of Precursor Mission 2, Stages 6-7 | 20 |
| 2.7-1 | Precursor Mission 3 | 21 |
| 2.8.1-1 | Flow of Launch Opportunity 1 | 23 |
| 2.8.1-2 | Launch Opportunity 1, MTS2 and CARGO1-A | 24 |
| 2.8.1-3 | Launch Opportunity 1, MTS3 and CARGO1-B | 26 |
| 2.8.1-4 | CARGO1 Deployment and Activation | 28 |
| 2.8.1-5 | MTS2 and MTS3 Return Following First Launch Opportunity | 28 |
| 2.8.2-1 | Flow of Launch Opportunity 2 Missions | 30 |
| 2.8.2-2 | CREW1 Transfer | 32 |
| 2.8.2-3 | Refueling of MTS1 | 34 |
| 2.8.2-4 | Landing Site Layout for First Manned Mission | 34 |
| 2.8.3-1 | Flow of CREW1 Return and Launch Opportunity 3 Missions | 36 |
| 2.8.3-2 | Flow of CREW1 Return | 38 |
| 2.8.4-1 | Flow of CREW2 Return and Launch Opportunity 4 Missions | 40 |
| 3.2-1 | Methodology Flowchart | 44 |
| 3.4-1 | Surface Reactor Value Tree | 50 |
| 3.4-2 | Overall Performance Index Graph | 54 |
| 3.4-3 | PI Contributors | 54 |
| 4.1.1-1 | Propellant Mass Required for Earth to Mars Transfer for Various Isp | 57 |
| 4.1.2-1 | NASA's Evolutionary Xenon Thruster (NEXT) | 58 |
| 4.1.2-2 | High Power Ion Engine for Interstellar Precursor Missions | 59 |
| 4.1.2-3 | NASA-457M Hall Thruster | 59 |
| 4.1.3-1 | VASIMR Engine Concept | 61 |
| 4.2.1-1 | Schematic View of the Space Power System | 62 |
| 4.2.2-1 | Pu Isotopic Composition as a Function of Burnup | 66 |
| 4.2.2-2 | 8.5% Am-242m Enriched Am Fuel: Infinite Medium Criticality | 66 |
| 4.2.2-3 | Achievable Fuel Burnup per Moderator Mass Investment | 67 |
| 4.2.2-4 | k-inf BOL for Am-242m Based Fuel | 68 |
| 4.2.2-5 | k-inf BOL vs. Reactivity Limited Burnup Capabilities for Am-242m Based Fuel | 68 |

| | | |
|---------|---|-----|
| 4.2.2-6 | Core Reactivity Control by Direct Leakage..... | 72 |
| 4.2.2-7 | Burnup Calculations Results..... | 73 |
| 4.2.2-8 | Coolant Void Coefficient..... | 74 |
| 4.2.2-9 | MSFR and Honeycomb Fuel Elements Grid..... | 77 |
| 4.3.2-1 | A Typical Solar Cell Structure..... | 80 |
| 4.3.2-2 | TPV Energy Conversion..... | 81 |
| 4.3.4-1 | Cross Section of the Monolithic Two-Junction Two-Terminal TPV Cell..... | 82 |
| 4.4.2-1 | Unit Cell..... | 86 |
| 4.4.3-1 | Space Power Conversion System..... | 91 |
| 4.5.2-1 | TEM Pump..... | 93 |
| 4.5.2-2 | ALI Pump..... | 93 |
| 4.6.6-1 | Cross Sectional View of the Space Reactor Shield..... | 97 |
| 5.1.6-1 | Study of H/HM_{eff} Dependence..... | 110 |
| 5.1.6-2 | Radial Unit Cell Diagram..... | 113 |
| 5.1.6-3 | Axial Unit Cell Diagram..... | 113 |
| 5.1.6-4 | Unit Cell Reactivity History..... | 114 |
| 5.1.6-5 | Evolution of K_{eff} vs. EFPY..... | 114 |
| 5.1.6-6 | Normalized Flux Energy Spectrum..... | 116 |
| 5.1.6-7 | Axial Power Shape during Burnup..... | 117 |
| 5.1.9-1 | Whole Core and Reflector..... | 120 |
| 5.2.2-1 | Brayton Cycle Layout..... | 124 |
| 5.2.2-2 | Plant-and-Fin Heat Exchanger..... | 126 |
| 5.2.2-3 | Printed Circuit Heat Exchanger..... | 126 |
| 5.2.3-1 | Effect of Core Pressure on the Fractional Pressure Drop..... | 128 |
| 5.2.3-2 | Effect of Core Fractional Pressure Drop on the Cycle Efficiency..... | 128 |
| 5.2.4-1 | Efficiency of Non-Regenerative Brayton Cycle..... | 132 |

Other Figures

| | |
|---|----|
| Conceptual View of Sample Return Lander..... | 16 |
| Conceptual View of Prototype Transit Hab Module at ISS..... | 20 |
| Conceptual View of CARGO1-A Descent..... | 22 |
| Conceptual View of CARGO1-A Deployment..... | 22 |
| Conceptual View of CARBO1-B Descent..... | 22 |
| Conceptual View of CREW1 Re-Positioning Habitats..... | 30 |
| Conceptual View of Mars Ascent..... | 35 |
| Conceptual View of CRW1 Earth Return..... | 35 |

List of Tables

| | | |
|---------|---|-----|
| 2.8.1-1 | CARGO#-A Mission Mass Breakdown..... | 25 |
| 2.8.1-2 | CARGO#-B Mass Breakdown..... | 27 |
| 3.3-1 | Constructed Scale | 46 |
| 3.3-2 | AHP Statements of Importance | 47 |
| 3.4-1 | Decision Matrix | 48 |
| 3.4-2 | Incompatible Combinations..... | 48 |
| 3.4-3 | Options Considered for Further Consideration..... | 49 |
| 3.4-4 | Goals for Surface Reactor..... | 49 |
| 3.4-5 | Objectives for the Surface Reactor | 49 |
| 3.4-6 | Performance Measures Scales..... | 51 |
| 3.4-7 | AHP Hierarchy | 52 |
| 3.4-8 | AHP Hierarchy Identifiers..... | 52 |
| 3.4-9 | Performance Measure Weights..... | 52 |
| 3.4-10 | Performance Indices..... | 53 |
| 4.1.2-1 | Key Performance Parameters of Advanced Electric Propulsion Systems..... | 59 |
| 4.2.1-1 | Refractory Metals Properties | 63 |
| 4.2.2-1 | Description of Selected Calculated Cases..... | 71 |
| 4.2.2-2 | Selected Results | 73 |
| 4.2.2-3 | Pu Isotopic Composition..... | 75 |
| 4.2.2-4 | Environmental Hazard Characteristics Comparison..... | 76 |
| 4.2.2-5 | Environmental Hazard Characteristics per Unit of Power Output..... | 76 |
| 4.2.2-6 | MSFR Core Description | 77 |
| 4.4.2-1 | Space Power System Characteristics | 89 |
| 4.6.6-1 | Cross Sections for Shielding Material | 96 |
| 4.6.6-2 | Different Shielding Thickness and Results..... | 98 |
| 4.6.9-1 | Exposure Limits for Different Groups..... | 99 |
| 4.6.9-2 | Estimated Dose Due to GCR on Martian Surface | 100 |
| 4.6.9-3 | Dose Rate (BFO) to Astronauts in Transit..... | 100 |
| 5.1.7-1 | Comparison of Potential Reflectors..... | 118 |
| 5.1.9-1 | CECR Core Description..... | 120 |
| 5.2.2-1 | Surface Characteristics..... | 126 |
| 5.2.2-2 | Heat Transfer and Friction Data | 127 |
| 5.2.4-1 | Brayton Cycle Reference Design..... | 131 |
| 5.2.4-2 | Non-Regenerative Open Brayton Cycle Reference Design..... | 133 |
| 5.3.3-1 | Shielding Material in MITR..... | 136 |
| 5.3.4-1 | Martian Soil Composition..... | 136 |
| 5.3.5-1 | Martian Soil Shielding Results | 137 |

ABSTRACT

The goal of the design project was to develop supporting nuclear technologies for a near-term manned mission to Mars. Through the application of different nuclear technologies in a series of precursory missions, the reactor and propulsion technologies necessary for a manned mission to Mars are demonstrated before humans are committed to the trip.

As part of the project, the NASA design reference mission was adapted to make use of highly efficient, low mass, nuclear power systems and electric propulsion systems. A scalable space fission reactor and power conversion unit was developed for near-term deployment. A long-life, slow response surface fission reactor was also developed for use with in-situ resource utilization (ISRU) plants on the Martian surface.

The space power system is capable of producing up to 4 MW of DC electric power for a full-power lifetime of 570 days. For a VASIMR engine, 570 full power days (FPD) is equivalent to 3 round trips between Earth and Mars. The molten salt cooled fast reactor (MSFR) core is very compact, and the working fluid reaches very high temperature.

The surface power system produces an average of 200 kWe for more than 25 effective full power years (EFPY). This targeted full power lifetime was chosen to reduce the cost of future Mars missions by allowing for long-term infrastructure to be deployed on the surface. The surface system is a CO₂ cooled epithermal conversion reactor (CECR) that is designed for simple control mechanisms, long full power life, and ease of remote operation.

1.0 INTRODUCTION

This report details the design development work done as part of a course at MIT (22.033 Nuclear Engineering Design Project). The goal of the design project was to enhance concepts for missions to Mars through the use of nuclear power.

The scope of the project quickly narrowed on two particular applications, a space power system and a surface power system. This report will discuss in detail the specifications for a space power fission reactor and conversion unit as well as the shielding design. The report will then describe the analogous features for the surface power plant.

A mission plan was developed to aid in establishing the requirements and boundary conditions for the design in terms of maximum weights and sizes of components and required power levels and operating lifetimes. Chapter 2 of this report gives a full description of the mission plans for a series of three manned missions to the Martian surface.

Chapter 3 discusses the numeric design methodology used to make some design decisions. As many different constraints are imposed with a variety of (often competing) design goals and features, this methodology was invaluable in selecting promising design alternatives for evaluation.

Chapter 4 describes the space power system and the propulsion technologies utilized. The details of electric propulsion (EP) technologies and power requirements are discussed, followed by a detailed description of the space core and conversion unit and lastly the shielding design.

Chapter 5 describes the surface power core and CO₂ Brayton cycle design, followed by a discussion of shielding options using local Martian resources. Chapter 6 gives a brief summary of major contributions and conclusions as well as identifying areas for future work in the area of space nuclear applications.

2.0 MARS EXPLORATION MISSION PLAN

2.1 INTRODUCTION TO MISSION PLAN

In order to facilitate the conceptual design of nuclear reactor systems to augment and empower Mars exploration, it is desirable to define some of the objectives of such exploration. The result of such an exercise is a better understanding of the requirements of the reactor power systems. Thus, boundary conditions for the design are set, resulting in systems optimized for the tasks they are employed to perform. To a large degree, the scientific community has already undertaken this process, and the key areas of focus for Mars exploration have been outlined in the NASA Design Reference Mission (DRM). [1] These objectives are as follows.

Mars Exploration Objectives:

- 1) Land people on Mars and return them safely to Earth.
- 2) Balance technical, programmatic, mission and safety risks.
- 3) Provide an operationally simple mission approach emphasizing the judicious use of common systems.
- 4) Provide a flexible implementation strategy.
- 5) Limit the length of time that the crew is continuously exposed to the interplanetary space environment.
- 6) Define a robust planetary surface exploration capacity capable of safely and productively supporting crews on the surface of Mars for 500 to 600 days each mission.
- 7) Define a capability to be able to live off the land. This means developing effective system designs and processes for using in-situ materials to replace products that otherwise would have to be provided from Earth.
- 8) Rely on advances in automation to perform a significant amount of the routine activities through the mission.
- 9) Ensure infrastructure is operational before a crew is committed.
- 10) Ensure that management techniques are available and can be designed into a program implementation that can substantially reduce costs.
- 11) Manage space operations capabilities including communications, data management, and operations planning to accommodate both routine and contingency mission operational situations; and understand abort modes from surface or space contingencies.
- 12) Design systems capable of utilizing the 2012 launch opportunity, which represents the most difficult opportunity in the 15-year Earth-Mars cycle.
- 13) Examine at least three human missions to Mars. The initial investment to send a human crew to Mars is sufficient to warrant more than one or two missions. Each mission may return to the site of the initial mission or establish a new site within roving distance of the other site(s). Thus there can be an evolutionary establishment of capabilities on the Martian surface.
- 14) Identify the characteristics of space transportation and surface operations systems consistent with sustaining a long-term program at affordable cost.
- 15) Provide for the achievement of a variety of defined science objectives.

In the course of developing a mission plan which satisfies these objectives, and given the nature of man’s past space flight experience, it is reasonable to require that systems essential for crew survival be flight tested prior to the commitment of a human crew. To provide opportunities for this testing to occur, smaller manned mission “precursors” are appropriate. These precursor missions prove the viability of key components and systems that will be used in the eventual manned exploration, while leveraging the unique advantages provided by those systems in order to achieve high levels of science return.

Another advantage of the precursor strategy is to break up the necessary system development for manned exploration into smaller portions. These portions are easier to obtain funding for and provide useful science data along each step. System performance data is returned and operational experience is gained. If a failure occurs, the data and experience collected can be used to improve the design and correct the issues. The mission can be flown again until the problems are solved.

With this strategy and set of objectives in mind, we have outlined in the sections that follow three precursor missions as well as the manned mission strategy. These missions establish values for design criteria including maximum allowable masses, required power levels, necessary life times, and other system limitations and constraints.

2.2 EARTH-MARS TRANSIT BREAKDOWN

The orbital alignments of the planets Mars and Earth in their paths around the sun create windows of opportunity for transfer between these two planets once every two years. Due to the inclination of their elliptical orbits, the closest distance between Mars and Earth, during each launch window, varies through a 15-year cycle as illustrated below in Figure 2.2-1. The minimum distance can vary between 0.4 AU at the best opportunities to nearly 0.7 AU at the worst. Any Earth-Mars transportation system should be designed to operate at the worst-case condition.

Plans for the initial manned missions to Mars should make use of the Earth-Mars launch opportunities occurring between 2016 and 2022, since these represent the least difficult launch

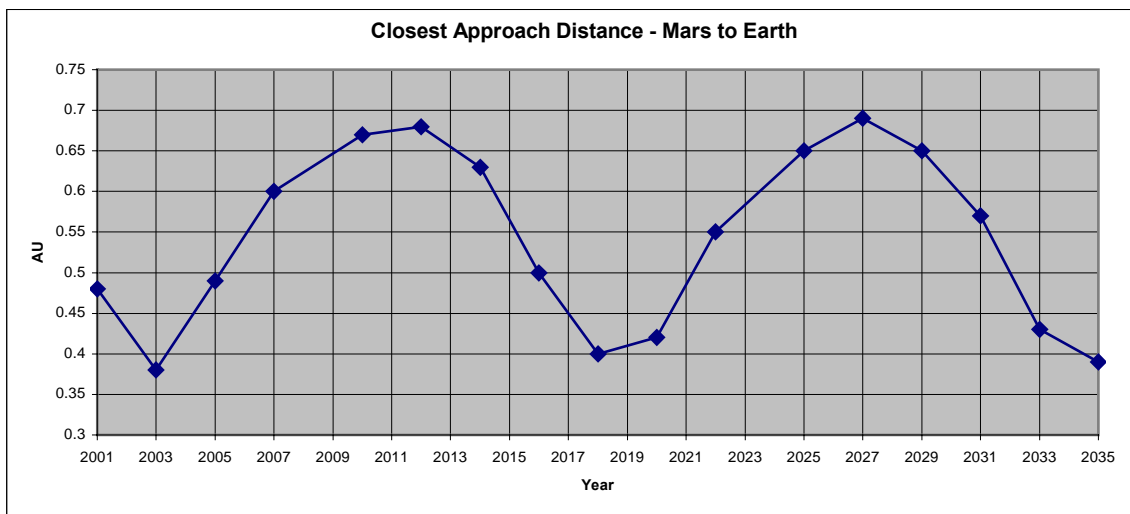


Figure 2.2 – 1 Closest Distances between Mars and Earth.

opportunities due to Earth-Mars distances. System design, however, should be based on the 2011 launch opportunity, which represents the most difficult opportunity in the 15-year Earth-Mars cycle. By designing the space transportation systems for this opportunity, missions can be flown in any opportunity with more favorable opportunities providing either faster transit times for the crew or increased payload delivery capability.

There exist a number of possible transfer trajectories, each with their own advantages and disadvantages. It will be necessary to utilize a number of different trajectories in the course of Mars exploration, depending upon individual mission requirements and propulsion system capabilities. An overview of the basic trajectories and maneuvers employed in the following mission plan is given below.

2.2.1 Hohmann Transfer

Hohmann transfers are the most propellant-efficient means of moving between two circular orbits (i.e. Earth orbit & Mars orbit), because they require the smallest change in spacecraft velocity. To accomplish a Hohmann transfer, two propulsive maneuvers are required. The first one breaks the spacecraft out of the initial orbit and puts it in an orbit that intersects the desired final orbit. The spacecraft is then in the Hohmann transfer ellipse, which is an orbit tangent to both circular orbits. After the spacecraft has coasted to the point that connects the transfer orbit to the desired final orbit, it fires its engine a second time, now to circularize its orbit, thus matching the target orbit. [4]

In the mission plan that follows, only the Mars sample return mission will utilize a Hohmann transfer. In this case, a chemical rocket will be used to return collected samples to Earth for analysis. All other missions have been designed to make use of reusable electric propulsion systems. Use of these systems will result in a different type of Earth-Mars transfer.

2.2.2 Early Nuclear - Electric Propulsion Transfers

In the following mission plan, for the precursor and unmanned cargo missions, highly efficient electric propulsion (EP) system transfers will take place utilizing near term EP technologies and space nuclear reactor systems. Characteristically, electric propulsion systems exhibit high specific impulse (ISP) making them far more efficient than chemical propulsion systems. However, they also produce much lower thrust levels. Thus, to change the velocity of a payload by a given amount takes a smaller mass of EP fuel than it would of chemical fuel. The tradeoff is that the transfer takes longer to occur. For unmanned missions, we are more than willing to trade transfer time for efficiency, since this reduces the mass of propellant that must be launched to low earth orbit (LEO), which ultimately reduces the total mission cost.

Other differences exist between chemical and electric propulsion transfers. Chemical transfers involve one or more short duration engine firings, which provide the necessary change in spacecraft velocity. Following these burns, the spacecraft effectively “coasts” to its destination. Electric propulsion systems however involve continuous thrusting, resulting in the gradual addition of energy to the spacecraft’s orbit over a long duration. Payloads launched to low earth orbit (LEO) require a period of continuous EP thruster firing which results in a spiral trajectory of increasing orbital energy, bringing the spacecraft to a high earth orbit (HEO). At a certain point, the spacecraft velocity will increase to the point where it escapes earth orbit and enters a heliocentric transfer orbit. The EP system continues to thrust increasing the energy of this orbit as the spacecraft proceeds on its way to Mars. This process is illustrated in Figure 2.2.2-1 below.

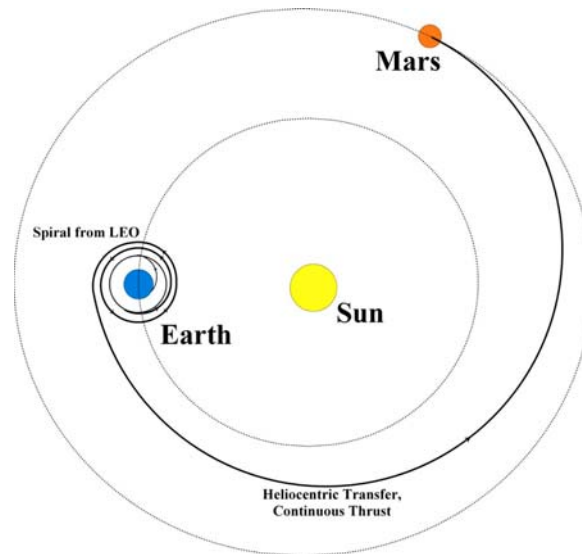


Figure 2.2.2 – 1 Nuclear-Electric Propulsion Transfer for Precursor and Cargo Missions.

Electric propulsion systems cannot provide a sufficiently large acceleration to allow payloads to follow Hohmann transfer orbits, due to the low thrust level. Despite being in less than the optimal transfer orbit (in terms of delta V required), because the EP system makes much more efficient use of propellant, the transfer is performed much more efficiently than is possible in a chemically derived Hohmann transfer.

2.2.3 Power and Propulsion System Return

Together the space nuclear reactor system and the electric propulsion system mentioned above and described in detail further on make up what will be referred to here as the re-usable Mars Transfer System (MTS). By creating a strategy to reuse these assets, significant cost savings can be realized. Many competing technologies, including chemical rockets and NTR systems are completely expendable. Thus, continued exploration using these systems requires the launch of significant additional mass to LEO. A reusable MTS virtually eliminates this requirement and thus significantly reduces the cost of continued exploration.

In order to re-use the Mars Transfer Systems, the mission plan requires their return to Earth after being used to propel each set of cargo to Mars. In order to accomplish this, it will be necessary for these systems to separate from their payloads at a certain point in the Earth-Mars transfer. The payloads will continue on to Mars where they will shed their excess velocity through aerocapture maneuvers. The power & propulsion systems will continue to operate so as to put themselves on a return trajectory to Earth. It is possible that the gravitational force of Mars can be used to assist this maneuver. The return of the MTS will be possible largely because the mass of the returning systems represents only a small portion of the outgoing mass.

2.2.4 Nuclear Powered VASIMR Fast Crew Transfer

The radiation environment in interplanetary space is more extreme than that typically experienced by astronauts in LEO. Additional shielding can be provided to block some of this radiation, however this constitutes a large increase in transfer habitat mass. A better solution is to

reduce the time that the crew is exposed to this high radiation environment. This approach has the benefit of reducing the total dose that the crew will receive, as well as reducing the crew's exposure to the de-habilitating effects of zero gravity, and the demands on spacecraft life support systems. For these reasons, when committing human crews for exploration of the planet Mars it is desirable to significantly reduce transit time.

In order to accomplish very short transit times while maintaining the high efficiency and reusability of electric propulsion systems, this mission plan assumes that the craft utilized for human crew transfers to and from Mars has a VASIMR based propulsion system. VASIMR stands for "Variable Specific Impulse Magnetoplasma Rocket." VASIMR is a high thrust, high efficiency plasma rocket engine being developed at the NASA Johnson Space Center for use in Mars exploration.

Unlike the NASA Design Reference Mission (DRM), this mission plan does not make use of a Nuclear Thermal Rocket (NTR) system for Earth-Mars transfer. This type of system was viewed as undesirable because of issues with public acceptance of NTR systems and because of its un-reusable nature. In addition, typical NTR based mission plans call for the NTR transfer of a chemical ERV to Mars orbit. Thus the return crew transit must be a slow chemically derived Hohmann transfer. The proposed mission plan relies on the nuclear fission powered VASIMR propulsion for both the Earth-Mars and Mars-Earth journeys.

The Earth-Mars transfer of the VASIMR propelled craft, like with other electric propulsion systems, would involve continuous thrusting providing a gradual addition of energy to the spacecraft's orbit. The first step would be a LEO to HEO spiral trajectory similar to that for other EP systems. Once it had reached HEO, the crew would then launch and transfer to this craft for the journey to Mars. The VASIMR engines would continue to thrust for almost the entire trip, resulting in a 90-day crew transfer. Near Mars the crew would board a capsule that would aerobreak and land while their transfer propulsion system and habitat would overshoot Mars and re-encounter it several months later. The VASIMR craft would remain in Mars orbit until the crew is ready to return to Earth. This process is illustrated in Figure 2.2.4-1 below.

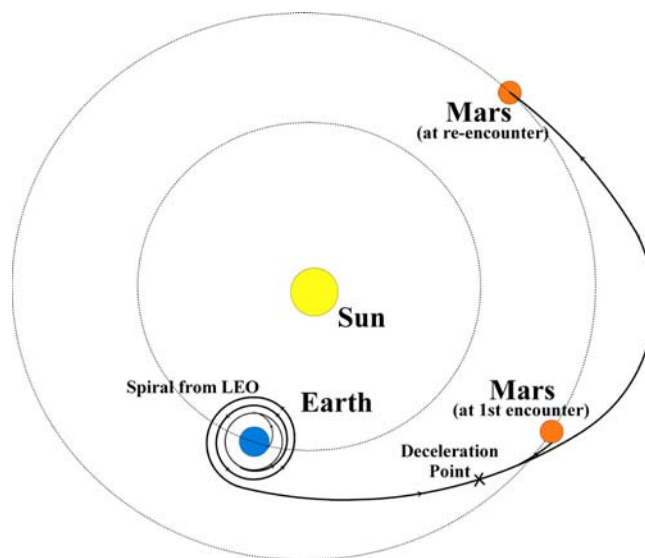


Figure 2.2.4 – 1 VASIMR Fast Transfer and Mars Overshoot.

The nuclear reactors presented later in this report have been designed to provide 4 MW of electric power each to meet the requirements outlined for the VASIMR mission plan [5]. At the point when VASIMR technology becomes available, three of the space fission reactors presented here could be combined with three VASIMR engines to create a reusable craft capable of Earth–Mars and Mars-Earth fast transits at high efficiencies.

2.3 OVERVIEW OF PROPOSED MISSIONS

This mission plan describes three precursor missions, as well as the manned mission strategy. The order of these missions is such that the lessons learned from one mission can be applied to the missions which follow, building capability and experience. The order and duration of these proposed missions is shown below in Figure 2.3-1.

The first proposed precursor mission is a Mars telecommunications satellite. This satellite would be launched in 2012 and would remain operational in Mars orbit throughout the first several manned Mars missions, providing high data rate communications between Mars and Earth. In addition, this mission would provide an opportunity to test the operation of a scaled-down version of the Mars Transfer System (space fission reactor and electric propulsion systems).

The second proposed precursor mission is a Mars sample return and technology demonstration mission. This mission would provide an opportunity to test some of the Mars surface infrastructure that will be needed for manned exploration, including a Mars surface fission reactor, while returning a large mass of surface samples to Earth. The mission would make use of the first full-scale Mars Transfer System for the Earth-Mars transfer, with the system returning to Earth for re-use. Launching in 2014, the mission would culminate with the return of surface samples in 2017.

The third, and final, proposed precursor mission would be space testing of the transfer habitat. This habitat is what the crew will live in for both their Earth-Mars and Mars-Earth journeys. Testing would consist of the launch of a prototype habitat to LEO near the International Space

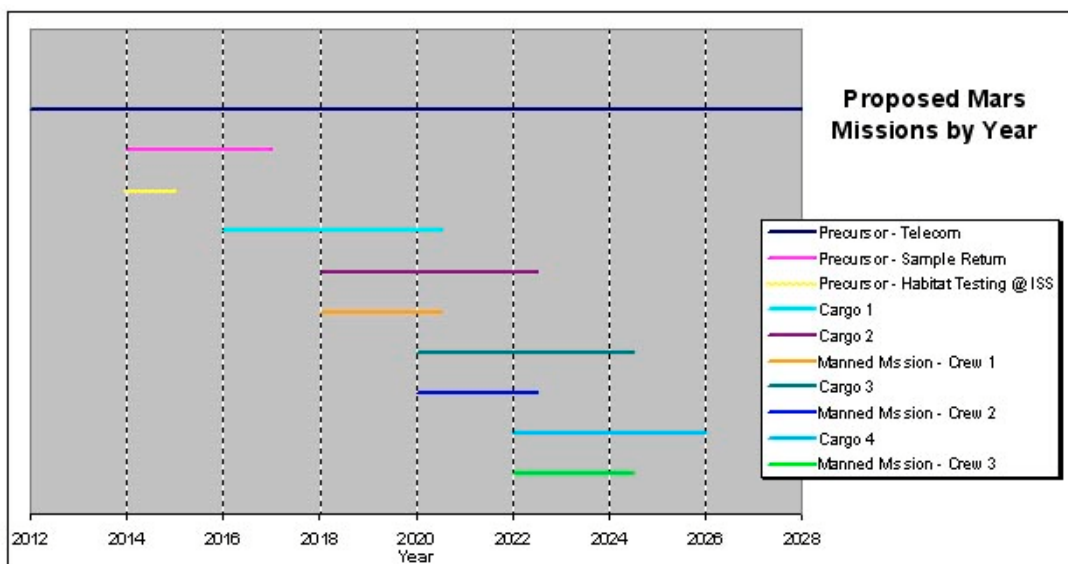


Figure 2.3 - 1 Order of Proposed Mars Missions.

Station (ISS) in 2014. With the habitat attached to the station, an in-depth analysis of its design and construction would take place to ensure that it would be robust enough to survive multiple round trips to Mars. This prototype habitat would then remain attached to the station, greatly expanding the working and living space provided for the astronauts of the ISS.

Following the successful completion of the precursor missions, significant testing and evaluation of the systems needed for the manned missions will have been completed. To further ensure success, and to meet the requirements defined by the scientific community, it is necessary to establish infrastructure on the surface of Mars prior to the commitment of a human crew. It is also necessary to provide backup capability should the initial infrastructure fail. A mission strategy has been developed, as depicted in Figure 2.3-1, to meet these objectives.

The manned mission strategy, beginning as early as 2016 and following the successful completion of the precursor missions, is described as follows. In the initial launch opportunity a set of cargo (CARGO1) consisting of a surface nuclear fission reactor, chemical resource plant and a surface habitat will be launched from Earth and sent, unmanned, to the surface of Mars. There this infrastructure will deploy and activate under remote control from Earth. Mission controllers will monitor the health of these systems, which are essential for life support and surface activity. The transfer of this cargo to Mars and its deployment and activation, should be completed within the two years between launch opportunities.

In the next launch opportunity, (as early as 2018) an informed decision then can be made concerning the deployment of the first crew (CREW1) based on the health of the surface infrastructure. Should there be a problem, the commitment of CREW1 can be delayed by one launch opportunity, and a full or partial replacement set of infrastructure can be sent to Mars instead. This pattern can continue until a healthy set of infrastructure is operational and waiting for the crew on Mars and at that time the first crew may be committed.

Provided there is no problem with the initial set of infrastructure (CARGO1), two missions will be launched in the next launch opportunity (2018). One will be the crew on a VASIMR driven fast transit and the other will be an additional set of surface infrastructure (CARGO2) identical to the first set of cargo. Both the crew and the second set of cargo will land near the existing infrastructure. CREW1 will use CARGO1 as their primary and CARGO2 as their secondary infrastructure, thus full backup capability has been provided. Following 600 days of surface activities, the crew will launch to their VASIMR craft and return to Earth. Each following launch opportunity will be identical in structure to this, with the next crew and a set of cargo being sent. In this manner, by the end of the third crew mission, considerable science will have been achieved and a well-established scientific station will be in place and ready for reuse in future exploration.

2.4 MARS NUCLEAR POWERED TELECOMMUNICATIONS SATELLITE

A reasonable first precursor mission would be a nuclear powered telecommunications satellite. This satellite can provide high data rate communications between Mars and Earth, which is seen as an essential capability for future exploration. It also provides an opportunity to make use of a scaled down space nuclear fission reactor power system and electric propulsion system, in order to validate and test those technologies.

Suggested Launch Window: 2012

Primary Objectives:

- To provide capability for high data rate communications between Mars and Earth. It can provide data storage and relay for both Mars orbital and surface operations. This increases the science yield of all present and future Mars missions by allowing the transmission of more data.
- To validate space nuclear fission reactor power system technologies, aiding their development and enabling this capability for future missions.
- To validate fission reactor powered electric propulsion technology for Earth-Mars transfer. (Scaled up versions of this reactor and propulsion system will be used for future Mars missions in the form of the Mars Transfer System.)

Secondary Objectives:

- To provide real-time orbital video and high resolution pictures.
- To provide a platform for high power Mars orbit experiments (active radar, etc.)

Earth Launch Manifest:

- Delta 4 or Atlas 5 – Mars Telecommunications Satellite

Payload :

- High Transmitting Power (200kW) Telecommunications System
- Space Nuclear Reactor System (Producing 200kWe)
- Electrical Energy Conversion System (Thermal to Electrical)
- Electric Propulsion (EP) System consisting of many thrusters in parallel
- EP Fuel (Xenon, etc.)
- High power experiments (radar, etc.)
- High resolution video and still camera system

The flow of this mission is illustrated in Figures 2.4-1 and 2.4-2 below. The mission can be subdivided into five stages which are Launch to LEO, Fission Reactor & Electric Propulsion System Activation, Earth-Mars Transfer & Mars Orbital Insertion (MOI), Early Mars Orbital Operations, and Late Mars Orbital Operations. These mission stages are described in detail below.

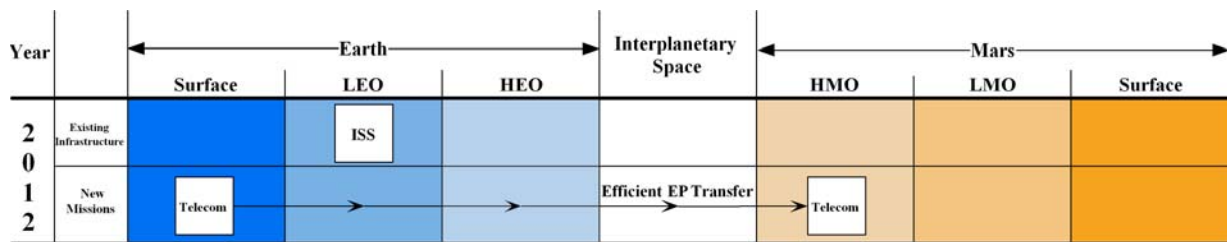


Figure 2.4 – 1 Flow of Precursor Mission 1.

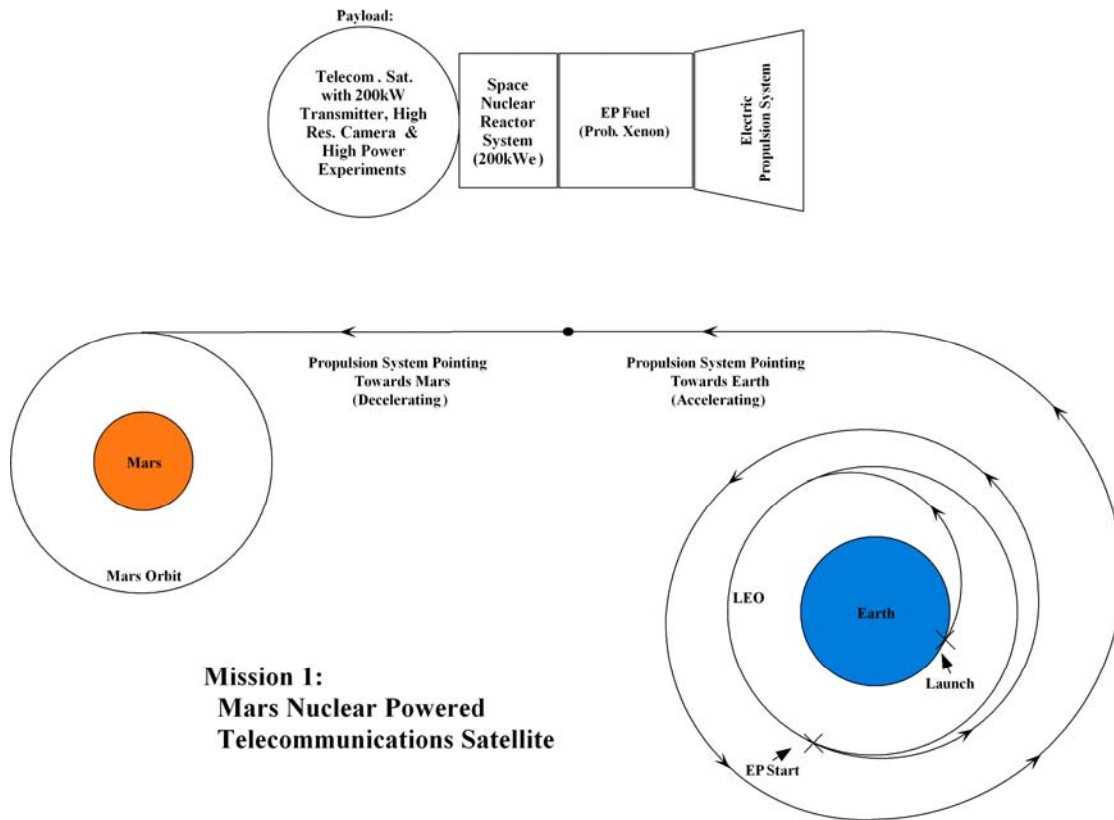


Figure 2.4 – 2 Flow of Precursor Mission 1.

Mission Stage 1 (Launch to LEO):

- Payload is launched via a chemical rocket and placed in Low Earth Orbit.
- Chemical launch stage is jettisoned.

Mission Stage 2 (Fission Reactor and Electric Propulsion System Activation):

- EP system is deployed.
- Thermal radiator system is deployed.
- Nuclear reactor is activated.
- EP system is activated. This begins a slow spiral trajectory, building up velocity until the spacecraft leaves earth orbit.

Mission Stage 3 (Earth-Mars Transfer and MOI):

- EP system propels the satellite halfway to Mars.
- Mid-journey the satellite reverses orientation.
- EP system slows the satellite into Mars orbit.

Mission Stage 4 (Early Mars Orbital Operations):

- The orbit is adjusted using the EP system to the point where a low polar orbit is achieved.
- This mapping orbit will allow the satellite to cross over most of the surface area of the planet. High-resolution video and pictures will be taken. Data will be collected from the high power experiments and relayed to Earth.

Mission Stage 5 (Late Mars Orbital Operations):

- Once a primary mapping mission is complete, the EP system will place the satellite in geo-stationary orbit over the location of a future surface mission. There it will be able to provide high data rate telecommunications capabilities.
- As other missions are flown and communication needs change, the orbit can be maintained or adjusted through use of the EP system.

It may be desirable to send a total of three or more telecommunications satellites to Mars orbit. This would allow non-stop communications capability between Earth and Mars as well as between virtually any two different locations on the planet surface. It also adds redundancy, should any one satellite fail. Three satellites in Mars orbit are depicted in Figure 2.4-3 below.

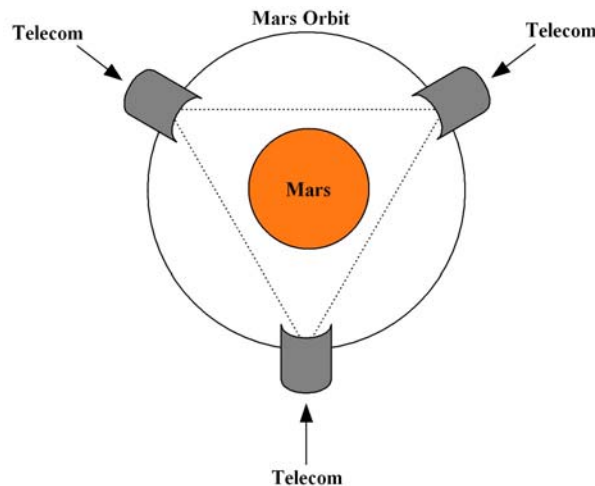


Figure 2.4 – 3 Three Telecommunications Satellites in Mars Orbit.

2.5 OVERVIEW OF PROPOSED MAGNUM LAUNCH VEHICLE

This mission plan makes use of a proposed Magnum Heavy Launch Vehicle to launch payloads to Low Earth Orbit. The NASA Design Reference Mission [2] describes this Magnum vehicle as one having an 80 metric ton to LEO capacity which can be used to launch the payloads and systems needed for Mars exploration. With this capability, payloads can be packaged and launched together rather than being launched on a large number of smaller rockets. This eliminates or greatly reduces the requirement of on-orbit assembly.

The Magnum rocket consists of an expendable inline core vehicle with diameter equal to the space shuttle external tank. Two space shuttle type boosters provide additional thrust at launch.

Magnum has been designed to make common use of existing space shuttle launch facilities so as to reduce launch costs.

The figures below have been taken from the NASA DRM. Figure 2.5-1 depicts the basic configuration of the Magnum vehicle. Figure 2.5-2 compares the launch capability of the Magnum vehicle with other proposed and existing launch systems. Finally Figure 2.5-3 gives more detailed launch capabilities of the proposed Magnum vehicle.

There is a possibility that Magnum or similar heavy launch vehicles will be unavailable for use in the Mars exploration program. Care has been taken in the design of the space and surface nuclear reactors to ensure that they can be packaged within existing rockets such as the Boeing Delta 4 or the Lockheed Atlas 5 should this be the case.

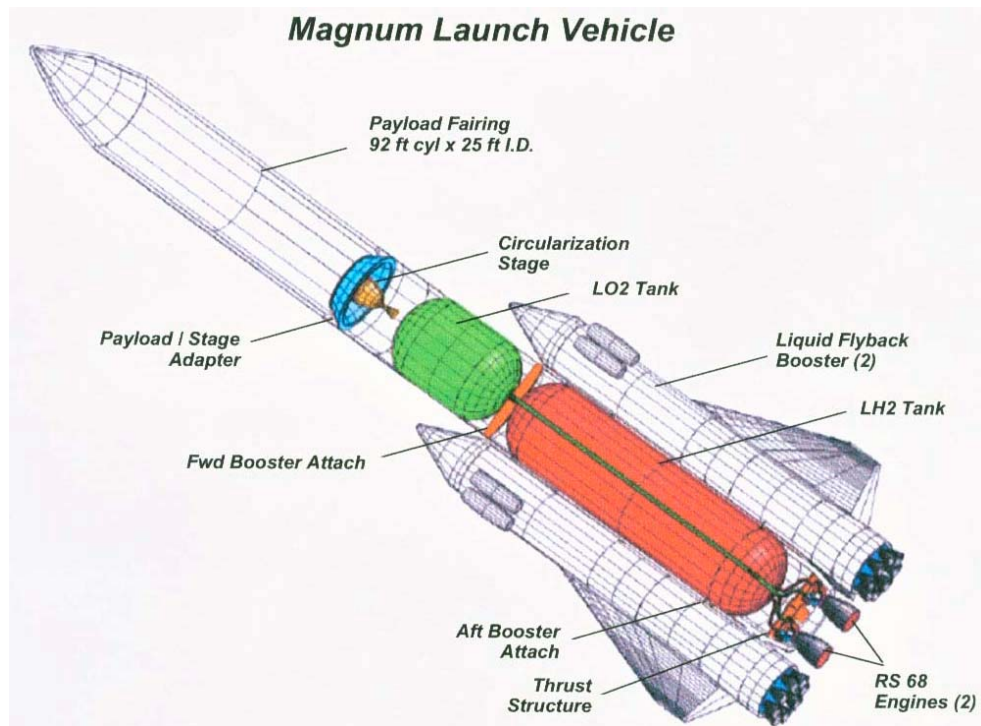


Figure 2.5 - 1 Basic Configuration of Magnum Launch Vehicle [2].

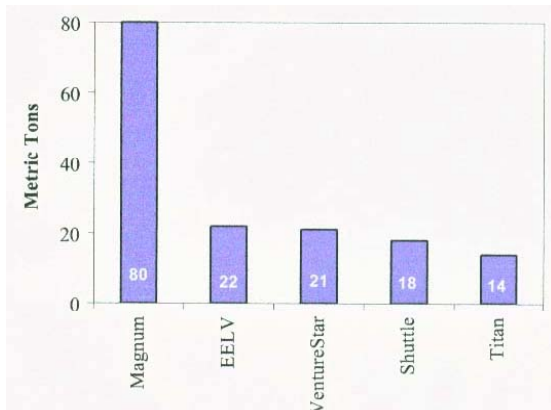
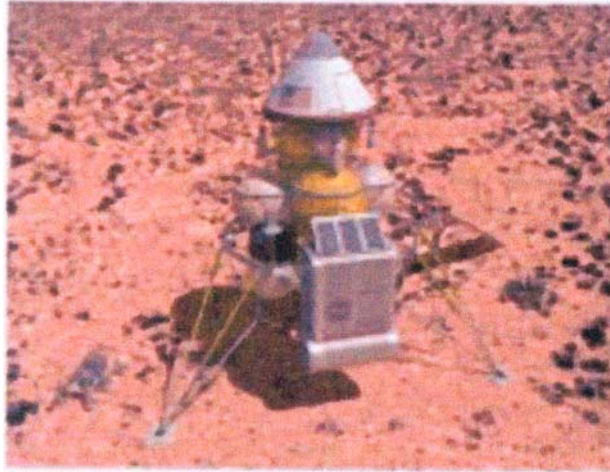


Figure 2.5 - 2 Magnum Payload (Capability to 407 km) [2].

| | Performance or Mass (mt) | |
|-----------------------------|--------------------------|-------------------|
| | Inclination 28.5° | Inclination 51.6° |
| Shroud Drop @ 400 Kft | 85.4 | 79.9 |
| Integrated Shroud/Aerobrake | | |
| Payload Only | 75.7 | 70.2 |
| Shroud / Aerobrake Wt. | 13.6 | 13.6 |
| Total Injected | 89.3 | 83.7 |

Figure 2.5 - 3 Magnum Launch Capabilities [2].

2.6 MARS SAMPLE RETURN AND TECHNOLOGY DEMONSTRATOR MISSION



Conceptual View of Sample Return Lander [1]

The second proposed precursor is a Mars sample return mission. This mission will employ a full-scale *space* fission reactor power system and electric propulsion system. It will also test a full-scale Mars *surface* fission reactor power system and In-situ Resource Utilization (ISRU) chemical plant. These are seen as essential technologies for the manned exploration of Mars.

Suggested Launch Window: 2014

Primary Objectives:

- To demonstrate the reusable *Mars Transfer System* or *MTS* (space fission reactor & electric propulsion system) for Earth to Mars cargo transfers.
- To validate Mars surface nuclear fission reactor technology, enabling this capability for future missions. This reactor will be identical to those to be sent on the manned missions.
- To validate large-scale ISRU technology by operating it on the surface of Mars and generating methane and oxygen largely from the CO₂ atmosphere. This enables this capability for future missions.

Secondary Objectives:

- To provide an energy recharging station to support surface rovers in sample collection.
- To collect a variety of samples from a selected area of the Martian surface.
- To fuel a sample capsule rocket with propellant and oxidizer produced from the Martian atmosphere.
- To use this rocket to return samples from the surface of Mars to Earth for analysis.

Earth Launch Manifest:

- Magnum Heavy launch – MTS1 & Fuel
- Delta 4 or Atlas 5 – Mars Sample Return Lander

Mars Transfer System (MTS):

- Space Nuclear Fission Reactor Power System
- Electric Propulsion (EP) System (array of thrusters)
- EP Fuel (Xenon, etc.)
- Docking mechanism (to dock with payload)

Payload:

- Aero-capture shield for Mars orbital capture & entry.
- Surface landing system (retro-rockets, landing legs).
- Surface Nuclear Fission Reactor Power System.
- (ISRU) In-Situ Resource Utilization System.
- Hydrogen feedstock for ISRU.
- One or more rechargeable battery powered surface rovers.
- Sample return capsule with rocket (for ascent & Trans-Earth Injection) and an empty fuel tank.
- Ablative heat shield (for Earth entry of samples).

In the proposed sample return mission, the surface fission reactor, ISRU plant, and the mass of hydrogen feedstock sent from Earth will be the same as those to be sent on the manned missions. The ISRU will therefore produce the same amount of fuel and oxidizer as it would to fuel a manned ascent capsule. In the case of the manned missions, this fuel and oxidizer is only used to lift the crew from the Martian surface to Low Mars Orbit. The propulsive force needed to return the crew to Earth is provided by their VASIMR craft. For the sample return mission, this same mass of fuel and oxidizer propels the much smaller payload mass all the way from the surface of Mars, to Mars orbit, and finally on a Hohmann transfer to Earth.

The flow of this mission is illustrated in Figure 2.6-1 below. The mission can be subdivided into seven stages which are *Launch to Low Earth Orbit*, *MTS Activation*, *Payload & MTS Docking*, *Earth-Mars Transfer*, *Aero Breaking & Landing*, *Lander Activation & Operations*, *Ascent*, *TEI & Continued Lander Operations*, and *Sample Entry and MTS Return*. These mission stages are described in detail below and are depicted in Figures 2.6-2 through 2.6-4.

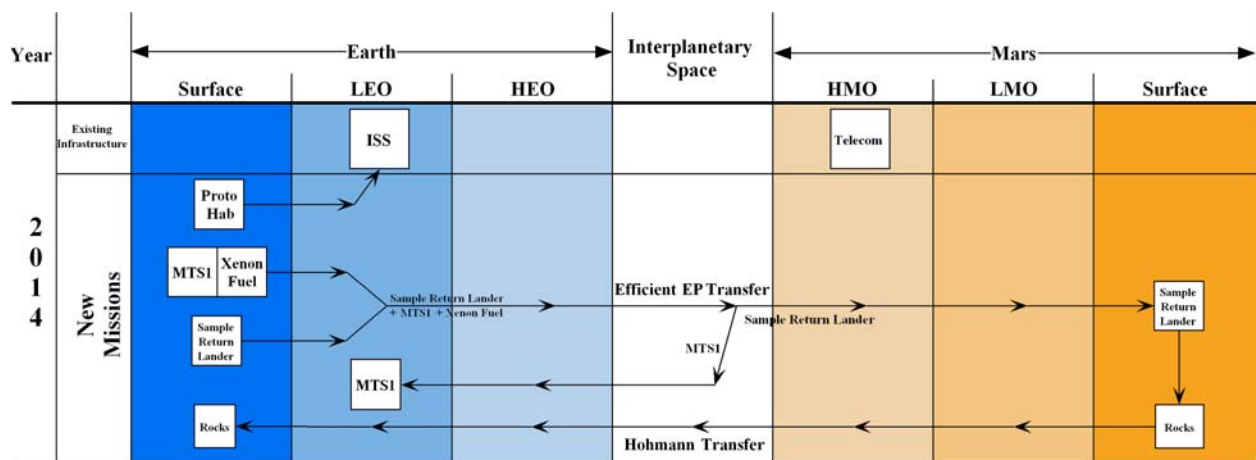


Figure 2.6 – 1 Flow of Precursor Missions 2 and 3.

Mission Stage 1 (Launch to Low Earth Orbit (LEO)):

- **(Launch 1)** Mars Transfer System (MTS1) and Xenon fuel is launched via a Magnum rocket to LEO.
- Chemical booster stage is jettisoned.
- **(Launch 2)** Sample Return Lander is launched via a Delta 4 or Atlas 5 rocket to LEO.
- Chemical booster stage is jettisoned.

Mission Stage 2 (MTS Activation):

- Electric Propulsion (EP) system is deployed.
- Thermal Radiator system is deployed.
- Nuclear Fission Reactor is activated.
- EP system is activated.

Mission Stage 2 (Payload and MTS Docking):

- MTS rendezvous with Payload
- Automated docking performed between MTS and payload.

Mission Stage 3 (Earth-Mars Transfer):

- MTS propels the payload partway to Mars.
- At a certain point, the MTS and Payload separate.
- MTS continues to fire as necessary to put it on a return trajectory to Earth.

Mission Stage 4 (Aero Breaking and Landing):

- Payload aerocaptures/aerobreaks in the Martian atmosphere, slowing it down.
- Landing rockets slow the descent further to land the payload.

Mission Stage 5 (Lander Activation and Operations):

- Thermal Radiators are deployed
- Surface Nuclear Fission Reactor is brought online.
- ISRU plant is activated and begins producing methane and oxygen.
- Rover is charged and deployed. It begins surface operations, locating and collecting samples. It returns and recharges as needed.
- Sample return rocket is fueled.
- Sample container is filled with samples.

Mission Stage 6 (Ascent, TEI and Continued Lander Operations):

- The fully loaded and fully fueled sample return craft launches to Mars Orbit.
- Once reaching Mars orbit, the sample return craft uses the same ascent rocket to make a firing to place it on a Hohmann transfer returning to Earth.
- The reactor and ISRU plant continue to operate on the surface until all available hydrogen feedstock has been exhausted. This can provide a small cache of backup consumables for future manned missions.
- The reactor will reduce its power output to the minimum necessary to supply energy to the rover(s). The rover(s) continue science operations until they or the reactor fail.
- This reactor and ISRU can serve as backup infrastructure for future manned missions.

Mission Stage 7 (Sample Entry and MTS Return):

- The Sample Capsule aero-captures/aero-breaks in the Earth atmosphere using its ablative heat shield. It splashes down and/or parachutes to a landing.
- MTS1 returns and captures into a high Earth orbit via its return trajectory. It then continues to thrust, reducing the energy of its orbit until it has reached LEO and expended all of its fuel. Here it remains until it is refueled and reused.

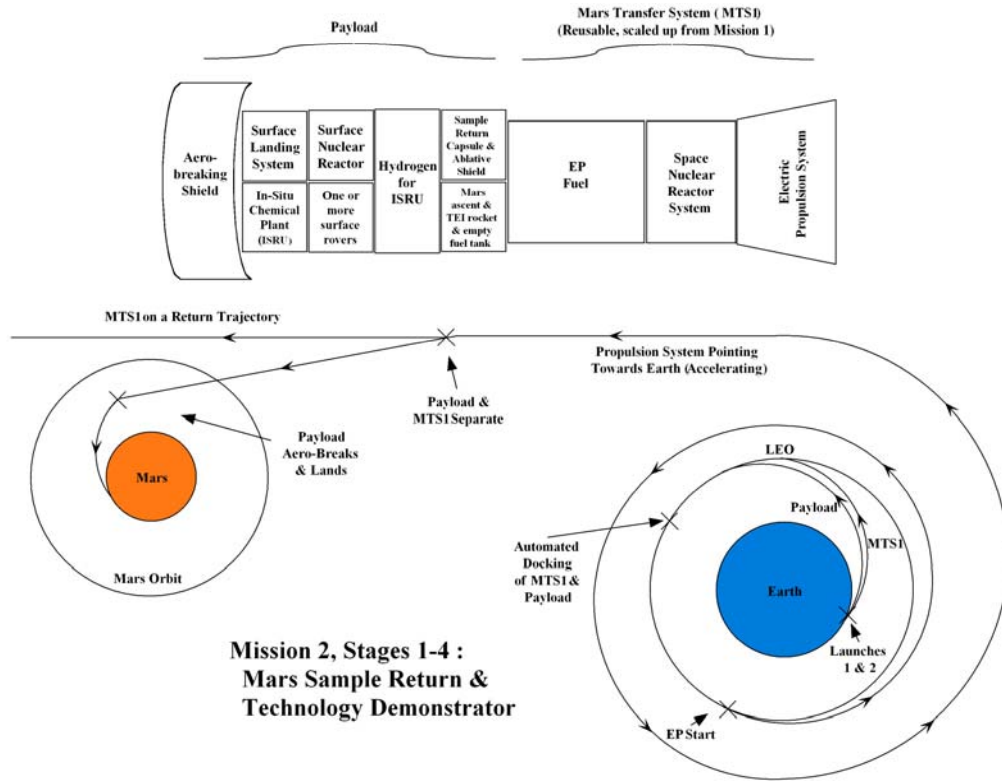


Figure 2.6 – 2 Flow of Precursor Mission 2, Stages 1-4.

Mission 2, Stage 5 (Surface Ops) :
Mars Sample Return &
Technology Demonstrator

- Nuclear Reactor Activation
- ISRU Activation
- Ascent/TEI Stage Fueling
- Rover Operation & Recharging
- Large Scale Sample Collection

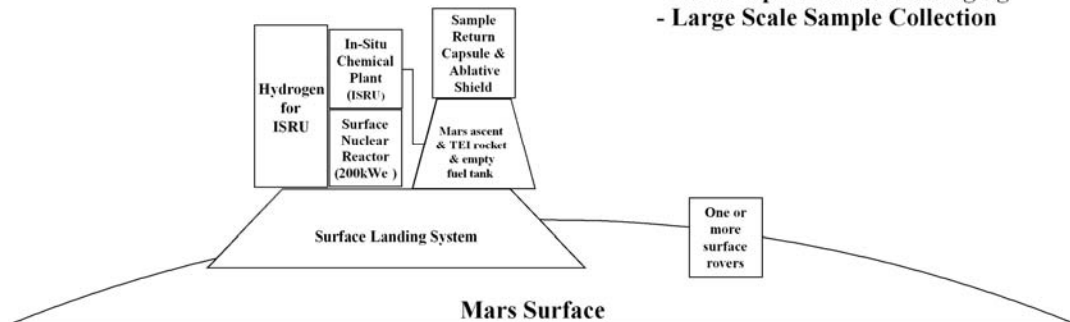


Figure 2.6 – 3 Flow of Precursor Mission 2, Stage 5.

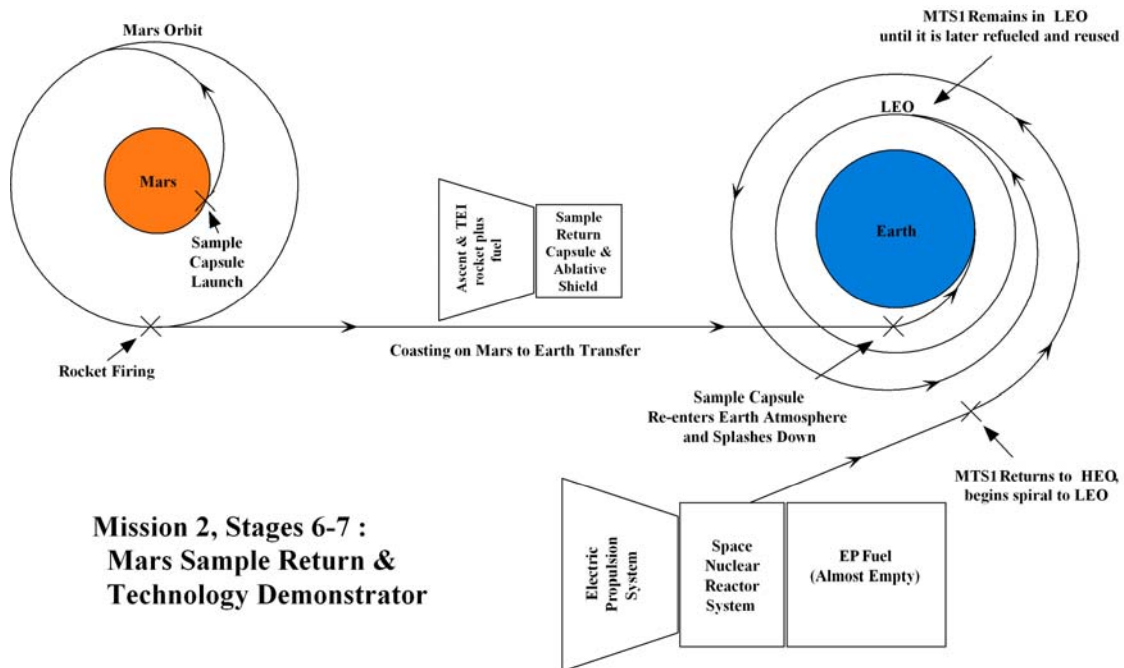
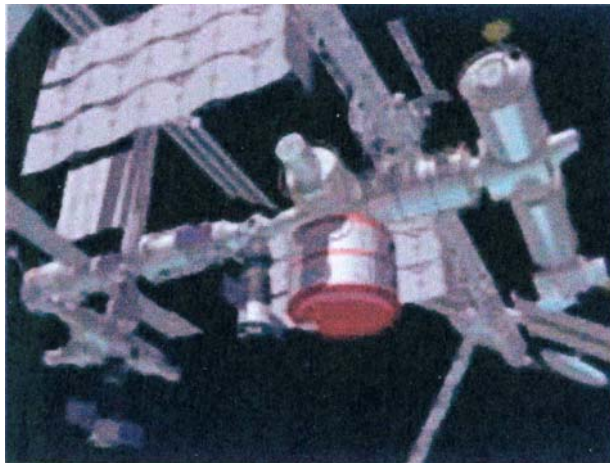


Figure 2.6 – 4 Flow of Precursor Mission 2, Stages 6-7.

2.7 TRANSIT HABITAT TESTING AND VERIFICATION AT THE INTERNATIONAL SPACE STATION



Conceptual View of Prototype Transit Hab Module at ISS [1]

The third proposed precursor mission provides an opportunity to flight test the transit habitat. This is the habitat that the crew will depend upon to survive both the Earth-Mars and Mars-Earth journeys. This test is important because it increases the chances for crew survival. Should a flaw in the design of the habitat be found, changes can be made to future habitats (including the one to be launched on the next launch opportunity). Additionally, this habitat could remain at the International Space Station, where it would greatly expand the living and working space aboard the station. The flow of this precursor mission is illustrated in Figure 2.6-1 and Figure 2.7-1 below.

Earth Launch Manifest:

- Magnum Heavy launch – Prototype Transit Habitat

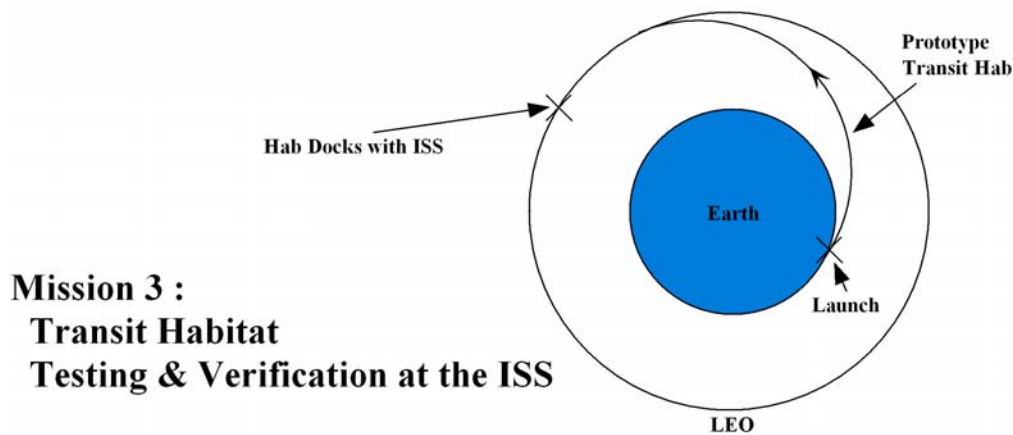


Figure 2.7 –1 Precursor Mission 3.

2.8 MANNED MISSIONS

2.8.1 Manned Missions: Launch Opportunity 1

In this initial manned mission launch opportunity, the cargo to be used by the first Mars exploration crew will be launched from Earth and sent, unmanned, to the Martian surface. It will be sent from Earth in two packages, CARGO1-A and CARGO1-B as described below. Once on the surface, the infrastructure will deploy and activate under remote control. Mission controllers will monitor the health of these systems, and ensure that they are fully operational prior to committing the first crew on the next launch opportunity.

Suggested Launch Window: 2016

Launch Opportunity Objectives:

- To launch two additional Mars Transfer Systems (MTS2, MTS3).
- To send the first set of cargo (CARGO1-A & CARGO1-B) to the Martian surface.
- To provide an operational beacon to assist with the precision landing of future craft near the existing infrastructure.
- To ensure the delivered infrastructure is fully deployed and operational prior to the next launch opportunity.

Earth Launch Manifest:

- Magnum Heavy launch – MTS2 & Fuel
- Magnum Heavy launch – MTS3 & Fuel
- Magnum Heavy launch – CARGO1-A
- Magnum Heavy launch – CARGO1-B

Payload (CARGO1-A):

- Aero-capture shield for Mars orbital capture and entry.
- Surface landing system (retro-rockets, landing legs).
- Earth Entry / Mars Ascent Capsule.
- Surface Nuclear Fission Reactor Power System on mobile truck.
- 1 km long power cable.
- (ISRU) In-Situ Resource Utilization System.
- Hydrogen feedstock for ISRU.
- Surface communications system and landing assist beacon.
- Inflatable mars surface labs.
- Un-pressurized rover.
- Water storage tank.
- Science equipment.

Payload (CARGO1-B):

- Aero-capture shield for Mars orbital capture & entry.
- Surface landing and repositioning system (retro-rockets, landing legs and wheels).
- Surface Habitat

The flow of this launch opportunity is illustrated in Figure 2.8.1-1 below. The opportunity can be subdivided into eight stages which are *Launches to Low Earth Orbit, MTS2 + MTS3 Activation, CARGO1-A & MTS2 Docking, CARGO1-B & MTS3 Docking, Earth-Mars Transfers, Aero Breaking & Landings, CARGO1 Activation & Operations, and MTS2 & MTS3 Return*. These mission stages are described in detail below and are depicted in Figures 2.8.1-2 through 2.8.1-5.



Conceptual View of CARGO1-A Descent [1]



Conceptual View of CARGO1-A Deployment [1]



Conceptual View of CARGO1-B Descent [1]

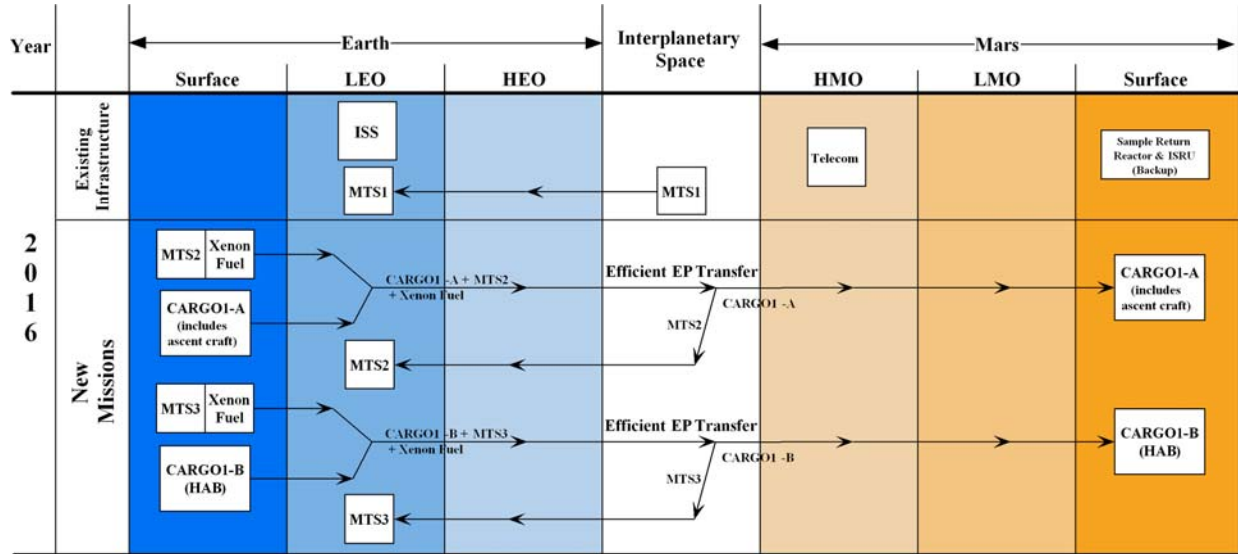


Figure 2.8.1 – 1 Flow of Launch Opportunity 1.

Stage 1 (Launches to Low Earth Orbit (LEO)):

- (**Launch 1**) Mars Transfer System (MTS2) and Xenon fuel is launched via a Magnum rocket to LEO.
- Chemical booster stage is jettisoned.
- (**Launch 2**) Mars Transfer System (MTS3) and Xenon fuel is launched via a Magnum rocket to LEO.
- Chemical booster stage is jettisoned.
- (**Launch 3**) CARGO1-A is launched via a Magnum rocket to LEO.
- Chemical booster stage is jettisoned.
- (**Launch 4**) CARGO1-B is launched via a Magnum rocket to LEO.
- Chemical booster stage is jettisoned.

Stage 2 (MTS2 and MTS3 Activation):

- Electric Propulsion (EP) systems are deployed.
- Thermal Radiator systems are deployed.
- Space Nuclear Fission Reactors are activated.
- EP systems are activated.

Stage 3 (CARGO1-A and MTS2 Docking):

- MTS2 rendezvous with CARGO1-A
- Automated docking performed between MTS2 and CARGO1-A.

Stage 4 (CARGO1-B and MTS3 Docking):

- MTS3 rendezvous with CARGO1-B.
- Automated docking performed between MTS3 and CARGO1-B.

Stage 5 (Earth-Mars Transfers):

- The transfer systems propel their respective payloads partway to Mars.
- At a certain point, the transfer systems and payloads separate.
- MTS2 and MTS3 continue to fire as necessary to put them on return trajectories to Earth.

Stage 6 (Aero Breaking and Landings):

- CARGO1-A and CARGO1-B aerocapture/aerobreak in the Martian atmosphere.
- Landing rockets slow their descent further to land the payloads.

Stage 7 (CARGO1 Activation and Operations):

- The reactor on its mobile platform travels up to 1km away from the rest of the infrastructure, trailing its power transfer cable behind it.
- Thermal Radiators are deployed.
- Surface Nuclear Fission Reactor is brought online, powering ISRU.
- ISRU plant is activated and begins producing methane and oxygen to fuel the ascent capsule. It also begins generating oxygen and water for life support systems.
- Landing assist beacon is deployed and activated.
- Systems are controlled and monitored from Earth.
- The CARGO1-B Habitat remains fixed at its landing site until the first crew arrives and repositions it near the other infrastructure.
- The deployed cargo is depicted below in Figure 2.8.1-4

Stage 8 (MTS2 and MTS3 Return):

- MTS2 & MTS3 return and capture into a high Earth orbit via their return trajectories. They then continue to thrust, reducing the energy of their orbits until they have reached LEO and expended all of their fuel. Here they remain until they are refueled and reused.
- The return of the Mars Transfer Systems is depicted below in Figure 2.8.1-5

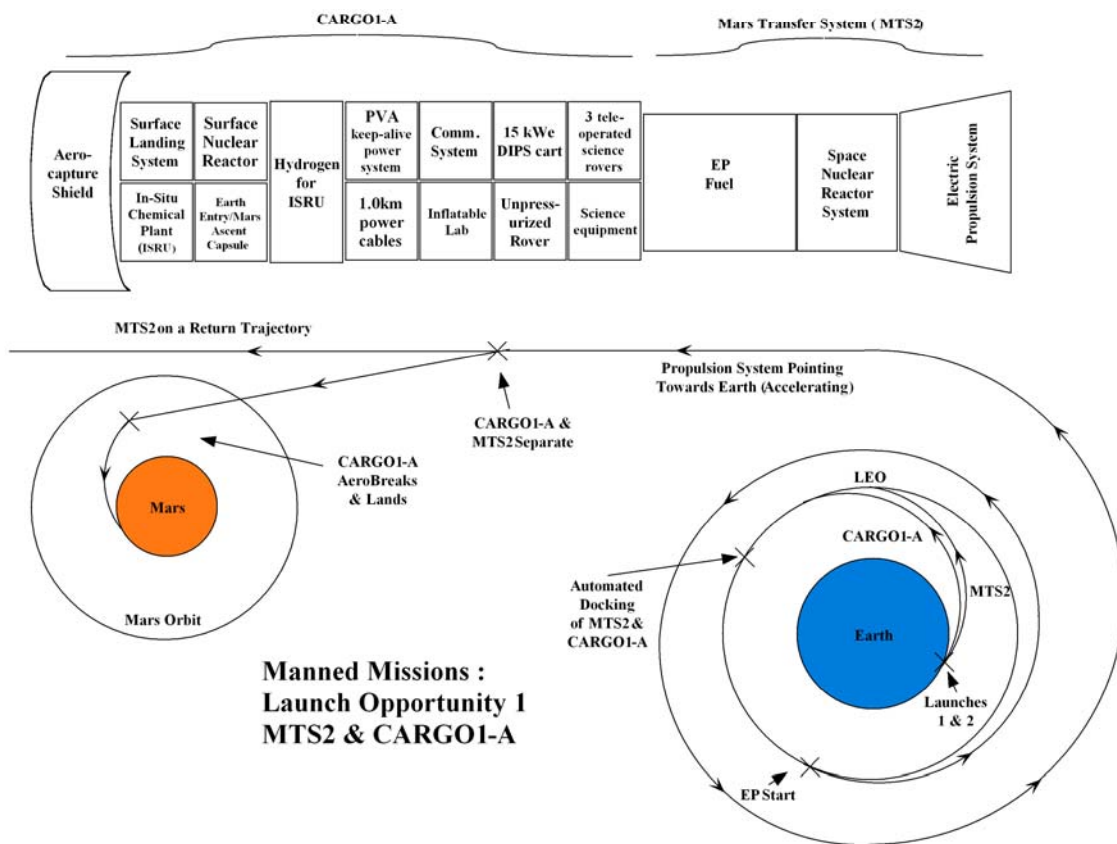


Figure 2.8.1 – 2 Launch Opportunity 1, MTS2 and CARGO1-A.

Table 2.8.1 – 1 CARGO# -A Mission Mass Breakdown

| | | | |
|--|----------------|-----------|-----------|
| Earth Entry / Mars Ascent Capsule | 4,829 | kg | DRM 3.0 A |
| Ascent stage dry mass | 4,069 | kg | DRM 3.0 A |
| ISRU plant | 3,941 | kg | DRM 3.0 A |
| Hydrogen feedstock | 5,420 | kg | DRM 3.0 A |
| PVA keep-alive power system | 825 | kg | DRM 3.0 A |
| 200kw surface nuclear power plant | 4,000 | kg | |
| 1.0km power cables, PMAD | 837 | kg | DRM 3.0 A |
| Communication system | 320 | kg | DRM 3.0 A |
| Inflatable Laboratory Module | 3,100 | kg | DRM 3.0 A |
| 15 kWe DIPS cart | 1,500 | kg | DRM 3.0 A |
| Un-pressurized rover | 550 | kg | DRM 3.0 A |
| 3 tele-operable science rovers | 1,500 | kg | DRM 3.0 A |
| Water storage tank | 150 | kg | DRM 3.0 A |
| Science Equipment | 1,770 | kg | DRM 3.0 A |
| Total Cargo Mass | 32,811 | kg | |
| Vehicle Structure | 3,186 | kg | DRM 3.0 A |
| Terminal propulsion system | 1,018 | kg | DRM 3.0 A |
| Total Landed Mass | 37,015 | kg | |
| Landing System Propellant | 10,985 | kg | DRM 3.0 A |
| Forward Aeroshell | 9,918 | kg | DRM 3.0 A |
| Parachutes and mechanisms | 700 | kg | DRM 3.0 A |
| Total Mass at Mars Entry (Also in LEO) | 58,618 | kg | |
| Space Reactor System | | | |
| Reactor | 250 | kg | |
| Shield | 4,500 | kg | |
| Coolant | 1,975 | kg | |
| Radiator | 2,700 | kg | |
| Collector / Armor | 2,100 | kg | |
| Pumps | 400 | kg | |
| Total Space Reactor System | 11,925 | kg | |
| Propulsion System | 10,000 | kg | |
| EP Xenon Fuel (for TMI) | 25,000 | kg | |
| Total Mars Transfer System Mass | 46,925 | kg | |
| Total Cargo & MTS Initial Mass in LEO | 105,543 | kg | |

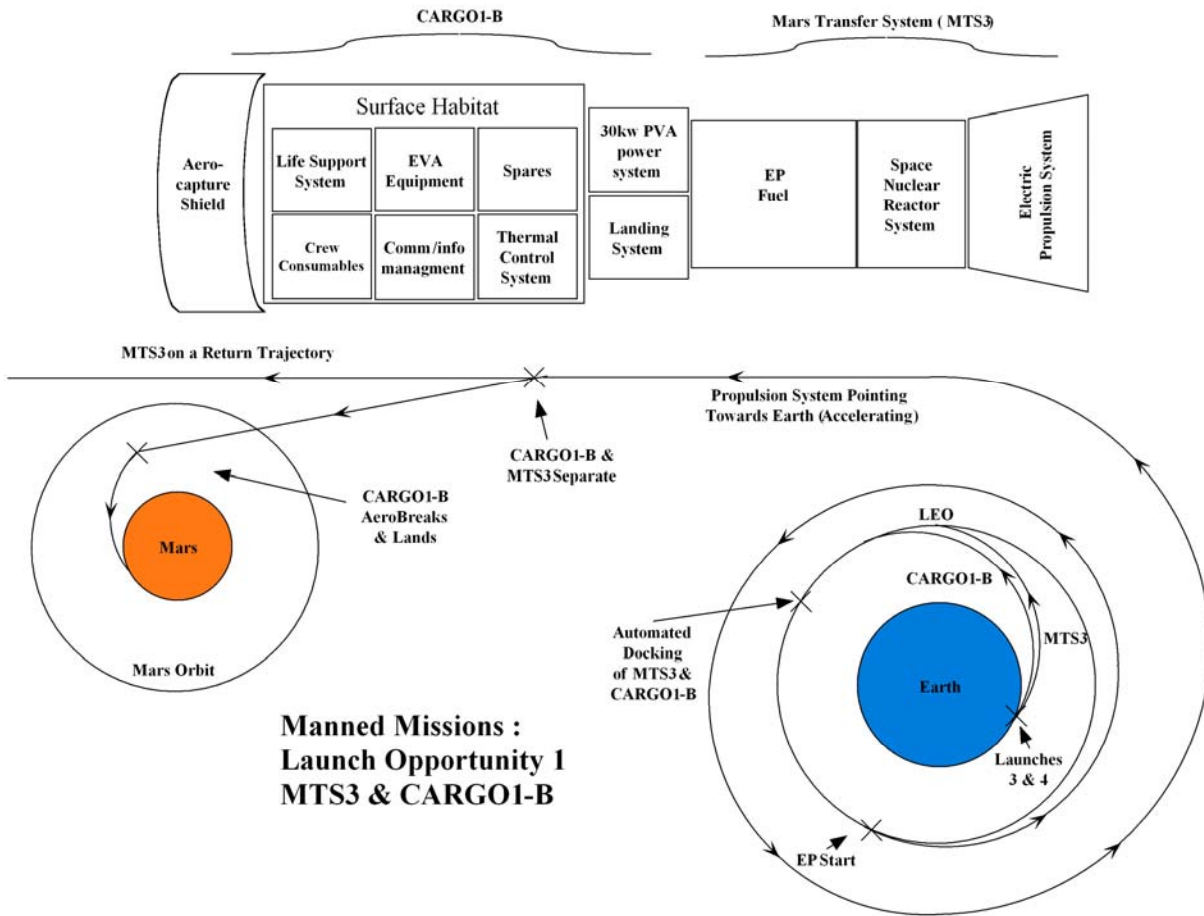


Figure 2.8.1 – 3 Launch Opportunity 1, MTS3 and CARGO1-B.

Table 2.8.1 – 2 CARGO# - B Mass Breakdown

| | | | |
|--|----------------|-----------|-----------|
| Surface Habitat | | | |
| Life Support System | 4,661 | kg | DRM 3.0 A |
| Crew Accommodations & Consumables | 12,058 | kg | DRM 3.0 A |
| EVA equipment | 243 | kg | DRM 3.0 A |
| Comm/info management | 320 | kg | DRM 3.0 A |
| 30 kW PVA power system (for surface) | 3,249 | kg | DRM 3.0 A |
| Thermal Control System | 550 | kg | DRM 3.0 A |
| Structure | 5,500 | kg | DRM 3.0 A |
| Spares | 1,924 | kg | DRM 3.0 A |
| Total Habitat Mass | 28,505 | kg | DRM 3.0 A |
| Vehicle Structure | 3,186 | kg | DRM 3.0 A |
| Terminal propulsion system | 1,018 | kg | DRM 3.0 A |
| Total Landed Mass | 32,709 | kg | DRM 3.0 A |
| Propellant (For Surface landing) | 11,381 | kg | DRM 3.0 A |
| Forward Aeroshell | 13,580 | kg | DRM 3.0 A |
| Parachutes and mechanisms | 700 | kg | DRM 3.0 A |
| Total Mass at Mars Entry (Also in LEO) | 58,370 | kg | DRM 3.0 A |
| Space Reactor System | | | |
| Reactor | 250 | kg | |
| Shield | 4,500 | kg | |
| Coolant | 1,975 | kg | |
| Radiator | 2,700 | kg | |
| Collector / Armor | 2,100 | kg | |
| Pumps | 400 | kg | |
| Total Space Reactor System | 11,925 | kg | |
| Propulsion System | 10,000 | kg | |
| EP Xenon Fuel (for TMI) | 25,000 | kg | |
| Total Mars Transfer System Mass | 46,925 | kg | |
| Total CHV & MTS Initial Mass in LEO | 105,295 | kg | |

**Manned Missions:
CARGO1 Deployment / Activation**

- Nuclear Reactor on small truck, wheels 1km away from the rest of the payloads
- Nuclear Reactor Activation
- ISRU Activation
- Generation of fuel for Ascent
- Deployment of Landing Beacon

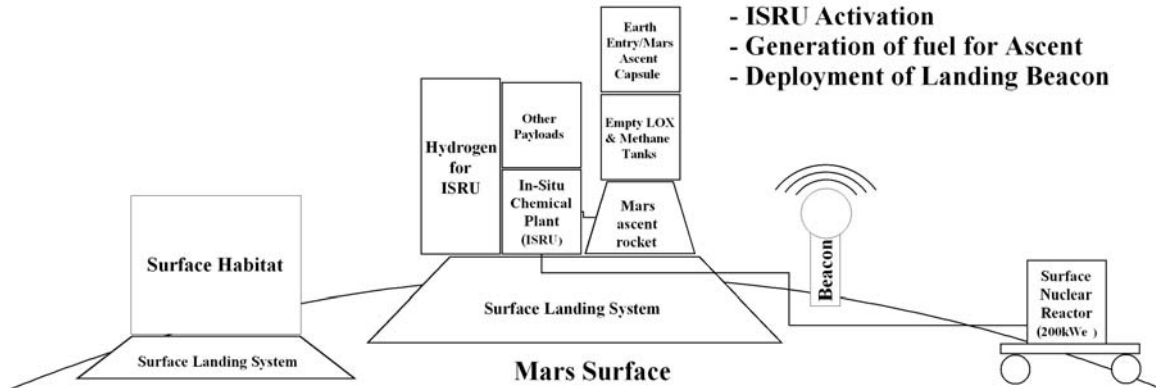
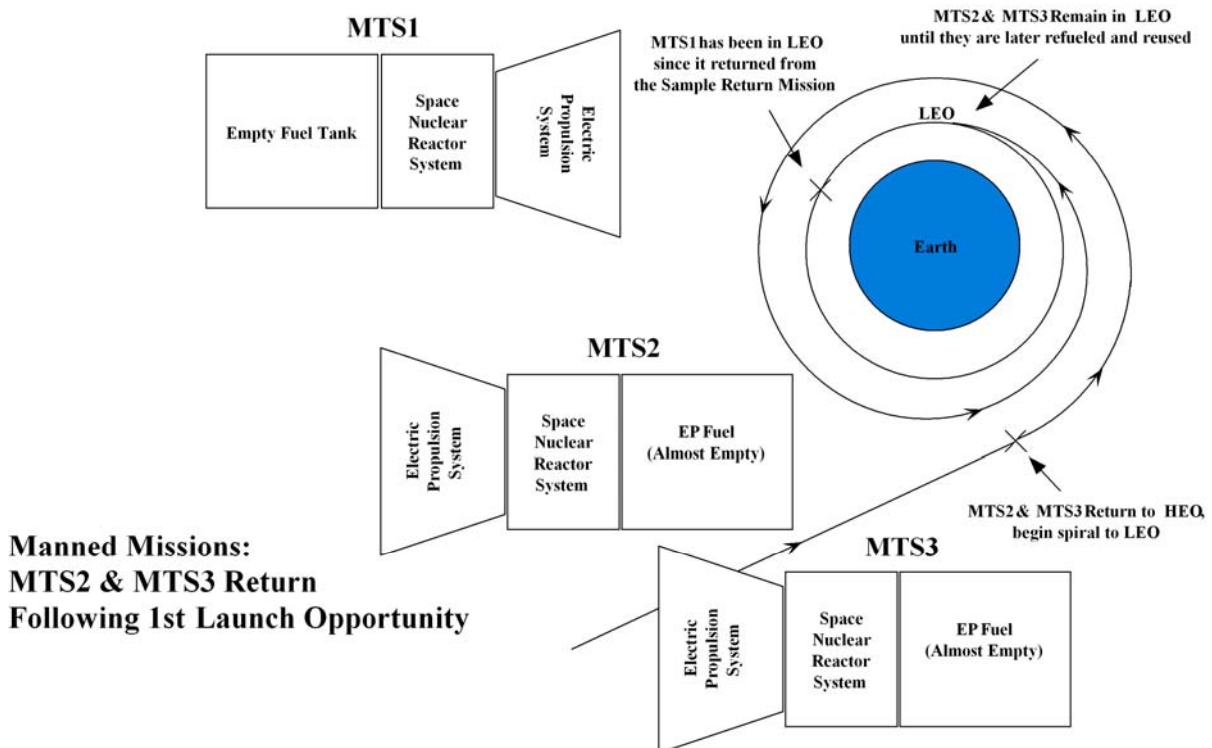


Figure 2.8.1 – 4 CARGO1 Deployment and Activation.



**Manned Missions:
MTS2 & MTS3 Return
Following 1st Launch Opportunity**

Figure 2.8.1 – 5 MTS2 and MTS3 Return Following First Launch Opportunity.

2.8.2 Manned Missions: Launch Opportunity 2

In the second launch opportunity, assuming that there is no problem with the initial set of infrastructure (CARGO1), two missions will occur. One will be the transfer of the first crew (CREW1) on a VASIMR driven fast transit (approx 90 days). The other will be the delivery of a

second set of surface infrastructure (CARGO2-A and CARGO2-B) identical to the first set of cargo. The crew will land and utilize the existing infrastructure for life support and Mars exploration.

Several months after crew arrival, CARGO2, which was on a slow efficient transfer, will land near the existing base and will serve as a backup habitat and set of infrastructure. Provided that this backup capability is not needed by CREW1, the second habitat and set of infrastructure will be prepared for the next crew (CREW2). Following 600 days of surface activities, CREW1 will board their ascent rocket and meet their VASIMR craft in Mars orbit. The VASIMR craft will propel them back to Earth.

Suggested Launch Window: 2018

Launch Opportunity Objectives:

- To launch and assemble the first of two VASIMR Transfer Craft (VTC1).
- To launch the first crew (CREW1) and have them meet the VASIMR Transfer Craft in HEO.
- To send the first crew (CREW1) to Mars.
- To refuel MTS1 (sitting in LEO).
- To launch the fourth and final Mars Transfer System (MTS4).
- To send the second set of cargo (CARGO2-A and CARGO2-B) to the Martian surface.

Earth Launch Manifest:

- Magnum Heavy launch – VASIMR Transfer Craft 1 Section 1
- Magnum Heavy launch – VASIMR Transfer Craft 1 Section 2
- Delta 4 or Atlas 5 – CREW1 in Earth Ascent / Mars Descent Capsule
- Delta 4 or Atlas 5 – Xenon Refueler Craft
- Magnum Heavy launch – MTS4 and Fuel
- Magnum Heavy launch – CARGO2-A
- Magnum Heavy launch – CARGO2-B

Payload (VASIMR Transfer Craft Sections 1 and 2):

- 3 VASIMR engines
- 3 Space Nuclear Fission Reactors (4 MWe each)
- Hydrogen fuel for engines
- Crew Transfer Habitat
- Crew consumables (air, water, food)

Payload (Earth Ascent/Mars Descent Capsule):

- CREW1
- Ablative Mars Entry Shield.
- Surface landing system (retro-rockets, landing legs).
- Docking adapter.

Payload (Xenon Refueler):

- 25 metric tons of Xenon Fuel
- Fuel Tank Connector System
- Refueler RCS and maneuvering system.

The crew transfer mission can be subdivided into six stages which are *VASIMR Transfer Craft (VTC1) Section Launches*, *VTC1 Assembly and Activation at ISS*, *CREW1 Launch and Rendezvous with VTC1*, *VTC1 Earth-Mars Transfer*, *VTC1 Mars Overshoot and Re-encounter*, and *CREW1 Landing*. These mission stages are described in detail below and are depicted in Figure 2.8.2-2.

CREW1 Transfer Mission Stages:

Stage 1 (VASIMR Transfer Craft (VTC1) Section Launches):

- (***Launch 1***) First section of VTC1 is launched via a Magnum rocket to LEO near the ISS.
- Chemical booster stage is jettisoned.
- (***Launch 2***) Second section of VTC1 is launched via a Magnum rocket to LEO near the ISS.
- Chemical booster stage is jettisoned.

Stage 2 (VTC1 Assembly and Activation at ISS):

- The two sections of VTC1 rendezvous with the ISS.
- Assembly and re-configuration of the sections take place, changing the spacecraft from its launch configuration to its interplanetary cruise configuration.
- A detailed analysis and inspection of the vehicle is done utilizing the resources and crew of the ISS. Any damage found is repaired.
- VTC1 and ISS separate. VTC1 is remotely instructed to move away from the ISS to a “safe” distance before activating the three space nuclear fission reactors and the EP system.
- VTC1 thrusts continuously for 30 days, adding energy to its orbit and taking it from LEO to HEO. The crew is not on board during this time because the craft will be traveling slowly through portions of the high radiation Van Allen belt.

Stage 3 (CREW1 Launch and Rendezvous with VTC1):

- (***Launch 3***) A Delta 4 or Atlas 5 rocket launches CREW1 to HEO in their Earth Ascent/Mars Descent Capsule.
- CREW1 in their capsule rendezvous with and transfer to VTC1 in HEO.

Stage 4 (VTC1 Earth-Mars Transfer):

- VTC1 with CREW1 aboard thrusts continuously, resulting in a 90 day Earth-Mars transfer. (See Figure 2.2.4-1 for an illustration depicting this transfer.)
- Near Mars, the crew re-boards their Earth Ascent/Mars Descent Capsule and separate from VTC1.

Stage 5 (VTC1 Mars Overshoot and Re-encounter):

- After dispatching CREW1, VTC1 adjusts its trajectory to overshoot Mars.
- VTC1 continues to thrust, changing its trajectory such that it re-encounters Mars several months later.
- Once VTC1 re-encounters Mars, it will capture into a High Mars Orbit where it will remain until the crew is ready to return.

Stage 6 (CREW1 Landing):

- CREW1 in their Earth Ascent/Mars Descent Capsule aero-break to shed their excess velocity. They make use of the landing assist beacon to land very close to the existing infrastructure.

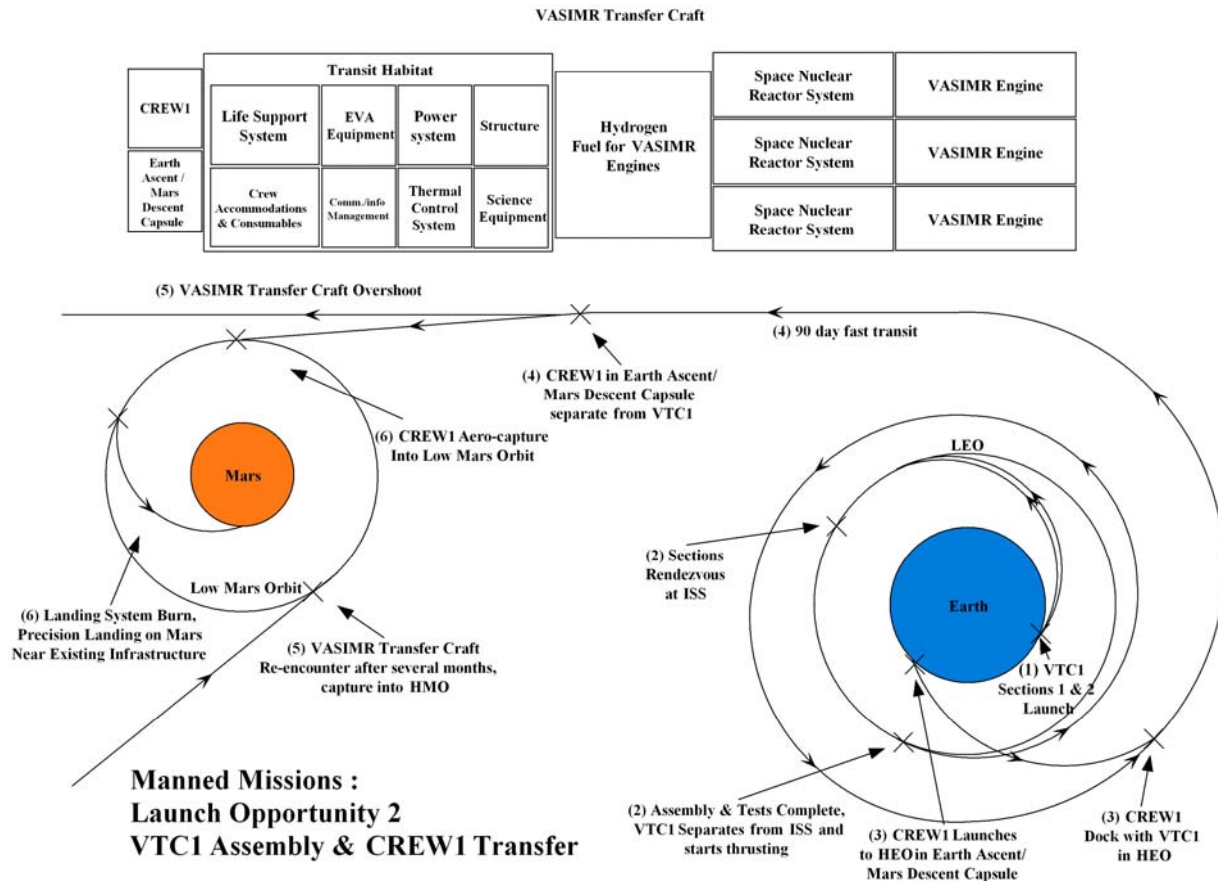


Figure 2.8.2 – 2 CREW1 Transfer.

The cargo transfer mission can be subdivided into ten stages which are *Xenon Refueler Launch and Refueling of MTS1, MTS4 Launch to Low Earth Orbit, CARGO2-A & CARGO2-B Launches, MTS4 & MTS1 Activation, CARGO2-A & MTS1 Docking, CARGO2-B & MTS4 Docking, Earth-Mars Transfers of CARGO2-A and CARGO2-B, Aero Breaking & Landings, CARGO2 Activation & Operations, and MTS1 & MTS4 Return*. These mission stages are described in detail below.

Cargo Transfer Mission Stages:

Stage 1 (Xenon Refueler Launch and Refueling of MTS1):

- **(Launch 4)** Xenon Refueler Craft is launched via a Delta 4 or Atlas 5 rocket to LEO.
- Chemical booster stage is jettisoned.
- Empty Xenon tank is jettisoned from MTS1.
- Xenon Refueler Craft rendezvous with MTS1.
- Xenon Refueler RCS jettisoned.
- This process is depicted in Figure 2.8.2-3 below.

Stage 2 (MTS4 Launch to Low Earth Orbit):

- **(Launch 5)** Mars Transfer System (MTS4) and Xenon fuel is launched via a Magnum rocket to LEO.
- Chemical booster stage is jettisoned.

Stage 3 (CARGO2-A and CARGO2-B Launches):

- (**Launch 6**) CARGO2-A is launched via a Magnum rocket to LEO.
- Chemical booster stage is jettisoned.
- (**Launch 7**) CARGO2-B is launched via a Magnum rocket to LEO.
- Chemical booster stage is jettisoned.

Stage 4 (MTS4 and MTS1 Activation):

- Electric Propulsion (EP) system is deployed.
- Thermal Radiator system is deployed.
- Space Nuclear Fission Reactor is activated.
- EP system is activated.
- MTS1 EP system is re-activated.

Stage 5 (CARGO2-A and MTS1 Docking):

- MTS1 rendezvous with CARGO2-A
- Automated docking performed between MTS1 and CARGO2-A.

Stage 6 (CARGO2-B and MTS4 Docking):

- MTS4 rendezvous with CARGO2-B
- Automated docking performed between MTS4 and CARGO2-B.

Stage 7 (Earth-Mars Transfers of CARGO2-A and CARGO2-B):

- The transfer systems propel their respective payloads partway to Mars.
- At a certain point, the MTSs and payloads separate.
- MTS1 and MTS4 continue to fire as necessary to put them on return trajectories to Earth.

Stage 8 (Aero Breaking and Landings):

- CARGO2-A and CARGO2-B aerocapture/aerobreak in the Martian atmosphere.
- Landing rockets slow their descent further. The landing assist beacon is used to land the payloads very close to the existing infrastructure and CREW1.

Stage 9 (CARGO2 Activation and Operations):

- Surface mobility systems are used by CREW1 to relocate the CARGO2 payloads to desired locations.
- The second reactor on its mobile platform positions itself near the existing reactor.
- Thermal Radiators are deployed.
- Surface Nuclear Fission Reactor 2 is brought online, powering ISRU2.
- ISRU2 plant is activated and begins producing methane and oxygen to fuel the second ascent capsule. This ascent capsule will serve as a backup for the first crew, should the first ascent capsule fail. The ISRU also begins generating oxygen and water for life support systems.
- Second Landing assist beacon is deployed and activated (serves as a backup).
- Systems are controlled and monitored from Earth and by CREW1 onsite.
- The layout of infrastructure on the surface of Mars at this time is depicted in Figure 2.8.2-4

Stage 10 (MTS1 and MTS4 Return):

- MTS1 & MTS4 return and capture into a high Earth orbit via their return trajectories. They then continue to thrust, reducing the energy of their orbits until they have reached LEO and expended all of their fuel. Here they remain until they are refueled and reused.

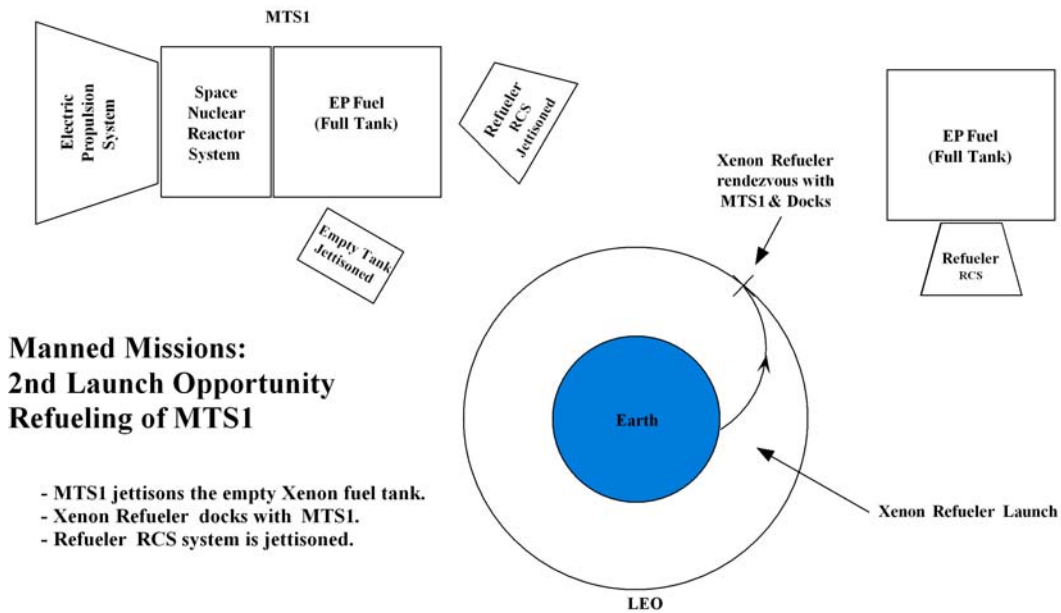


Figure 2.8.2 – 3 Refueling of MTS1.

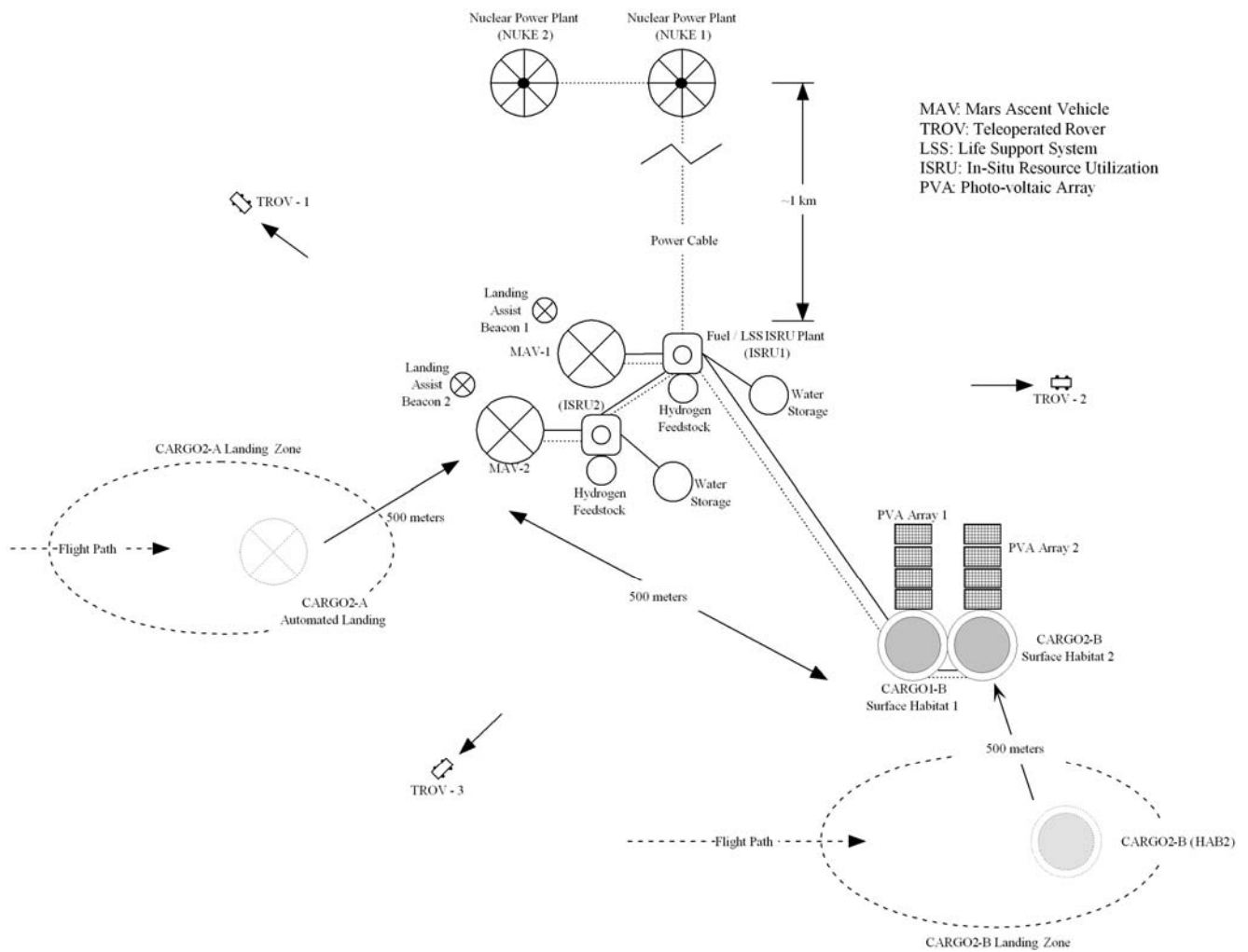


Figure 2.8.2 – 4 (Landing Site Layout for First Manned Mission)

2.8.3 Manned Missions: Crew 1 Return and Launch Opportunity 3

CREW1 Return

After conducting surface operations for 600 days or more, CREW1 will climb into the Earth Entry/Mars Ascent capsule. The crew in their capsule will launch and meet the VASIMR Transfer Craft (VTC1) in high Mars orbit. All of the fuel needed for this ascent has been generated on the surface of Mars. This “living off the land” approach represents a major enabling capability for Mars exploration, reducing the initial mass launched from Earth.

Once the crew has docked with VTC1, the VASIMR engines will begin to thrust placing the crew on a fast transit trajectory return to Earth (approximately 90 days). Near Earth, CREW1 will re-board their Earth Entry/Mars Ascent capsule and separate from the VASIMR Transfer Craft. The crew will shed their excess velocity by making use of an ablative heat shield, then will parachute and/or splash down to Earth. Meanwhile, VTC1 will overshoot Earth and re-encounter it several months later so that it can be reused in the next opportunity.

Launch Opportunity 3

In this third launch opportunity, two additional missions will occur. One will be the transfer of the second crew (CREW2) on a second VASIMR Transfer Craft. The other will be the delivery of the third set of surface infrastructure (CARGO3-A and CARGO3-B) identical to the first and second sets of cargo. The crew will land and utilize the existing infrastructure for life support and Mars exploration.

Similar to CARGO2, several months after crew arrival, CARGO3 will land near the existing base. It will serve as a backup habitat and set of infrastructure for CREW2 and the primary for CREW3. Following 600 days of surface activities, CREW2 will board their ascent rocket and meet their VASIMR craft in Mars orbit. The VASIMR craft will propel them back to Earth.



Conceptual View of Mars Ascent [1]



Conceptual View of CREW1 Earth Return [1]

Suggested Launch Window: 2020

Launch Opportunity Objectives:

- To return CREW1 to Earth.
- To launch and assemble the second of two VASIMR Transfer Craft (VTC2).
- To launch the second crew (CREW2) and have them meet the VASIMR Transfer Craft in HEO.
- To send the second crew (CREW2) to Mars.
- To refuel MTS2 and MTS3 (sitting in LEO).
- To send the third set of cargo (CARGO3-A & CARGO3-B) to the Martian surface.

Earth Launch Manifest:

- Magnum Heavy launch – VASIMR Transfer Craft 2 Section 1
- Magnum Heavy launch – VASIMR Transfer Craft 2 Section 2
- Delta 4 or Atlas 5 – CREW2 in Earth Ascent / Mars Descent Capsule
- Delta 4 or Atlas 5 – Xenon Refueler Craft
- Delta 4 or Atlas 5 – Xenon Refueler Craft
- Magnum Heavy launch – CARGO3-A
- Magnum Heavy launch – CARGO3-B

The flow of the three missions (CREW1 Return, CREW2 transfer & CARGO3 transfer) taking place this launch opportunity is illustrated in Figure 2.8.3-1 below.

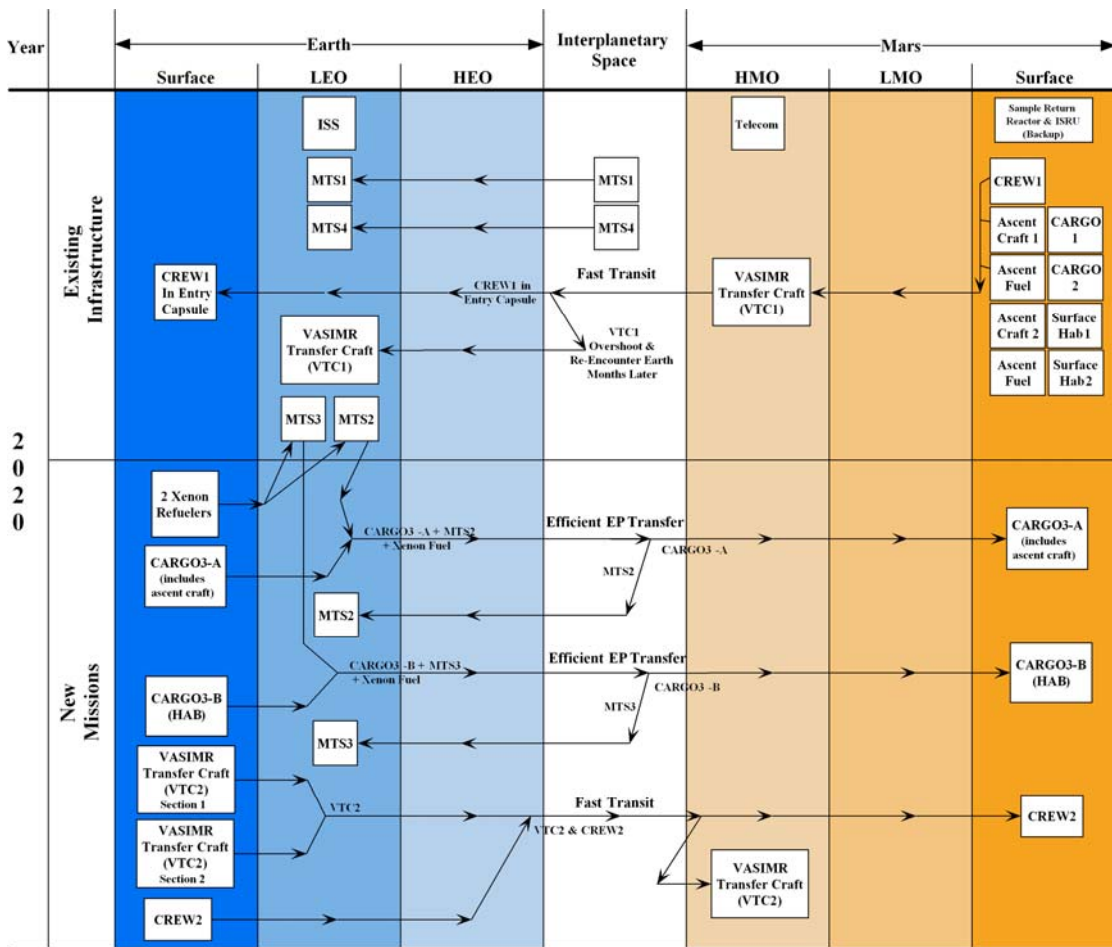


Figure 2.8.3 – 1 Flow of CREW1 Return and Launch Opportunity 3 Missions.

The CREW1 Return mission can be subdivided into five stages which are *CREW1 Mars Ascent*, *VTC1 Rendezvous*, *Mars-Earth Transfer*, *VTC1 Earth Overshoot and Re-encounter*, *CREW1 Earth Landing*. These mission stages are described in detail below and depicted in Figure 2.8.3-2.

CREW1 RETURN Mission Stages:

Stage 1 (CREW1 Mars Ascent):

- CREW1 boards Earth Entry/Mars Ascent Capsule.
- Capsule launches to HEO.

Stage 2 (VTC1 Rendezvous):

- Earth Entry/Mars Ascent Capsule with CREW1 docks with VTC1 in HEO.

Stage 3 (Mars-Earth Transfer):

- VTC1 with CREW1 aboard thrusts continuously, resulting in a 90 day Mars-Earth transfer.

Stage 4 (VTC1 Earth Overshoot and Re-encounter):

- Near Earth, the crew re-boards their Earth Entry/ Mars Ascent Capsule and separate from VTC1.
- After dispatching CREW1, VTC1 adjusts its trajectory to overshoot Earth.
- VTC1 continues to thrust, changing its trajectory such that it re-encounters Earth several months later.
- One it re-encounters Earth, it will continue to thrust, spiraling down to LEO where it can be refueled and re-used in the next launch opportunity.

Stage 5 (CREW1 Earth Landing):

- Earth Entry/Mars Ascent Capsule sheds excess velocity through use of ablative heat shield.
- Capsule parachutes and/or splashes down.

The CREW2 transfer mission can be subdivided into 6 stages which are *VASIMR Transfer Craft (VTC1) Section Launches*, *VTC1 Assembly and Activation at ISS*, *CREW1 Launch and Rendezvous with VTC1*, *VTC1 Earth-Mars Transfer*, *VTC1 Mars Overshoot and Re-encounter*, and *CREW1 Landing*. These mission stages are identical to those for the 2018 transfer of CREW1, which is described in Section 2.8.2 and depicted in Figure 2.8.2-2.

The cargo transfer mission can be subdivided into 10 stages which are *Xenon Refueler Launches and Refueling of MTS2 & MTS3*, *CARGO3-A & CARGO3-B Launches*, *MTS2 & MTS3 Activation*, *CARGO3-A & MTS2 Docking*, *CARGO3-B & MTS3 Docking*, *Earth-Mars Transfers of CARGO3-A and CARGO3-B*, *Aero Breaking & Landings*, *CARGO3 Activation & Operations*, and *MTS2 & MTS3 Return*. These mission stages are virtually identical to those for the 2018 transfer of CARGO2-A and CARGO2-B, which is described in Section 2.8.2.

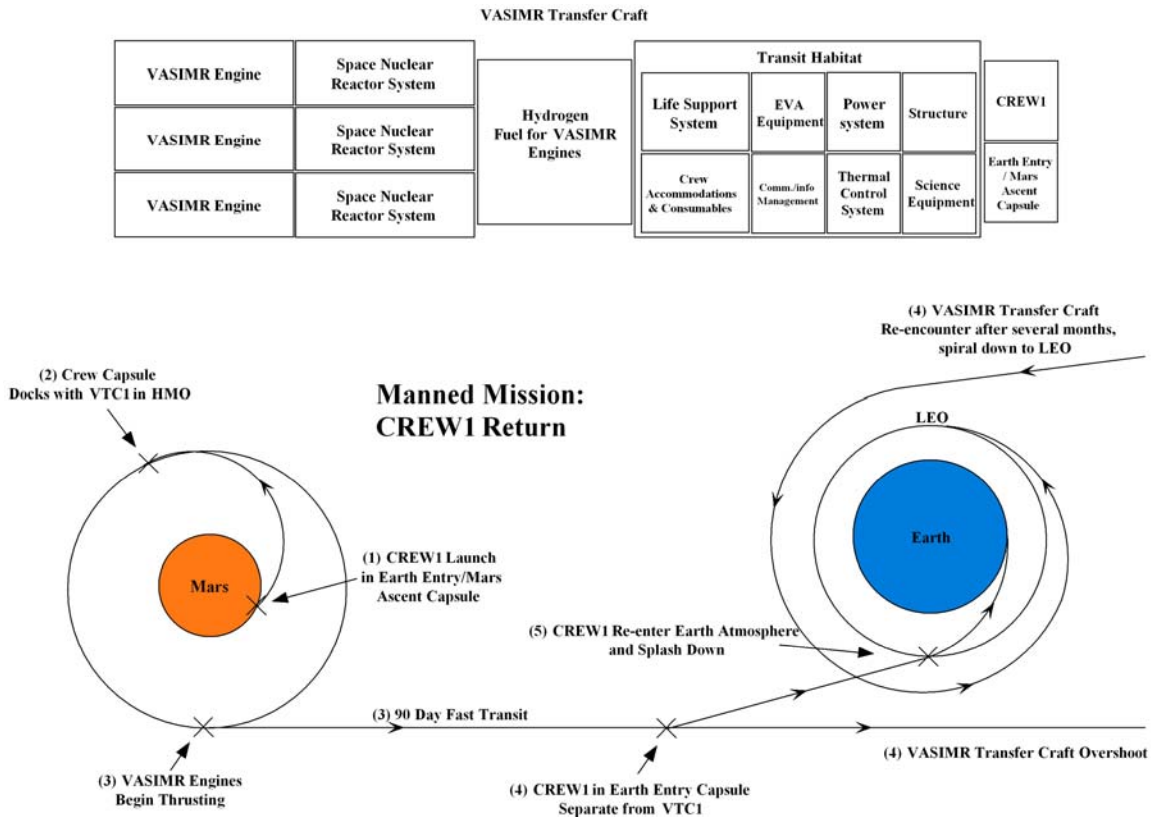


Figure 2.8.3 – 2 Flow of CREW1 Return.

2.8.4 Manned Missions: Crew 2 Return & Launch Opportunity 4

CREW2 Return

CREW2 will return after 600 days on the surface. Their return trip is identical to the return of CREW1, only using the second VASIMR Transfer Craft (VTC2).

Launch Opportunity 4

In this fourth launch opportunity, only one new mission is required to continue Mars exploration. This mission is the transfer of the third crew (CREW3) on the refueled VASIMR Transfer Craft (VTC1). The crew will land and utilize the existing infrastructure for life support and Mars exploration. Following 600 days of surface activities, CREW3 will board their ascent rocket and meet their VASIMR craft in Mars orbit. The VASIMR craft will propel them back to Earth.

If it is desirable, additional cargo and infrastructure can be sent to Mars as well in this opportunity, but it is not required in order to accomplish the initially defined goal of sending three manned missions to Mars. Up to two cargo missions may be optionally launched in this opportunity, making use of the existing two Mars Transfer Systems parked in LEO. These cargo missions would be similar in structure to those launched in previous launch opportunities.

Suggested Launch Window: 2022

Launch Opportunity Objectives:

- To return CREW2 to Earth.
- To refuel the VASIMR Transfer Craft (VTC1) in LEO.
- To launch the third crew (CREW3) and have them meet the VASIMR Transfer Craft in HEO.
- To send the third crew (CREW3) to Mars.

Earth Launch Manifest:

- Delta 4 or Atlas 5 – Hydrogen VASIMR Refueler Craft
- Delta 4 or Atlas 5 – CREW3 in Earth Ascent / Mars Descent Capsule

- Optional Launch Opportunity Objectives:

- To refuel MTS1 and MTS4 (sitting in LEO).
- To send a fourth set of cargo (CARGO4-A & CARGO4-B) to the Martian surface.

- Optional Earth Launch Manifest:

- Delta 4 or Atlas 5 – Xenon Refueler Craft
- Delta 4 or Atlas 5 – Xenon Refueler Craft
- Magnum Heavy launch – CARGO3-A
- Magnum Heavy launch – CARGO3-B

The flow of the missions taking place this opportunity is illustrated in Figure 2.8.4-1 below.

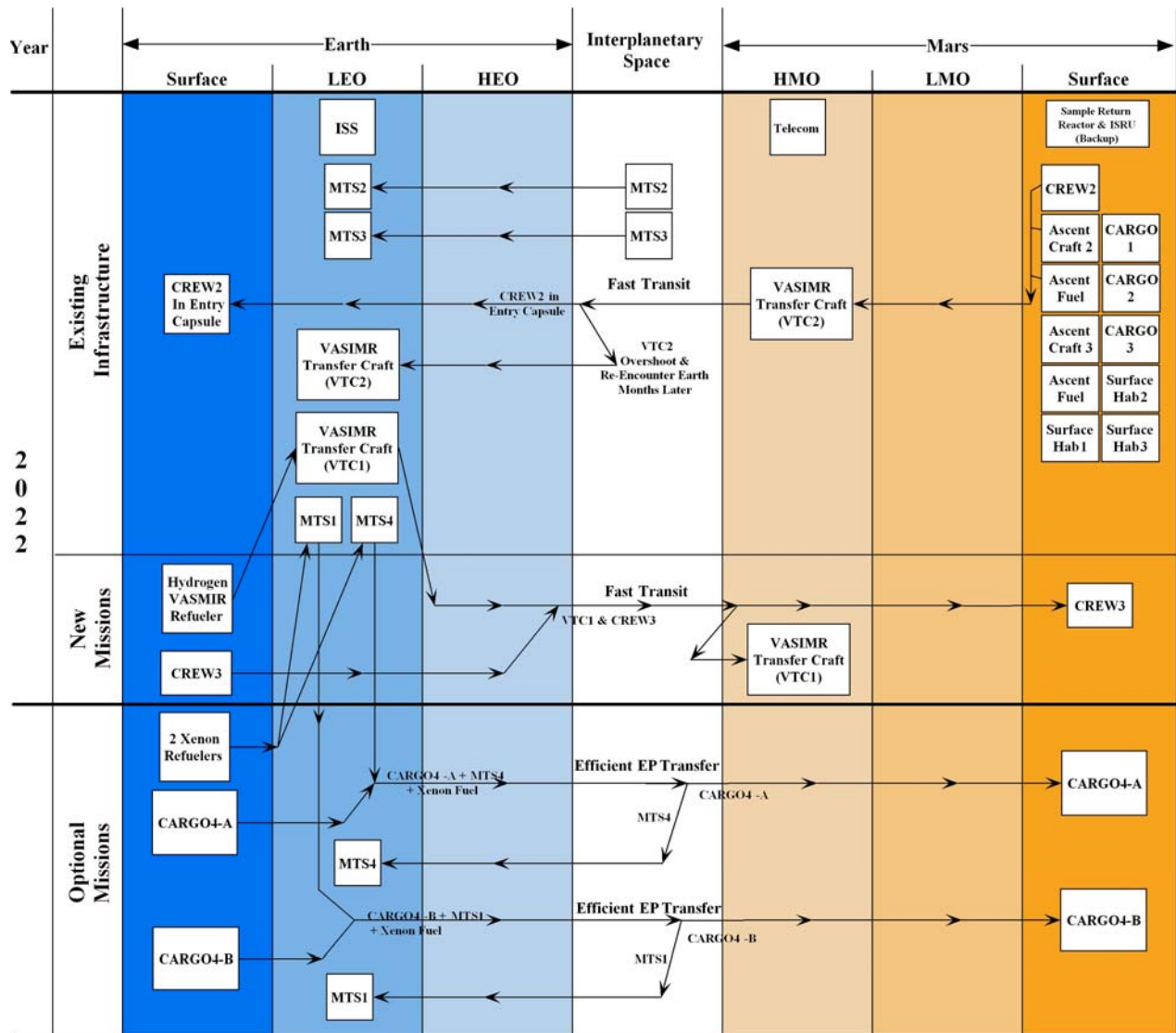


Figure 2.8.4 – 1 Flow of CREW2 Return and Launch Opportunity 4 Missions.

2.9 PROSPECTIVE ON CONTINUED EXPLORATION AND CONCLUSION

Prospective on Continued Exploration

Following the return of CREW3 in 2024, three complete manned Mars expeditions will have been completed. A wealth of science data, pictures, and samples will have been returned from the surface. It is at this point that NASA, the general public, and Congress must make the decision to continue manned Mars exploration. Unfortunate as it would be, cancellation even of a completely successful Mars program is not outside the realm of possibility, just as a completely successful Moon exploration program was canceled after six landings. Hopefully a good case can be made to continue the program.

If the decision were made to continue manned Mars exploration, NASA would be extremely well prepared to do so because of the large amount of infrastructure they will have established. Four

Mars Transfer Systems capable of sending large payload masses to Mars would be in low earth orbit ready to be refueled and reused. Two VASIMR Transfer Craft capable of transferring crews to and from Mars would also be in low earth orbit ready to be refueled and reused. Mars surface infrastructure consisting of three 200kWe nuclear fission reactors, three ISRU chemical plants, and three surface habitats would be in place, as well as a number of surface rovers and a large quantity of scientific instruments.

Should funding for this program be severely reduced at some point after 2022, in fact, the manned exploration of Mars can continue. Significant cost savings can be afforded by increasing the self-sufficiency of the surface base as much as possible so as to eliminate otherwise required cargo flights. Indigenous sources of hydrogen feedstock, building materials derived from the Martian regolith and food grown in greenhouses on the surface of Mars all will increase this self-sufficiency.

2.10 CONCLUSION

Throughout the course of this Mars exploration mission plan, each successive mission has added redundancy on the surface and increased the overall mission success rate. Reusable, nuclear fission powered Mars Transfer Systems and VASIMR Transfer Craft have reduced the number and mass of launches required from Earth. ISRU technology has been utilized where it can make the most impact, which is in producing fuel and oxidizer for launching mass from the surface of Mars to high Mars orbit.

With this mission plan fully outlined, the required capabilities of both space and surface nuclear fission reactor systems become clearer. It is these systems, described in detail in the sections which follow, that can truly enable manned Mars exploration in the near future.

2.11 REFERENCES FOR CHAPTER 2, MISSION PLAN SECTION

[1] The Reference Mission of the NASA Mars Exploration Study Team, Editors Stephen J. Hoffman, David L. Kaplan, NASA, Lyndon B. Johnson Space Center, Houston, TX, July 1997.

[2] Reference Mission Version 3.0 Addendum to the Human Exploration of Mars, The Reference Mission of the NASA Mars Exploration Study Team, Offices of Exploration & Advanced Development, NASA, Lyndon B. Johnson Space Center, Houston, TX, June 1998.

[3] Zubrin, Robert and Richard Wagner, *The Case for Mars*, The Free Press, New York, 1996. ISBN 0-684-82757-3.

[4] DAWN Mission Website, <<http://www-ssc.igpp.ucla.edu/dawn/>>, September 12, 2002.

[5] Hines, Gerald D., *The First Mars Outpost: Planning & Concepts*, Sasakawa International Center for Space Architecture, College of Architecture, University of Houston, 2001-2002

3.0 DECISION METHODOLOGY

3.1 OVERVIEW

From the start of this project, it was clear that a formal decision making process would be beneficial in the down selection of technologies used in the mission to Mars. A methodology was defined and implemented to at least some extent throughout the project. Many of the decision problems encountered required down-selection of technologies with competing objectives. It is in these decision problems that the full rigors of the process were of greatest benefit.

Initially, a single one set of objectives were defined for the entire project. While our initial belief was that one set of objectives would be sufficient for the entire project, it was clear that each part of the mission was unique despite the dependencies on other portions of the project. Therefore, each decision problem was handled independently while keeping the larger picture in mind. Furthermore, objectives for the specific decision problems did consider the impacts on the other parts of the mission. An example is the desire to keep the mass of the surface reactor as small as practical as it would have a direct impact on the initial launch and transport from Earth.

The initial goals were to keep costs low, ensure the crew survived, and the crew made it to Mars and back. However, these goals, while all important, were not necessarily equal. While keeping the costs low was important, ensuring the crew survives the mission is paramount (otherwise the mission would not likely occur). These preferences are indicated by the weights placed on the objectives (as will be demonstrated later in the case study).

Other goals were identified as well. Initially it was thought that as long as the crew survives the trip, everyone would be happy. However further discussion lead to the realization that if the trip to Mars took much longer than a few months, it would be difficult to find anyone willing to take the trip. Reducing the time of the trip required a faster rocket which meant better technology and more money. Thus trade-offs developed.

3.2 FOUR-STEP METHODOLOGY

To systematically analyze decision problems, a four-step methodology is employed. An overview of the methodology is presented in Figure 3.2-1.

In the first step, all plausible decision options are identified regardless of the feelings of individuals involved in the decision making process. By identifying every conceivable decision option, subjectivity is initially removed from the decision making process. It prevents less than favorable options from being repeatedly analyzed when people ask why it was not considered. By including it initially, it can be screened out in the second step thus documenting that it was initially considered.

This is not to say that ridiculous options should be included for the sake of generating options. The important part is that decision options that are expected to be unacceptable because they do not fulfill a goal should be included in the initial list so they can be removed by a formal process in the second step.

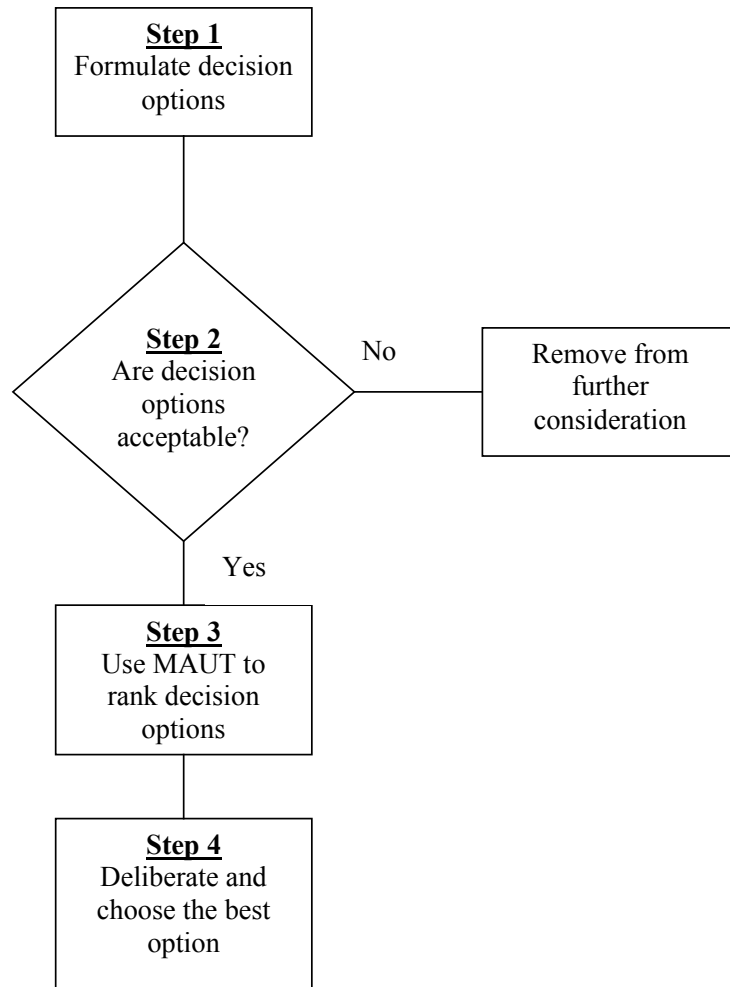


Figure 3.2 – 1 Methodology Flowchart.

The second step removes “unacceptable” decision options. The definition of an unacceptable decision option is left up to the decision maker but should be consistent as it is applied to all decision options. Care must be taken when removing decision options in this step. The removal of decision options is intended to make the process more realistic and reduce the burden of analyzing possible decisions that are clearly unacceptable. The decision options are removed based on external criteria that they violate. The criteria may include physical, sociological, political, economic, and other reasons. The end result is that the decision option and the criteria that eliminated it from further consideration are documented. This helps to ensure time is not wasted reconsidering decision options that were already screened.

In the third step, the Multi-Attribute Utility Theory (MAUT) is applied to the remaining decision options [1]. MAUT establishes formal rules for the rank-ordering of decision options. This ensures that the decision-making process stays consistent despite the number and complexity of the decision option. It also helps the decision maker characterize the relevant uncertainties which might otherwise be lost. MAUT assigns a performance index to each decision options.

The performance index is a relative weight that can be compared to the indices assigned to the other decision options. This facilitates a better understanding as to how much one decision option is better (or worse) than another.

The fourth step of the methodology is the actual deliberation between all involved parties. This step ensures that any shortcomings of the methodology are addressed and the best decision is chosen. While the performance index is a valuable tool in the identification of the most desirable option, it should still be scrutinized. This is especially the case if two decision options have similar indices but are physically different.

It is expected during deliberations that the criteria in Steps 2 and 3 will be questioned and modified. This is expected and encouraged. The methodology presented is meant to be a dynamic, iterative process. The number of iterations is limited only by the amount of time the decision maker wishes to spend on the problem. Even if only a single iteration is performed, it is expected that the results will be more consistent than if the methodology had been skipped. However, the methodology benefits from the continual refinement and therefore multiple iterations are encouraged.

3.3 APPLICATION OF MAUT

Before a Performance Index (PI) can be assigned to a decision option, the MAUT framework must be setup. The framework consists of defining the mission, objectives, performance measures, weights, utilities, and the analysis. The mission is a single statement about the overall goal of the project. In the case of this project, the overall mission of the project is “Safe, Reliable, and Cost Effective Mission to Mars.” For each decision problem, a specific mission was defined which reflects the overall mission.

Objectives are defined which, if fulfilled, meet the mission for the given decision problem. In many cases, the same objectives apply to all of the decision problems encountered. These typically include those involved with cost and safety.

The objectives are defined in a value tree. The main objectives are known as the fundamental objectives [4]. Fundamental objectives are things people really care about. Means objectives are defined in the analysis and are those things that people care about to achieve the fundamental objectives [5]. An example is time. Time is defined as a means objective as people care about time as it directly affects the crew, mission costs, and reliability. Fundamental objectives can be broken down into more specific objectives if need be.

Once the objectives are broken down enough to adequately describe the objectives directly above them, performance measures are defined. Performance measures serve to measure the level to which the objectives above them are fulfilled. The performance measures can take either a qualitative or quantitative input. In either case, they are divided into scales with each level of the scale being assigned a utility value.

The utility values used in this project are all linear. They consist of a range of values from zero to unity. A utility value of zero represents the least desirable outcome (the objective is not

fulfilled) where as a utility value of one is considered the most desirable outcome (the objective is completely fulfilled). Ideally, the utility functions are not linear but curved to indicate the risk attitude of the decision maker.

For the quantitative performance measures, subjective descriptions are used. They can range from the least desirable condition to the most desirable. A typical set of these descriptions could include Very Bad, Bad, Ok, Good, and Very Good. Table 3.3-1 provides a typical scale used with a qualitative utility function.

For the qualitative performance measures, a lower and upper bound must be defined. The bounds should represent the limit for all possible decision options regardless of the probability of a decision option reaching the limit.

Analytic Hierarchy Process (AHP) is one method to generate non-linear utility functions thus allowing the risk attitude of the decision maker to be quantified [7,8]. However, it was not used in this project for the generation of utility functions.

It should also be mentioned that the utility functions can be curve fitted to allow for values that are between two steps in the scale. However, if one utility function is curve fitted, all utility functions should be curve fitted (as practical). Otherwise, the use of discrete utility values to describe a range of values is acceptable.

Since people generally have preferences of one objective over another, weights must be assigned. An example is cost and safety. Safety is typically more important than cost. Therefore, a larger weight is applied to safety than cost.

To generate the weights on the objectives, an AHP exercise was setup for the project participants [7]. They were asked to make subjective judgments about their feelings of the objectives. The objectives used were generic but were applicable to the variety of decision problems encountered. The AHP exercise consists of a matrix with the row and column headings representing the objectives being compared. At the intersection of a row and column, an integer is inserted which represents the decision makers feeling about one objective over another. The integers are defined in Table 3.3-2.

Table 3.3 – 1 Constructed Scale

| Scale | Range |
|-------|-----------|
| 1 | Very Good |
| 2 | Good |
| 3 | Weak |
| 4 | Bad |
| 5 | Very bad |

Table 3.3 – 2 AHP Statements of Importance

| Scale | Statement of Importance |
|-------|--|
| 1 | A is Equally Important as B |
| 3 | A is Moderately More Important than B |
| 5 | A is Strongly More Important than B |
| 7 | A is Very Strongly More Important than B |
| 9 | A is Extremely More Important than B |

With the weights applied to the performance measures, the connection between the decision options and the PMs can be made. The process used to make the connections will be described later in this report.

Once the weights have been assigned, the expected performance index for each option can be computed. Below is the equation used for MAUT [2,3].

$$\bar{PI}_j = \sum_{i=1}^{N_{PM}} w_i \bar{u}_{ij}$$

where

\bar{PI}_j expected value of the Performance Index for the j^{th} decision option

w_i weight assigned to the i^{th} PM

u_{ij} expected disutility of the i^{th} PM with respect to the j^{th} decision option

This equation is applied to each decision option and the indices are compared. The results can be presented in tabular and/or graphical format.

3.4 CASE STUDY ON SURFACE REACTOR

To demonstrate the usefulness of the technology, the decision problem involved in choosing the best nuclear reactor for operation on the surface of Mars is presented. The reactor had five parameters that had to be decided upon. Each of the parameters had a number of possible options. The parameters and options are provided in Table 3.4-1.

The first step of the methodology requires that all possible options are formulated. This results in 196 possible combinations (every option combined with every other option).

Table 3.4 – 1 Decision Matrix

| Neutron Spectrum | Coolant | Fuel | Matrix | Geometry |
|------------------|-----------------|-----------------|------------------|----------|
| Thermal | CO ₂ | UO ₂ | BeO | Pin |
| Epithermal | LBE | UC | SiC | Block |
| Fast | | US | ZrO ₂ | |
| | | UN | MgO | |

Step 2 defines the criteria used to screen those options that are not acceptable. In this case study, the criteria are based upon the physical incompatibilities of the reactor parameters. Incompatible combinations of reactor components are listed in Table 3.4-2. These incompatible combinations are the expert opinion of members of our team. Some of the incompatibilities are due to competing phenomena (Fast Spectrum reactor with BeO matrix material) whereas other incompatibilities are due to concerns over the safety and reliability of the reactor (such as the chemical incompatibilities between CO₂ coolant and certain fuel materials).

Table 3.4 – 2 Incompatible Combinations

| |
|--|
| Fast Spectrum – BeO Matrix |
| Fast Spectrum – UO ₂ Fuel |
| Fast Spectrum – UN Fuel |
| Fast Spectrum - MgO Matrix |
| Epithermal Spectrum – MgO Matrix |
| Thermal Spectrum – ZrO ₂ Matrix |
| Thermal Spectrum – SiC Matrix |
| Thermal Spectrum – MgO Matrix |
| Thermal Spectrum – Pin Geometry |
| CO ₂ Coolant – UC Fuel |
| CO ₂ Coolant – UN Fuel |

As a result, many combinations are removed from further consideration. From the remaining decision options, only four are carried forward to Step 3. Ideally, all decisions not eliminated in Step 2 are subjected to Step 3. However, only the four listed in Table 3.4-3 are considered in this paper. The four represent the expert opinion of our team as to which combinations result in the best options.

Table 3.4 – 3 Options Considered for Further Consideration

| Neutron Spectrum | Coolant | Fuel | Matrix | Geometry |
|------------------|---------|------|--------|----------|
| Epithermal | CO2 | UO2 | BeO | Block |
| Fast | CO2 | US | SiC | Block |
| Fast | LBE | UC | SiC | Pin |
| Thermal | CO2 | UO2 | BeO | Block |

To apply Multi-Attribute Utility Theory, both fundamental and means objectives are identified. First, the goals associated with successful operation of the surface reactor are identified. These goals are listed in Table 3.4-4.

Table 3.4 – 4 Goals for Surface Reactor

| |
|---|
| 25 years operation Low Mass Slow Reactivity and Thermal Transients Low Reactivity Swing Chemically Inert in CO2 |
|---|

With the goals identified, objectives are identified. The objectives are listed in Table 3.4-5. While goals and objectives are similar, objectives have a broader definition.

Table 3.4 – 5 Objectives for the Surface Reactor

| |
|---|
| Long-Term Operation Lightweight Reactor Package Remote Controlled Operation Simple Reactivity Control Compatible with Environment |
|---|

The objectives are organized in a value tree shown in Figure 3.4-1. The value tree is a hierarchal representation of the objectives associated with the surface reactor. The value tree starts with the overall objective (mission) and descends down to the performance measures. The decision options are connected to the value tree through the analysis.

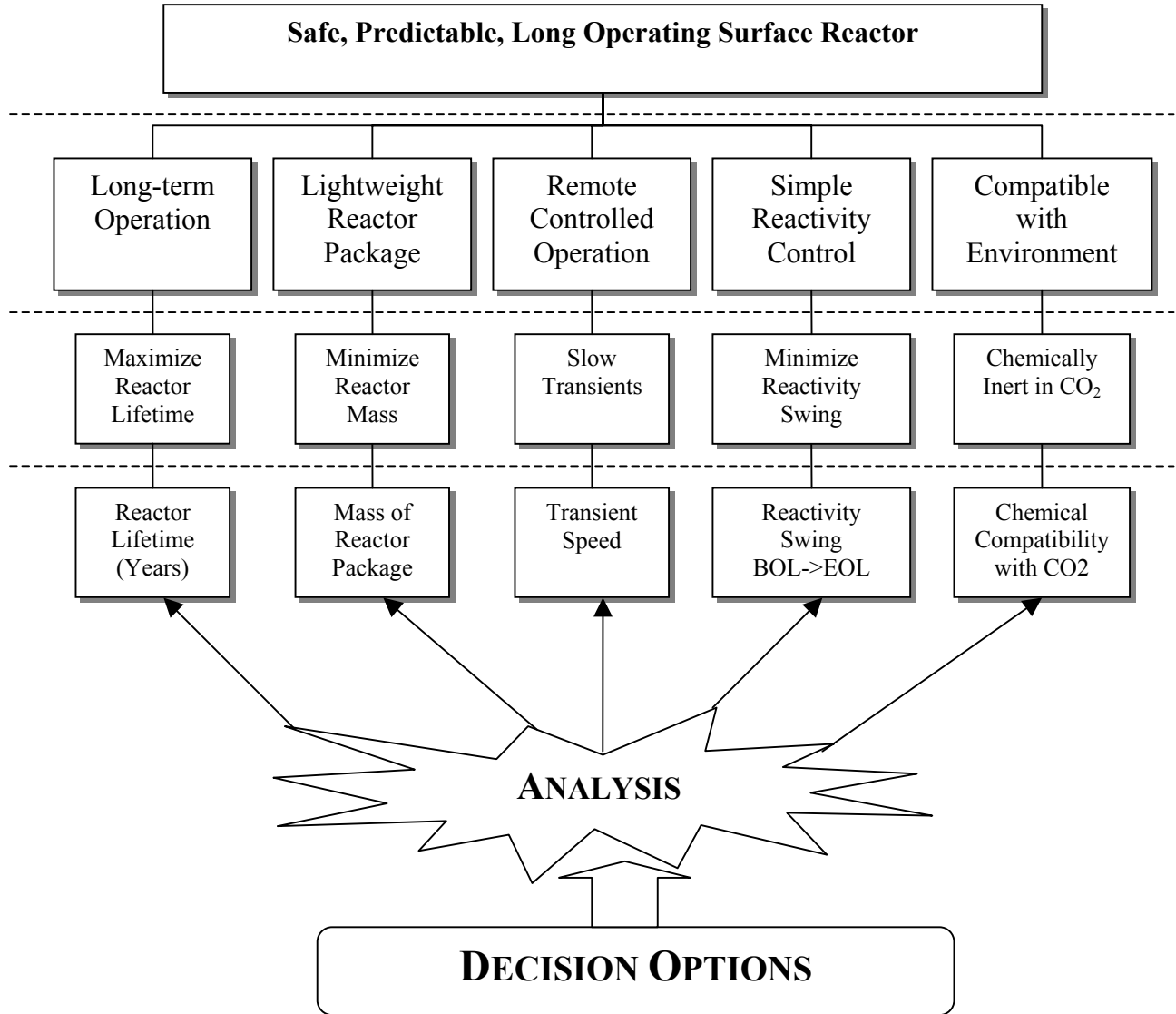


Figure 3.4 – 1 Surface Reactor Value Tree

The analysis contains the “means” objectives, which typically influence more than one fundamental objective [5]. The analysis may also contain decision trees, event trees, and fault trees to systematically bridge the decision options to the performance measures. A typical event tree might contain a number of branches representing the results of different types of accidents along with the associated frequencies. This is especially useful when analyzing design trade-offs (such as the number of safety systems for example).

To simplify the performance measures, scales are built. Table 3.4-6 shows the scales used to quantify the performance measures in the value tree. In the case of quantitative performance

Table 3.4 – 6 Performance Measures Scales

| Reactor Lifetime (years) | Mass | Transients | Reactivity Swing | Chemically Inert in CO ₂ |
|--------------------------|------------------------------------|------------|------------------|-------------------------------------|
| 0 – 5 | Very Low | Very Slow | Very Small | Very Bad |
| 6 – 10 | Low | Slow | Small | Bad |
| 11 – 15 | Somewhat Low | Medium | Medium | OK |
| 16 – 20 | Moderate | Fast | Large | Good |
| 20 – 25 | Somewhat High High Very High | Very Fast | Very Large | Very Good |

measures, it is possible to normalize the entire range of possible inputs from zero to one thus producing a continuous utility function. However, in the case of qualitative performance measures, it is not possible to produce a continuous curve from the discrete points as there are only a finite number of qualitative descriptions. Therefore, the utility function is broken into discrete steps representing the qualitative descriptions. A discrete utility value is assigned to each step.

To stay consistent with the qualitative utility functions, a scale is used to assess the quantitative utility functions as well. The quantitative inputs are broken into discrete ranges of values, which represent the steps. A utility value is assigned to each step.

For the sake of simplicity, linear utility functions are used. Ideally, utility functions which capture the risk attitude of the decision maker are used. A utility of zero is assigned to the least desirable scale step. A utility of unity is assigned to the most desirable scale step. The remaining utility values divided equally and assigned to the intermediate scale steps.

The next step is to assign weights on the performance measures. The weights represent the preference the decision maker has for one objective over another. AHP is used to assist the decision maker in producing the weights. The AHP hierarchy used to calculate the weights for this case study are presented in Table 3.4-7. The values inserted into the cells were the expert opinion of one team member. Table 3.4-8 defines the definitions for the rows and columns in the AHP hierarchy [7].

Table 3.4 – 7 AHP Hierarchy

| | A | B | C | D | E |
|---|-----|-----|-----|---|-----|
| A | 1 | 4 | 5 | 7 | 2 |
| B | 1/4 | 1 | 1/3 | 5 | 1/3 |
| C | 1/5 | 3 | 1 | 6 | 1/2 |
| D | 1/7 | 1/5 | 1/6 | 1 | 1/7 |
| E | 1/2 | 3 | 2 | 7 | 1 |

Table 3.4 – 8 AHP Hierarchy Identifiers

| Letter | Performance Measure |
|--------|-------------------------------------|
| A | Reactor Lifetime |
| B | Mass |
| C | Transients |
| D | Reactivity Swing |
| E | Chemically Inert in CO ₂ |

Table 3.4-9 provides the respective weights calculated using the AHP hierarchy in Table 3.4-7.

Table 3.4 – 9 Performance Measure Weights

| Performance Measure | Weight |
|-------------------------------------|--------|
| Reactor Lifetime | 45.21% |
| Mass | 9.76% |
| Transients | 16.49% |
| Reactivity Swing | 3.41% |
| Chemically Inert in CO ₂ | 25.13% |

It is apparent from the weights that the PM Reactor Lifetime is judged to be the most important factor in choosing the best surface reactor. After assigning the PM weights, it was decided that all of the reactors considered are capable of operating for 25 years. The performance measures were evaluated assuming that for the given decision option, the reactor would be designed for and operated a full 25 years of operation. If this time period was changed, it is likely that the impact the decision options have on the performance measures would be different thus resulting in different performance indices. If time permitted, a sensitivity analysis would have been

performed by varying the number of reactor operating years. However, the decision to mandate a 25-year lifetime was made towards the end of the project.

The next step is to assess to what extent each decision option fulfilled the objectives. When using MAUT, a formal analysis using event or fault trees is desirable especially when dealing with systems that have a probability of failing. Since our interest at this point is only to assess the different options, we assume that all reactor designs would operate for the entire lifetime without failure. Given this, a formal analysis was not used but instead, expert opinion was used to evaluate the performance measures with respect to each decision option.

The actual values inserted used for the performance measures can be found in the attached Appendix. It was assumed that the inputs to the performance measures were 100% certain. However, it is expected that the inputs to the performance measures will involve some degree of uncertainty. A probability distribution can be readily applied to the inputs thus producing better results.

Table 3.4-10 provides the expected performance indices for the four decision options considered in this case study. The expected performance indices are calculated using equation 1 in this report.

Figure 3.4-2 provides a graphical representation of the decision options and their respective performance indices. It is clear that the first decision is the best option as it has the largest performance index. Decision 3 appears to be the worse option. Decisions 2 and 4 have roughly the same performance index values and are the intermediate options.

Figure 3.4-3 provides a visual breakdown of the performance indices for all decision options. Each bar represents the utility value for the performance index multiplied by the respective weight on the performance measure. Therefore, the bars can be compared to one another within a decision option. The bars for a given performance measure can be compared for the different decision options as well. The higher the bar, the greater the respective objective is fulfilled. It is important to note that the reactor lifetime performance objective is fulfilled to the fullest extent yet it has a utility of zero for all decisions. This was done as they all have the same impact on that performance measure.

Table 3.4 – 10 Performance Indices

| Decision Number | Decision Option (Spectrum, Coolant, Fuel, Matrix, Geometry) | Expected Performance Index |
|-----------------|---|----------------------------|
| 1 | Epithermal, CO ₂ , UO ₂ , BeO, Block | 1.1683 |
| 2 | Fast, CO ₂ , US, SiC, Block | 0.9802 |
| 3 | Fast, LBE, UC, SiC, Pin | 0.9426 |
| 4 | Thermal, CO ₂ , UO ₂ , BeO, Block | 0.9798 |

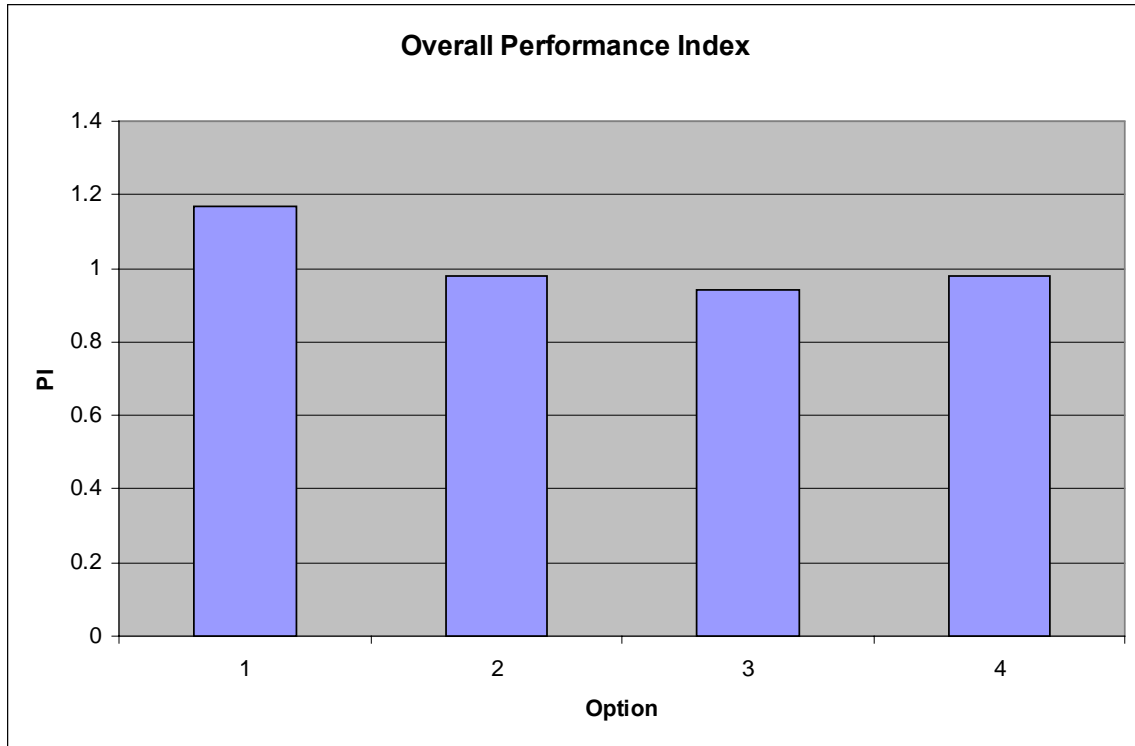


Figure 3.4 – 2 Overall Performance Index Graph.

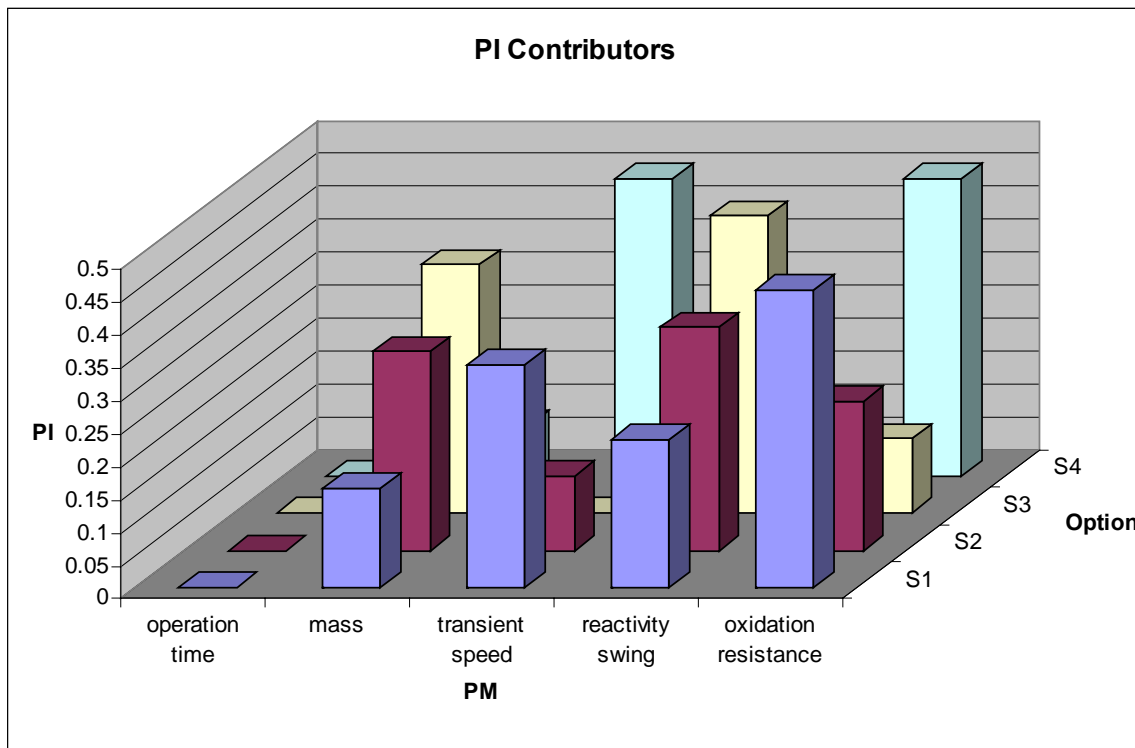


Figure 3.4 – 3 PI Contributors.

3.5 CONCLUSION

The application of the formal decision methodology by no means produces the absolute best answer. It is only through deliberation that the best option can be identified. This is not to say that the methodology is inadequate. The methodology in a way is a black box but with the advantage of a window. In many cases, the decision maker might choose to let the methodology produce the results and then only investigate the top options that are identified. However, the best way for the decision maker to employ the methodology is to look inside at the details and understand why a decision achieves the rank it does. By breaking down the performance indices and understanding their inner workings, the decision maker can not only obtain the best option but might develop new insight. This is especially true when multiple decision makers are involved each bringing their own experiences and beliefs. In the end, everyone gets a better understanding of what the overall mission is really about.

Another important note to make is that many decisions did not use all of the steps in the four-step methodology. In many cases, the rigors of Step 3, the Application of MAUT, was simplified to using one's own opinion as to which decision option was best without the rigors of building utility functions and calculating performance indices. This is not to say that the best decision was not obtained. There were many cases where we decided that innovation outweighed the better mathematical answer. This was the case in the choice to use TPVs. In the case of the surface reactor, a two-pronged approach was taken. We worked down through the methodology, working to assign indices to our decision options while at the same time, we worked upwards already having an idea what would represent the best set of options.

3.6 REFERENCES

- [1] R. Clemen, *Making Hard Decisions*, Duxbury Press, Belmont, CA, 1991.
- [2] R. Keeney and H. Raiffa, *Decisions with Multiple Objectives*, Cambridge University Press, Cambridge, U.K., 1993.
- [3] R. Weil and G. Apostolakis, "A Methodology for the Prioritization of Operating Experience in Nuclear Power Plants," *Reliability Engineering and System Safety*, **74**, 23-42, 2001.
- [4] G.E. Apostolakis and S.E. Pickett, "Deliberation: Integrating Analytical Results into Environmental Decisions Involving Multiple Stakeholders," *Risk Analysis*, **18**, 621-634, 1998.
- [5] National Research Council, *Building Consensus through Risk Assessment and Management of the Department of Energy's Environmental Remediation Program*, National Academy Press, Washington, DC, 1994.
- [6] R. Gregory and R. Keeney, "Creating Policy Alternatives Using Stakeholder Values," *Management Science*, **40**, 1035-1048, 1995.
- [7] T.L. Saaty, *The Analytic Hierarchy Process: Planning, Priority Setting, Resource Allocation*, McGraw-Hill, Suffolk, 1980.
- [8] W.R. Hughes, "Deriving Utilities Using the Analytic Hierarchy Process," *Socio-Economic Science*, **20**, 393-395, 1986.

4.0 SPACE POWER SYSTEM

4.1 SPACE PROPULSION OPTIONS

4.1.1 Introduction

The main objective of the space reactor design is to satisfy the propulsion system power requirements while minimizing the total mass of the system.

The power of the propulsion system is directly proportional to the product of its specific impulse (I_{sp}) and thrust.

$$P \sim I_{sp} \times T$$

The I_{sp} is a function of exhaust velocity of the propellant and the thrust is related to the propellant mass flow rate. High thrust engines provide faster transfer while high I_{sp} helps to save on the mass of the propellant and therefore on the total mass of the spacecraft. The sensitivity of the propellant mass to various I_{sp} for different Earth to Mars transfer times is illustrated in Figure 4.1.1-1.

Obviously, high power propulsion systems with preferably both high I_{sp} as well as with high thrust are necessary for fast transfer, low total mass, and, ultimately, to ensure the success of the mission.

Other important factors considered in the design are availability and maturity of the technology, amount and costs of research, development and testing programs required. The main emphasis is made on step-by-step development and potential scalability of applied technologies where future missions rely on accumulated data and experience as well as on the technologies proved and verified in previous missions.

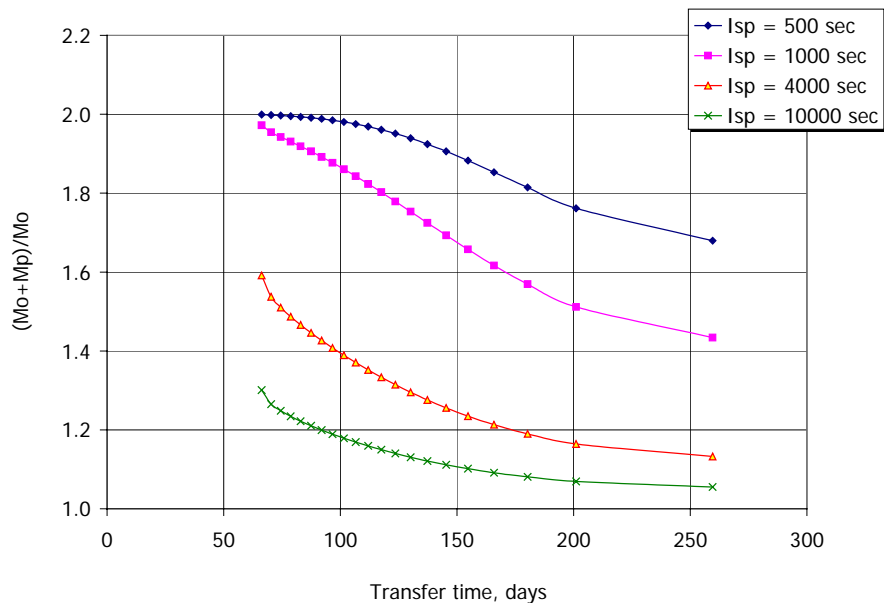


Figure 4.1.1 - 1 Propellant Mass Required for Earth to Mars Transfer for Various I_{sp} .

4.1.2 Choice of Propulsion System for Precursor Missions

All unmanned cargo precursor missions share two common specific features.

- Large cargo mass must be transferred, and therefore the propellant mass is limited.
- Travel time and exposure to cosmic radiation are of a less concern than for the manned mission

These basic considerations drive the choice of the propulsion system for the precursor missions.

Electric propulsion systems are being widely used for the purposes of satellite orbit correction. Such systems are characterized by very efficient utilization of propellant (high I_{sp}) but generally operate at relatively low power and, consequently, they provide relatively low thrust. These features, however, adequately reflect the needs of the precursor missions.

High I_{sp} allows for small propellant mass, thus maximizing the payload mass, while relatively low thrust can still be tolerable because travel time is not a limiting constraint for cargo missions. Though, it has to be noted that for the low thrust propulsion systems, the time required to achieve desirable ΔV can be considerably long especially for massive cargo shipments.

For example, the ion thruster known as NSTAR (NASA’s Solar Electric Propulsion Technology Applications Readiness) [1] and used for the New Millennium Deep Space-1 (DS-1) mission, operates at up to 2 kW of power and provides about 0.09 N of thrust.

The Hohman orbit transfer from LEO to Mars orbit will require total ΔV on the order of 6 km/sec. For a 20,000 kg spaceship, it would require some dozens of years (depending on engine’s I_{sp} and propellant mass) to achieve such ΔV , which does not comply with the constraints of the proposed mission.

A potential solution for that problem would be to utilize an array of thrusters, which would collectively provide the required thrust. In addition this would provide improved reliability and redundancy of the propulsion system and a greater degree of flight control flexibility.

A number of high-power / high-thrust electric propulsion systems are currently under development at NASA that can be suitable for the cargo precursor mission. These include, NEXT (NASA’s Evolutionary Xenon Thruster) [2], High power ion engine for interstellar precursor missions [3] and high-power high-thrust Hall thruster NASA-457M [4]. The key technical parameters for these engines are presented in Figures 4.1.2-1 through 4.1.2-3 and summarized in Table 4.1.2-1.

| | | |
|---|---------------------------|---------|
|  | Max. Input Power, kW | Up to 8 |
| | Max. Specific Impulse, S | 4,050 |
| | Efficiency @ Full Power | 68% |
| | Propellant Throughput, kg | >300 |
| | Specific Mass, kg/kW | 3.6 |

Figure 4.1.2 – 1 NASA’s Evolutionary Xenon Thruster (NEXT).

| | |
|---|---|
|  | <p>Engine Array Specifications total number of engines 10 total beam area 1.96 m² total engine and gimbal mass 248 kg cluster size - 10 cm clearances side-to-side 4.4 m x 1.8 m maximum array length 0.5 m specific mass, engine and gimbal 2.39 kg/kW</p> |
| | <p>Engine Array Performance (BOL) input power, max 103.3 kW thrust 1.12 N total flow rate 8.0x10⁻⁶ kg/s propellant krypton</p> |
| | <p>Engine performance efficiency 0.76 specific impulse 14,230 s input power 10.3 kW beam power 9.99 kW thrust 0.112 N total propellant efficiency 0.82 total flow rate 8.0x10⁻⁷ kg/s</p> |

Figure 4.1.2 - 2 High Power Ion Engine for Interstellar Precursor Missions.

| | |
|---|---|
|  | <p>Power Up To 72 Kw Thrust Up To 3 N Isp Up To 4100 S Efficiency >0.63</p> |
|---|---|

Figure 4.1.2 - 3 NASA-457M Hall Thruster

Table 4.1.2 - 1 Key Performance Parameters of Advanced Electric Propulsion Systems

| | NEXT | NASA-457M | Interstellar Ion Engine |
|----------------------|------|---------------|-------------------------|
| Power, kW | 8 | 50 (up to 72) | 10.3 |
| Thrust, N | 2-3 | up to 3 | 1.12 |
| Isp, s | 4050 | 2747 | 14,230 |
| Efficiency, % | 68 | 63 | 76 |
| Specific Mass, kg/kw | 3.6 | N/A | 2.4 |

The electric propulsion systems mentioned above are in the advanced stages of their development and they are based on mature technologies. Their performance was tested and verified under various conditions. The reliability and lifetime expectancy tests are currently ongoing or scheduled to be performed in the near future.

The limited lifetime of the ion optics components appears to be the main weakness of the electric propulsion systems. The advanced systems currently under development, however, have been demonstrated to operate for 20,000 hours and beyond [5].

As a result of the brief review of currently available technologies, we concluded that it would be practically feasible to develop an electric propulsion system/thruster with the following key characteristics:

| | |
|------------------------|------------|
| Power input, kW | 50 |
| Isp, s | up to 4000 |
| Thrust, N | up to 3 |
| Efficiency | 65% |
| Specific mass, kg/kW | 3 |
| Engine lifetime, hours | 20,000 |

For the purposes of current study, a generic electric propulsion system with the described set of performance parameters is adopted as a reference point for the design of systems for the precursor missions.

4.1.3 Manned Mission Propulsion System

Variable Specific Impulse Magnetoplasma Rocket (VASIMR) is a high power highly flexible engine that can ensure fast Earth to Mars transfer in less than 90 days [6,7] (Figure 4.1.3-1). The specific advantages of this concept include

- High payload capacity.
- Mission flexibility.
- Variable specific impulse for high-efficiency orbit transfer, trajectory optimization, high efficiency for interplanetary cruise.
- High thrust for faster escape from planetary orbits.
- Magnetoplasma technology is relevant to more advanced fusion systems.
- No moving parts, no electrodes, therefore higher reliability and longer lifetime.
- Hydrogen propellant: plentiful, inexpensive, and can be efficiently used as a radiation shield.

The VASIMR type propulsion system is currently under extensive development by NASA and collaborators. The first in space demonstration tests of the engine are planned for the near future and the multi-megawatt VASIMR engine can be ready for deployment within the timeframe that agrees with the current mission plan (by the year 2018). The VASIMR engine is suitable for manned missions to Mars and will require an electric power supply on the order of 12 MW in a direct current form.

In this study, we made an attempt to design a spacecraft power system that will satisfy the requirements of the VASIMR engine with specific weight of less than 3 kg/kWe.

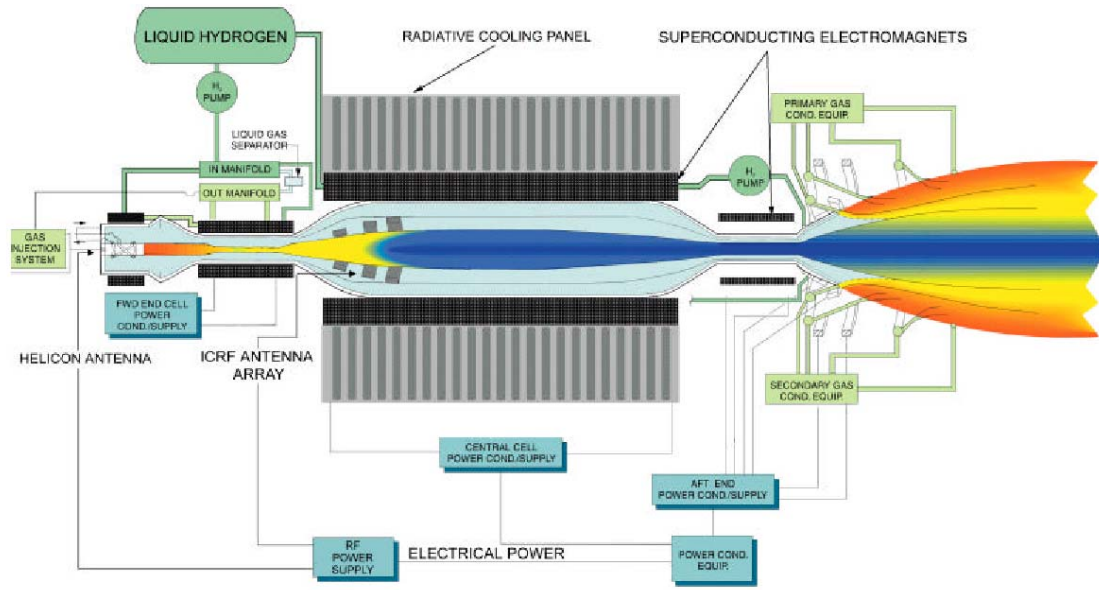


Figure 4.1.3 - 1 VASIMR Engine Concept

4.1.4 References

- [1] T. A. Bond, G. Benson, J. Christensen, J. T. Gallagher, M. Matranga, "The NSTAR Ion Propulsion Subsystem for DS1," AIAA-1999-2972, 1999.
- [2] M. J. Patterson, J. E. Foster, T. W. Haag, V. K Rawlin, G. C. Soulas, R. F. Roman, "NEXT: NASA's Evolutionary Xenon Thruster," AIAA 2002-3832, 2002.
- [3] M. T. Domonkos, M. J. Patterson, R. S. Jankovsky, "Ion Engine and Hall Thruster Development at the NASA Glenn Research Center," IMECE2002-39444, *Proceedings of IMECE'02: 2002 ASME International Mechanical Engineering Congress and Exposition*, New Orleans, Louisiana, November 17–22, 2002.
- [4] M. J. Patterson, R. F. Roman, and J. E. Foster, "Ion Engine Development for Interstellar Precursor Missions," AIAA 2000-3811, 2000.
- [5] M. T. Domonkos, M. J. Patterson, J. E. Foster, V. K. Rawlin, G. C. Soulas, J. S. Sovey, S. D. Kovaleski, R. F. Roman, and G. J. Williams, "Extending Ion Engine Technology to NEXT and Beyond," <http://www.grc.nasa.gov/www/ion/>
- [6] F.R. Chang Diaz, J.P. Squire, R.D. Bengtson, B.N. Breizman, F.W. Baity, M.D. Carter, "The Physics and Engineering of the VASIMR Engine," AIAA 2000-3756, *36th AIAA/ASME/SAE/ASEE Joint Propulsion Conference*, Huntsville, Alabama, 17-19 July, 2000.
- [7] F.R. Chang Diaz, J.P. Squire, A.V. Ilin, G.E. McCaskill, T.X. Nguyen, D.S. Winter, A.J. Petro, G.W. Goebel, L.D. Cassady, K.A. Stokke, C.E. Dexter, T.P. Graves, L. Amador Jr., J.A. George, M.D. Carter, F.W. Baity Jr., G.C. Barber, R.H. Goulding, D.O. Sparks, S.W. Schwenterly, R.D. Bengtson, B.N. Breizman, V.T. Jacobson, A.V. Arefiev, R.Z. Sagdeev, K. Karavasilis, S.V. Novakovski, A.A. Chan, T.W. Glover, "The Development of the VASIMR Engine," *International Conference on Electromagnetics in Advanced Applications*, Torino, Italy. Sept 13 - 17, 1999.

4.2 SPACE REACTOR POWER SYSTEM (Molten Salt Fast Reactor - MSFR)

4.2.1 Introduction

The proposed VASIMIR power system consists of three 4 MWe ultra compact high temperature molten salt cooled fast reactors (MSFR) combined with a thermo-photovoltaic (TPV) power conversion system.

The heat from the reactor core is transported by molten salt coolant to an internal radiator and then a thermal radiation field transfers energy from the radiator to the TPV collector. The TPV units partially absorb the heat and convert it to electric energy. The residual heat not absorbed by the TPV collectors is then dissipated to outer space. The schematic view of the space power system is shown in Figure 4.2.1-1.

Use of highly neutronically reactive Pu fuel and fast neutron spectrum enables designing ultra compact reactor core. Small size of the core reduces the mass of the shielding which is approximately proportional to the core dimensions (core diameter). The nuclear fuel used is in the form of Pu carbide. Carbide fuels have high HM density and good thermal conductivity. Carbide fuel fabrication and irradiation behavior, although currently under extensive research, remains to be evaluated.

The ultra compact fast reactor core has a very high power density, and therefore requires a working fluid with very good heat transfer properties. Molten salt (MS) is chosen as a heat transfer medium because it has very good heat transfer properties and high boiling temperature. These features enable the design to achieve very high core power densities while maintaining low flow velocity and low operating pressure in the system. Low system pressure improves the reliability of the system. Electromagnetic induction pumps can be used to provide molten salt

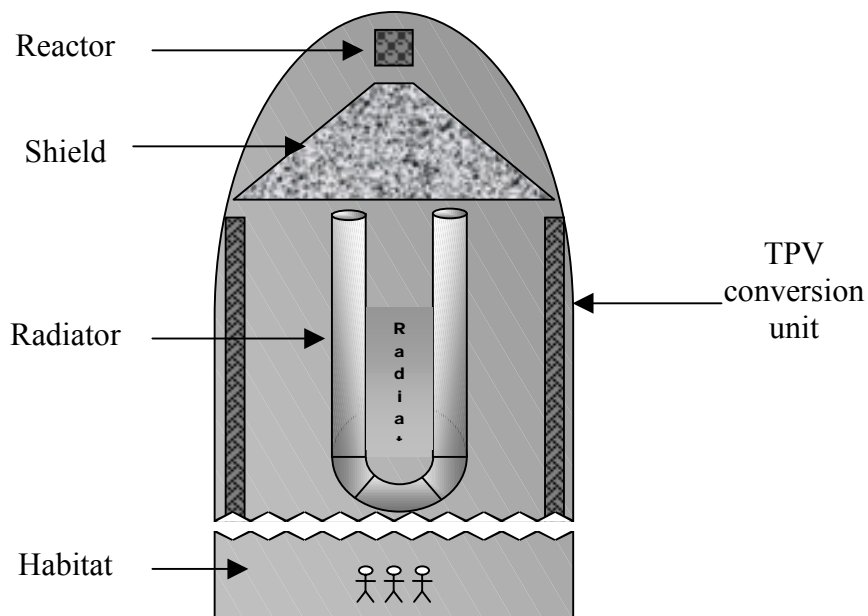


Figure 4.2.1 - 1 Schematic View of the Space Power System.

coolant circulation. Such pumps have no moving parts and do not need any external electricity source and therefore are very reliable. The induction pumps are expected to have higher efficiency with MS than with liquid metal coolants due to the high electric conductivity.

Photovoltaic power conversion efficiency can be as high as 40% for the operating temperature on the order of 1600K. (However, the conversion efficiency decreases substantially with the temperature.) It is very compact and has no moving parts. We suggest using the same power supply for the precursor cargo missions and the manned mission. The precursor missions' power supply system will operate at lower temperatures and will have lower power conversion efficiency. However, it will rely on more mature technology, will have larger design margin, higher probability of success and will serve for the purpose of proof and verification of the more advanced technologies for the future manned mission.

High operating temperature allows more efficient heat rejection by thermal radiation and therefore results in dramatic savings in the radiator mass. For precursor missions, the radiator mass for the low power systems may not be scaled down substantially with the power because of the lower operating temperatures and therefore less efficient heat rejection.

Refractory metal alloys with high (<2500K) melting temperatures are used as structural materials. Some properties of the refractory metals are summarized in Table 4.2.1-1. [1] Preliminary review suggests the use of Nb and Mo based alloys as primary structural materials because these metals have relatively low density and they are inexpensive and have low neutron absorption. Ti-based alloys have very low density and seem very attractive for use as piping and support structures.

Table 4.2.1-1 Refractory Metals Properties

| | $T_{melt}, ^\circ C$ | P, g/cc | A |
|----|----------------------|---------|--------|
| Nb | 2468 | 8.57 | 92.91 |
| Mo | 2622 | 10.28 | 95.94 |
| W | 3387 | 19.25 | 183.84 |
| Re | 3180 | 21.02 | 186.21 |
| Ti | 1668 | 4.51 | 47.87 |

4.2.2 Space Nuclear Reactor Design

The main objectives of the space reactor design are to minimize the mass and the volume of the reactor. The major constraints are the feasibility of the reactor control and thermal-hydraulic design.

In order to meet the requirements of small core mass and volume, highly neutronically reactive fuels are advantageous in order to compensate for the large neutron leakage.

We performed a preliminary evaluation of fast and thermal spectrum options for the design of the space power reactor. Our investigation was focused on the most neuronically reactive isotopes in fast and thermal spectra.

High fuel burnup allows saving on the total fuel mass but simultaneously creates the reactor controllability concern due to the large reactivity swing over the core lifetime. For example, the SAFE-400 reactor that uses highly enriched uranium fueled core has fairly small reactivity swing but the fuel burnup is very low – on the order of 1 a/o [2]. This means that 99% of the fuel weight was not used for the purpose of energy production.

In addition, exotic fuel candidates can appear to be very costly which may constitute a considerable part in the total cost of the mission. In that case, high fuel burnup will also provide better value for the investment.

In this study, we explore fuel types that can potentially achieve high burnup levels while maintaining reasonably small lifetime reactivity swing. Such a fuel would consist of a mixture of highly neutronically reactive fissile and fertile isotopes. Initially, fertile isotopes act as a poison. Fertile material reduces the core reactivity at the beginning of life (BOL) and later on the fertile material is gradually converted into fissile isotopes enhancing the fuel burnup.

30 a/o atomic burnup was chosen as a reference point for the analysis. This value represents a reasonable trade off between fuel performance under irradiation and the objective of minimum fuel mass to launch to the orbit.

We also assumed that the space power system will provide energy equivalent to the 4 MWe (11 MW_{th}) power units operating for 540 effective full power days (EFPD) which corresponds to three 180 days round trips from LEO to Mars orbit.

10% of heat losses by radiation were assumed due to the very high operating temperatures, i.e., for every 11 MW_{th} produced by the core just 10 MW are transferred to the radiator. These losses include radiation from the core as well as the pumps.

Under the assumptions stated above, the amount of fuel necessary to provide the energy equivalent to 5940 MW_{th}-days is on the order of 6 kg of heavy metal (HM) atoms. The 30 a/o burnup brings the total mass of the fuel to about 20 kg of HM.

Thermal spectrum core evaluation

The main advantage of thermal spectrum systems is very small fuel mass required to sustain criticality because of the large thermal cross-sections. The drawbacks are: the addition of moderator mass to the system, and generally large core lifetime reactivity swing due to the high reactivity worth of the fission products.

In the thermal spectrum, the isotope Am-242m is the best known fissile material. It has the highest fission cross-section on the order of 7000b [3] and very high fission neutrons yield of about 3.25. It is produced as a result of (n,γ) reaction in Am-241. Large quantities of Am-241 are available from the spent fuel from commercial power reactors as a result of the decay of relatively short lived (~14 years [2]) Pu-241 isotope.

The highest enrichment of Am-242m in Am-241 (on the order of 8.5%) can be obtained by irradiation of pure Am-241 chemically separated from the old spent commercial reactors fuel in very hard neutron spectrum [4,5].

Higher than 8.5 % enrichment of Am-242m will require isotopic separation techniques and therefore will substantially increase the fuel cost.

Choice of fertile poison material

Although Am-241 has a very large thermal capture cross-section and resonance integral, the branching ratio to the production of meta-stable isotope of interest Am-242m is small – about 10%. The ground state isotope Am-242 is of a smaller importance due to its very rapid decay to fertile Cm-243.

Alternative candidate fertile isotope considered is Pu-240 with resonance integral on the order of 10000 barns. The result of the (n,γ) reaction in Pu-240 is production of rather good fissile Pu-241 isotope.

Plutonium with high concentrations of Pu-240 isotope can be obtained by the long irradiation of reactor grade Pu in a well-thermalized neutrons spectrum. A sample set of burnup calculations in unit cell geometry was performed by the CASMO-4 [6] computer code. The fuel pin containing homogeneous mixture of RG Pu with ZrO₂ inert matrix was surrounded by large volume ($V_m/V_f \sim 100-600$) of D₂O providing a well thermalized spectrum. Figure 4.2.2-1 shows an example of the burnup calculations results. At about 50% atomic burnup the concentration of Pu-240 isotope can be as high as 55%. We believe that even higher concentrations of Pu-240 isotope are practically achievable with more sophisticated optimization and spectrum filtering techniques and different initial Pu-239 concentrations.

Considerably more expensive isotopic separation technologies are needed if much higher purity of Pu-240 is required.

A number of different fuel compositions with different Am-242m:Am-241:Pu-240 ratios were evaluated in this part of the study with respect to their reactivity limited burnup capabilities, reactivity swing over the fuel lifetime, and the total mass and the volume of the core (including fuel, moderator and coolant).

First, an evaluation of Am-242m – Am-241 mixture with 8.5% isotopic enrichment in Am-242m was performed to assess its achievable burnup potential.

The calculations were performed in infinite plane unit cell geometry. The thickness of the fuel slab was fixed at 50 μ . Am HM density used was 13.5 g/cm³. BeO moderator slab thickness was varied to provide V_m/V_f ratios in a range between 1 and 6000. Monte Carlo particle transport code MCNP-4C [7] was used for these calculations.

Figure 4.2.2-2 reports the results of criticality calculations for the 8.5% enriched Am-242m – Am-241 mixture.

The infinite system is barely critical at relatively high V_m/V_f ratios (1500 – 4000). These findings indicate that substantially higher Am-242m enrichment is required for feasible reactor design.

As a next step, a number of different mixtures of fissile Am-242m and fertile Am-242m – Am-241 mixtures were evaluated in terms of their initial excess reactivity and reactivity limited burnup capabilities. CASMO-4 was used for the burnup calculations. We assumed that the results obtained from CASMO-4 calculations are reasonably valid for the purposes of the current scoping study since it was designed for thermal reactor analysis and uses appropriate cross-sections set.

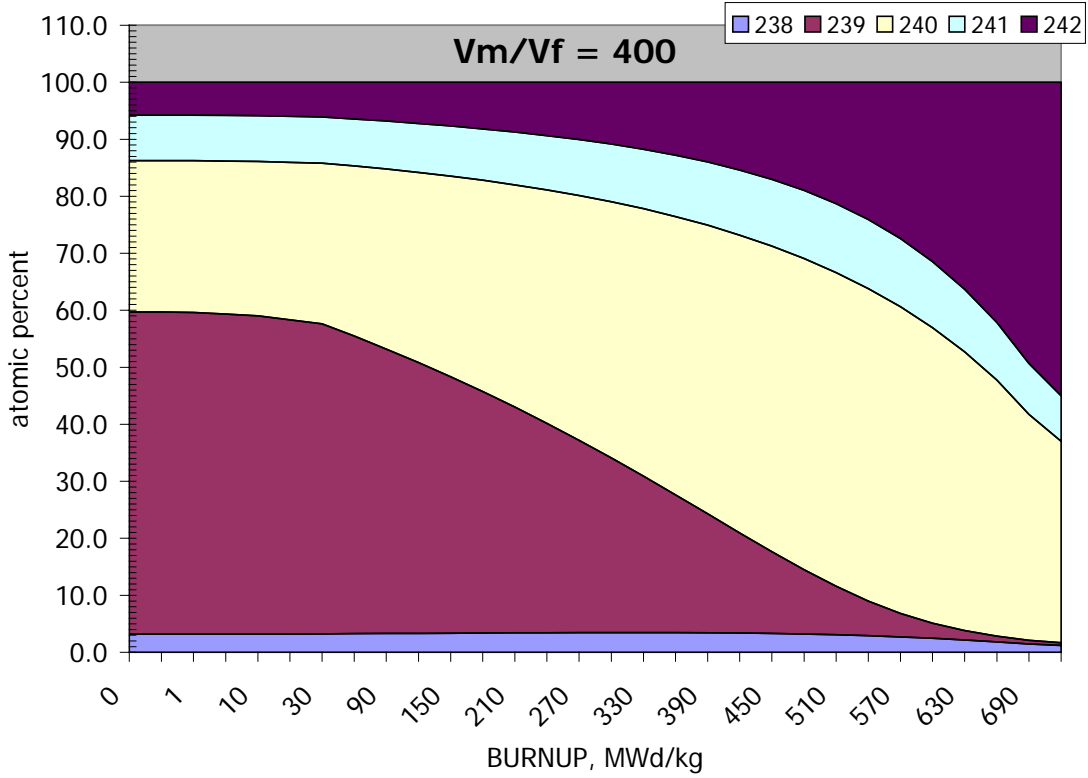


Figure 4.2.2 - 1 Pu Isotopic Composition as a Function of Burnup.

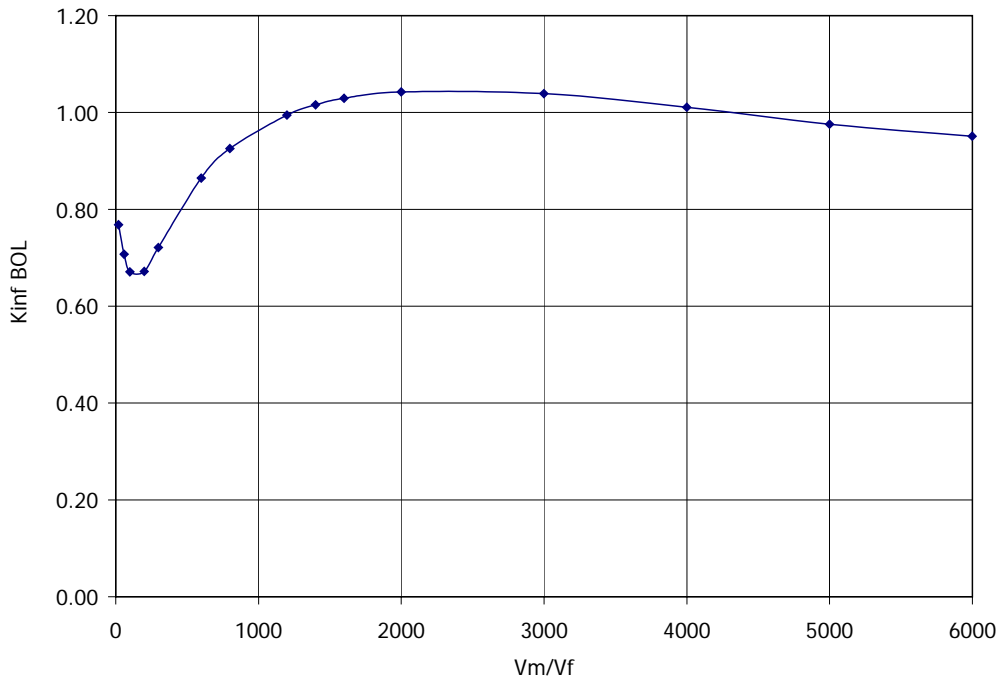


Figure 4.2.2 - 2 8.5% Am-242m Enriched Am Fuel: Infinite Medium Criticality.

The cylindrical geometry unit cell consisted of the fuel and moderator regions. The fuel region included Na heat pipe identical to SAFE-400 design covered on the outside with thin layer (200 μ) of Am (Am-Pu) fuel (13.5 g/cm³ HM density). The fuel pins were dispersed in BeO moderator matrix. The square pitch of the fuel pins was varied to cover a wide range of V_m/V_f ratios.

Figure 4.2.2-3 presents selected results of the burnup calculations for various fuel mixtures. The following can be concluded from the results. In order to achieve the goal of 30% atomic burnup high isotopic enrichments (>25%) of Am-242m are required which significantly increases the fuel cost.

Alternatively, high atomic burnup can be achieved with relatively large moderator volumes and substantially increases the core mass. About 3 MT of BeO is needed per about 20 kg of Am-242m – Am-241 (50:50) fuel to achieve 30 atomic burnup.

Substitution of fertile Am-241 with Pu-240 has relatively small effect on reactivity limited burnup.

Figures 4.2.2-4 and 4.2.2-5 report BOL reactivity for a number of different fuel compositions. The results indicate that initial excess reactivity is very high for the cases that have reasonable burnup potential (>15 a/o). The compensation of such a high initial reactivity will require sophisticated control mechanisms, which will in turn considerably complicate the system. Here again, the substitution of Am-241 with Pu-240 has a minor impact on BOL reactivity of the core.

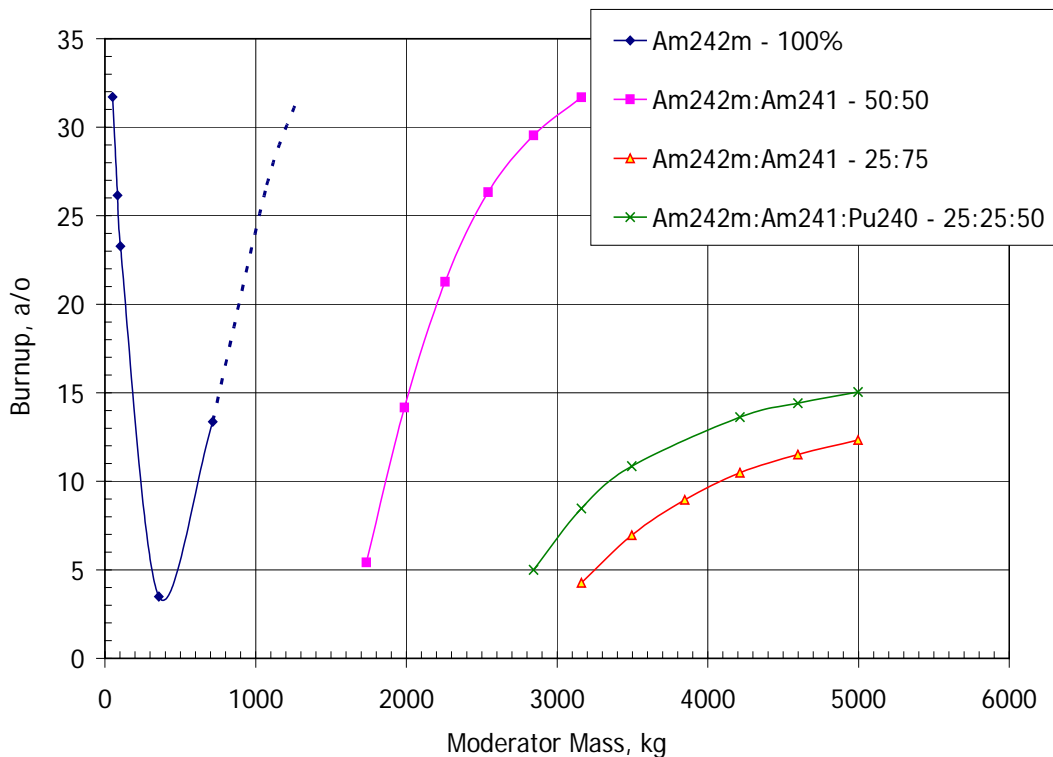


Figure 4.2.2 - 3 Achievable Fuel Burnup per Moderator Mass Investment.

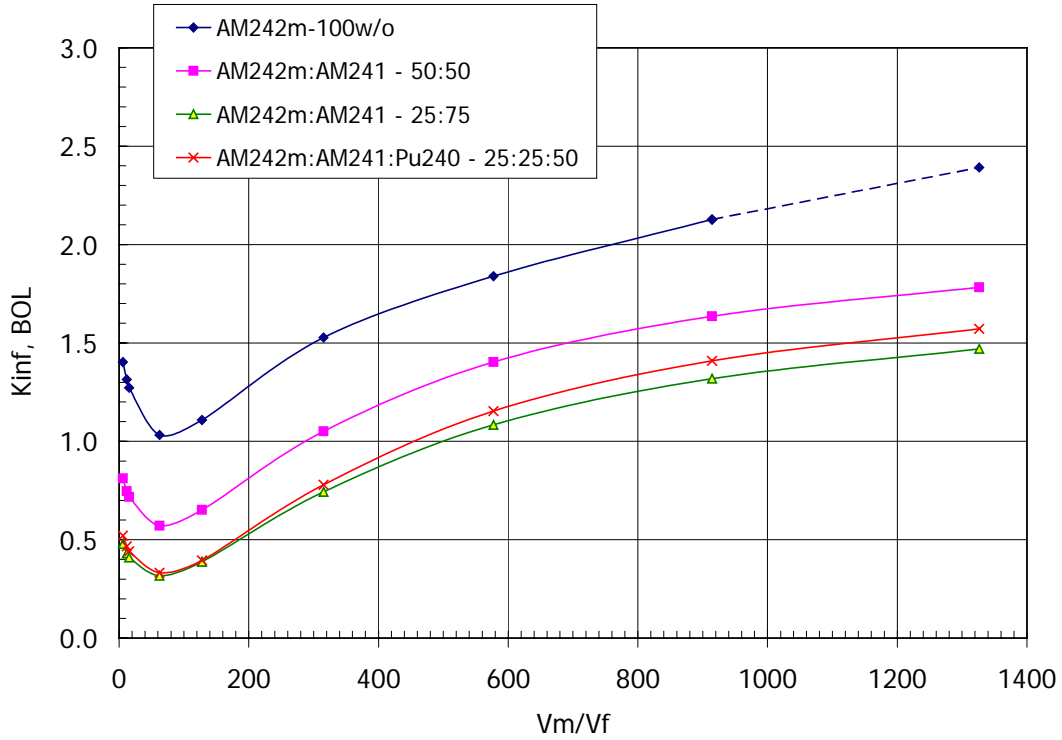


Figure 4.2.2 - 4 k-inf BOL for Am-242m Based Fuel.

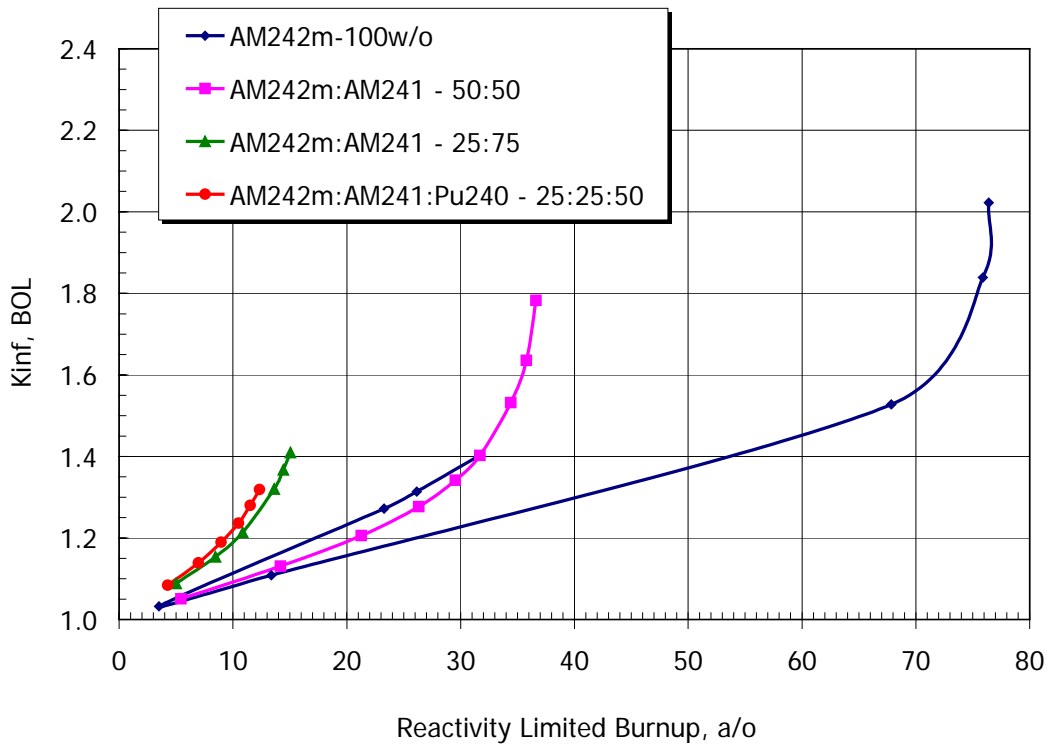


Figure 4.2.2 - 5 k-inf BOL vs. Reactivity Limited Burnup Capabilities for Am-242m Based Fuel.

In summary, we concluded that thermal spectrum Am-242m based systems are less attractive due to: large moderator mass required to maintain criticality and provide high burnup capabilities, high BOL excess reactivity that would be challenging to control, and isotopic separation required to boost Am-242m enrichment and achieve high burnup.

Fast spectrum core evaluation

The main advantages of the systems operating in the fast neutron energy region are small dimensions and high power density. Neutron leakage from the fast spectrum core is expected to be very high due to the small core dimensions and large migration area of the fast neutrons. Therefore, the reactivity worth of the reflector is very high which makes it possible to control the core entirely by external means without any in-core control mechanisms.

In the fast spectrum core, the transients occur much more rapidly than in thermal system due to the short prompt neutrons lifetime and due to the fact that some actinides that are very reactive in the fast spectrum have small delayed neutrons yield. Therefore, the reactor core and its control system should be carefully designed to provide negative reactivity feedbacks under accident conditions and safe reactor operation under normal operating conditions.

For the fast reactor core, the fuel mass required to sustain criticality is much larger than for the thermal systems due to considerably smaller cross-sections in the fast energy region. On the other hand, nearly all actinides are fissionable by fast neutrons and, thus, fast cores have favorable neutron economy, which makes it possible to design the core with very flat reactivity over the lifetime by choosing the fissile and fertile components of the fuel and optimizing the conversion ratio to be around unity.

The effects of fission product poisoning and the presence of structural materials in the core are minor due to their small reactivity worth in the fast spectrum. The present design attempts to take advantage of the fast spectrum core features and address most of the concerns related to the fast systems disadvantages.

Following the logic of the discussion presented earlier, the fast reactor design described in this section has the following main objectives:

- provide 11MW_{th} power for 540 effective full power days (EFPD)
- minimize the mass and the size of the reactor
- ensure feasibility of thermal hydraulic design
- ensure feasibility of control by leakage (external means)
- ensure negative reactivity feedback

A molten salt cooled fast reactor (MSFR) is proposed as a potential reactor that meets the goals. The following sections describe the methods for designing the reference MSFR for space applications.

Methods

All neutronic design calculations were performed with Monte Carlo particles transport code MCNP-4C. The burnup calculations were performed using the MCODE [8] – MCNP-ORIGEN [9] linkage utility program. The JEF-2.2 based continuous energy cross-sections library set was used for the MCNP calculations.

The core was modeled as a single homogeneous region with the top, bottom and radial reflectors. The homogeneous core representation is a reasonable approximation because the core components dimensions are, in general, much smaller than the migration length of neutrons in a fast spectrum system.

Description of Calculated Cases and Selected Results

A large number of sensitivity and crude optimization calculation were performed to address the reactor design objectives listed above.

Selected cases calculated in this section are described in Table 4.2.2-1.

Various fuel compositions were analyzed. The fuel was assumed to be in a carbide form because of the high HM density and fairly good thermal conductivity of U-Pu carbides.

Plutonium was chosen as a primary fuel material because all of its isotopes are very reactive in the fast spectrum and, therefore, allow for very compact and low HM mass core design. Several Pu isotopic compositions were considered:

- reactor grade (RG) Pu from commercial LWR type spent fuel because it is widely available
- weapons grade (WG) Pu available from dismantled nuclear weapons because Pu-239 is the most reactive isotope in the fast spectrum
- fertile rich Pu with high content of Pu-240 and Pu-242 isotopes (can be produced by long irradiation of RG Pu in well thermalized spectrum) because it can potentially reduce reactivity swing of the core.

In addition, mixtures of depleted uranium (U-238) with Pu of different grades in various proportions were evaluated to enhance breeding potential, reduce reactivity swing and increase burnup of the fuel.

In some calculations, Pu based fuel was assumed to be dispersed in neurotically inert fertile free matrix in case high priority will be attributed to improved irradiation stability or thermal performance of the fuel.

The fuel cladding and other structural materials present in the core were assumed to occupy up to 5 v/o. Nb based alloy or SiC coating were considered as a cladding material. It should be noted that because of the small dimensions of the core, honeycomb grid structure of the fuel and absence of gravity, the fuel cladding does not perform a function of structural material but rather serves as a barrier for preventing the fission products from escaping from the fuel. It does need, though, some structural and mechanical stability to maintain the fuel plates' integrity under temperature and irradiation induced changes (i.e., pressurization due to accumulation of fission gas).

The molten salt coolant used in the analysis was eutectic solution of NaF-ZrF₄ (50:50). It has been proposed for use in different nuclear systems and its properties have been widely studied. Molten salt is a very attractive coolant because of its very good heat transfer properties and it allows low pressure operation at the high temperatures of interest. The neutronic performance of the core is quite sensitive to the molten salt coolant volume fraction because the presence of large amounts of F atoms shifts the neutron spectrum to epithermal region, which reduces

Table 4.2.2 - 1 Description of Selected Calculated Cases

| Case | Coolant, v/o | Structure, v/o | Fuel, v/o | Fuel comp. | | Fuel mass, kg | Ref. thickness, cm |
|-----------|-----------------|-------------------|--------------|----------------------------|-------|---------------------|--------------------------------|
| 1 | 50 | 5 (SiC) | 45 | Fertile rich PU | | 40 | 5 |
| 2 | 50 | 5 (SiC) | 45 | RG Pu | | 40 | 5 |
| 3 | 40 | 0 | 60 | RG Pu | | 40 | 5 |
| 4 | 50 | 0 | 50 | RG Pu | | 40 | 5 |
| 5 | 50 | 0 | 25F- 25M | RG Pu | | 40 | 5 |
| 6 | 40 | 5 (SiC) | 55 | RG Pu | | 40 | 10 |
| 7 | 40 | 5 (Nb) | 55 | RG Pu +U ²³⁸ | 50:50 | 40 | 10 |
| 8 | 40 | 5 (Nb) | 55 | RG Pu | | 40 | 10 |
| 9 | 40 | 5 (Nb) | 55 | WG Pu +U ²³⁸ | 75:25 | 40 | 10 |
| 10 | 40 | 5 (Nb) | 55 | RG Pu +U ²³⁸ | 70:30 | 60 | 5 |
| 11 | 40 | 5 (Nb) | 55 | RG Pu +U ²³⁸ | 70:30 | 60 | 10 |
| 12 | 40 | 5 (Nb) | 55 | RG Pu +U ²³⁸ | 70:30 | 80 | 10 |
| 13 | 40 | 5 (Nb) | 55 | RG Pu | | 60 | 10 |
| 14 | 40 | 5 (Nb) | 55 | RG Pu | | 60 | 5 |
| 15 | 40 | 5 (Nb) | 55 | RG Pu +U ²³⁸ | 65:35 | 80 | 10 |
| 16 | 40 | 5 (Nb) | 55 | RG Pu | | 50 | 5 |
| 17 | 40 | 5 (Nb) | 55 | RG Pu | | 50 | 6 |
| 18 | 40 | 5 (Nb) | 55 | HEU | | 50 | 6 |
| 19 | 40 | 5 (Nb) | 55 | RG Pu | | 50 | 0 |
| 20 | 40 | 5 (Nb) | 55 | RG Pu | | 50 | rad. 0cm ax. 6cm |
| 21 | 40 | 5 (Nb) | 55 | RG Pu | | 50 | rad 6cm 50% dens. ax 6cm |

reactivity and degrades breeding. The calculations were performed for different coolant volume fractions to assess the sensitivity of k -eff and achievable burnup to this parameter. The minimal coolant volume fraction of 40 v/o was determined by the thermal hydraulic analysis and described in details in a separate section.

As expected, the core reactivity and the achievable burnup are extremely sensitive to the reflector thickness. The reflector dimensions were chosen such that the beginning of life core excess reactivity can be controlled by direct leakage. The possible options for the reflector control mechanisms are rotating slabs of reflector material located around the core or “sliding doors” type reflector plates that can be opened or shut varying the direct neutron leakage. Both conceptual options are schematically sketched in Figure 4.2.2-6.

Reflector material has marginal impact on reactivity and burnup. We considered graphite, BeO and Zr_3Si_2 . All of these materials have comparable performance. In the future, more attention should be devoted to the reflector design and optimization to find a compromise solution for the tradeoff between reflector effectiveness, mass and geometry. In the present study, the feasibility of control was evaluated by calculating the core criticality at the beginning of life with radial reflector with variable reflector material density between 50 and 100% of nominal reflector density.

The results of some of the calculated cases are summarized in Table 4.2.2-1. Figure 4.2.2-7 reports the results of the burnup calculations. Several observations can be made from the results presented in Figure 4.2.2-7 and Table 4.2.2-2.

It was found that addition of U-238 to the fuel does not reduce significantly the core reactivity swing. As expected, the mass of HM required to sustain criticality for 540 EFPD is significantly larger than for the thermal reactor system. However, the total mass of the reactor (including reflector mass) is on the order of a few hundred kilograms, which is substantially smaller than that of the thermal system.

Reflector contributes significant fraction to the total mass of the core, but still, the total reactor mass is very small compared with the masses of the rest of the systems.

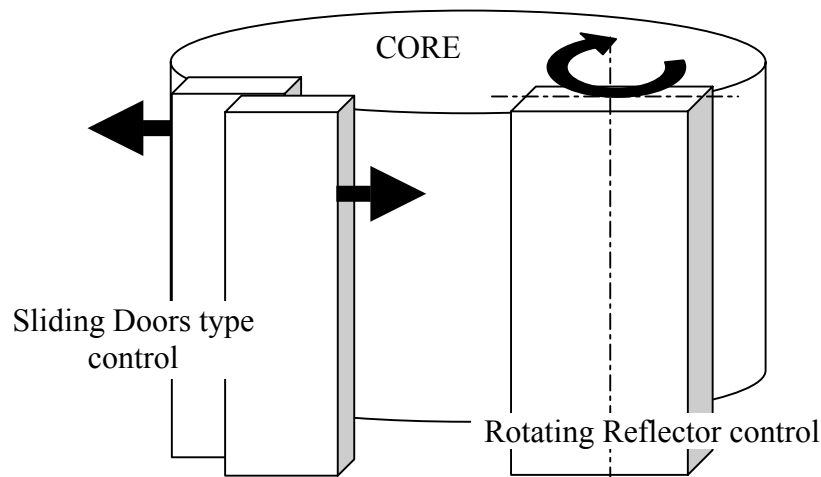


Figure 4.2.2 - 6 Core Reactivity Control by Direct Leakage.

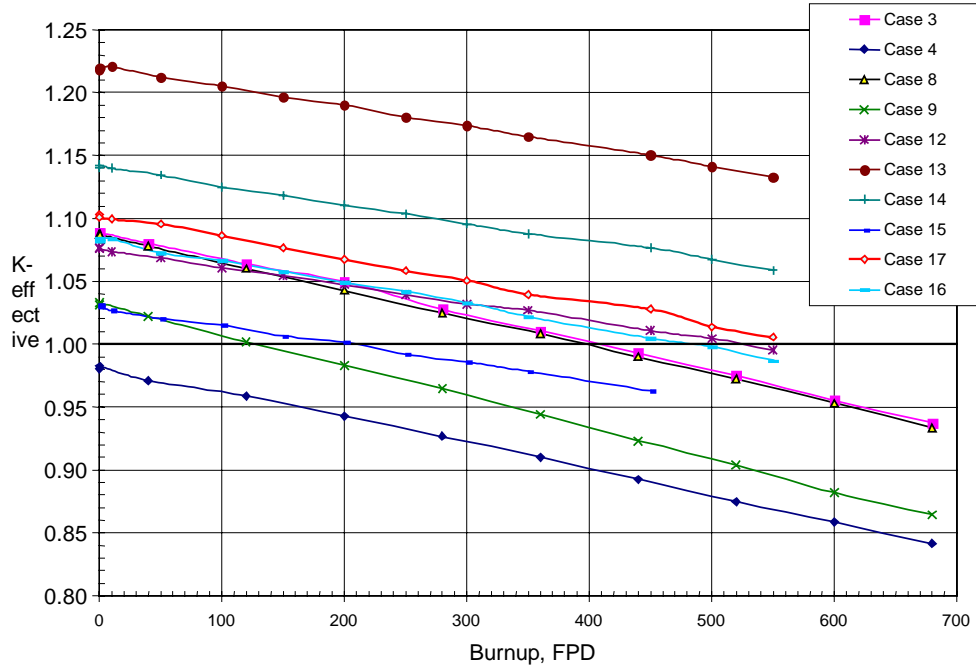


Figure 4.2.2 - 7 Burnup Calculations Results.

Table 4.2.2 - 2 Selected Results

| Case | Fuel mass, kg | Ref. thickness, cm | k_{eff} BOL | BU, MWd/kg | BU, EFPD | Core mass | Ref mass | Total Mass |
|-----------|---------------|-----------------------|---------------|------------|------------|-----------|-----------|------------|
| 1 | 40 | 5 | 0.71 | *NE | NE | 53 | 68 | 120 |
| 2 | 40 | 5 | 0.94 | NE | NE | 53 | 68 | 120 |
| 3 | 40 | 5 | 1.14 | ~100 | 410 | 47 | 58 | 105 |
| 4 | 40 | 5 | 0.98 | 0 | 0 | 50 | 64 | 114 |
| 5 | 40 | 5 | 0.76 | NE | NE | 77 | 94 | 172 |
| 6 | 40 | 10 | 1.09 | ~100 | 395 | 48 | 170 | 218 |
| 7 | 40 | 10 | 0.91 | NE | NE | 50 | 170 | 220 |
| 8 | 40 | 10 | 1.09 | ~100 | 400 | 50 | 170 | 220 |
| 9 | 40 | 10 | 1.03 | ~30 | 130 | 50 | 170 | 220 |
| 10 | 60 | 5 | 0.91 | NE | NE | 75 | 76 | 151 |
| 11 | 60 | 10 | 0.99 | NE | NE | 75 | 206 | 280 |
| 12 | 80 | 10 | 1.08 | 65 | 525 | 100 | 236 | 336 |
| 13 | 60 | 10 | 1.21 | 232 | 1400 | 75 | 206 | 280 |
| 14 | 60 | 5 | 1.14 | 175 | 950 | 75 | 76 | 151 |
| 15 | 80 | 10 | 1.03 | 26 | 210 | 100 | 236 | 336 |
| 16 | 50 | 5 | 1.08 | 100 | 480 | 62 | 69 | 131 |
| 17 | 50 | 6 | 1.1 | 117 | 570 | 62 | 88 | 150 |
| 18 | 50 | 6 | 0.6 | NE | NE | 62 | 88 | 150 |
| 19 | 50 | 0 | 0.92 | NE | NE | 62 | 0 | 62 |
| 20 | 50 | rad. 0cm ax. 6cm | 0.965 | NE | NE | 62 | - | - |
| 21 | 50 | rad. 50% dens ax. 6cm | 1.008 | NE | NE | 62 | - | - |

*NE – not evaluated

Case 18 in Tables 4.2.2-1 and 4.2.2-2 illustrates the main advantage of Pu in the fast spectrum. Substitution of RG Pu fuel with the same mass of U-235 reduces the core k-eff from 1.10 to about 0.6. Therefore, highly enriched uranium fueled cores will have much larger fuel and total system mass.

Case 17 in Tables 4.2.2-1 and 4.2.2-2 represents the tentative reference core design that meets most of the design objectives. Therefore, it was evaluated in terms of reactivity feedback coefficients and feasibility of control by direct leakage.

The results of the coolant void coefficient (VC) calculations are shown in Figure 4.2.2-8. The VC is negative through the whole range of possible coolant void fractions from 0 to 100% void. This very important feature can be attributed again to the large impact of neutron leakage on the core reactivity. Voiding in the coolant hardens the spectrum and increases the reactivity of the fuel but this is totally offset by the increased leakage of fast neutrons.

The fuel temperature coefficient was found to be very slightly positive – about 0.1 pcm/K. This positive reactivity effect is expected to be offset by the thermal expansion of fuel which is always negative and it is also a prompt fuel temperature feedback mechanism. Addition of some fertile isotopes Th-232 or U-238 to the fuel can potentially improve the Doppler temperature coefficient.

The estimation of the effective delayed neutron fraction (β -eff) and prompt neutrons lifetime (Λ) resulted in values of about 0.0025 and 0.08 μ sec respectively. The estimation of β -eff was based on the β -eff values of individual isotopes in the fuel and their relative contribution to the total power. This is a conservative estimation because delayed neutrons are born with lower energies and therefore will leak less than prompt neutrons in the finite dimensions system. The values of β -eff and Λ are relatively small and therefore rather fast reactor kinetics is expected in transients. Careful evaluation of the reactor control and safety mechanisms is required for the feasible reactor design. The β -eff value can be slightly improved by addition of U-238 isotope with very

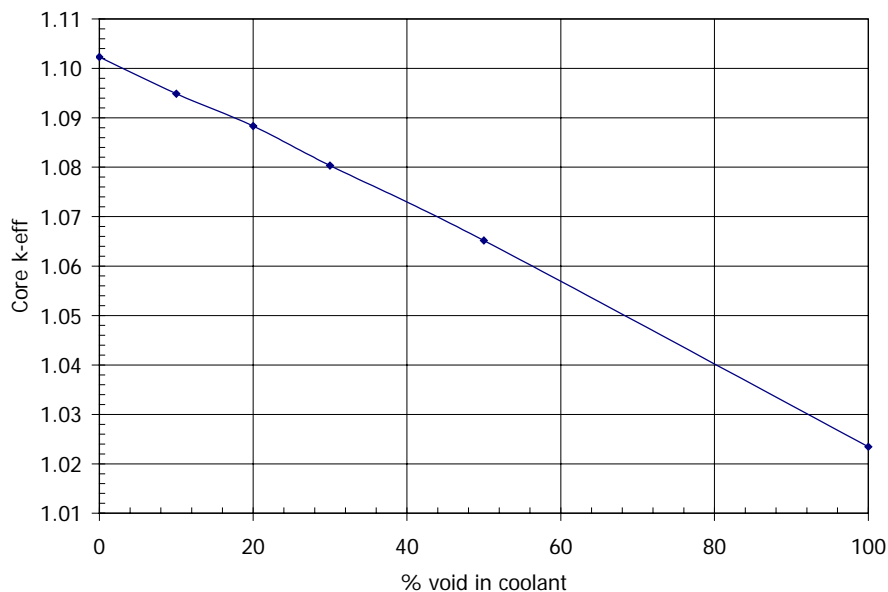


Figure 4.2.2 – 8 Coolant Void Coefficient.

high β -eff into the fuel. Another potential problem with the current reactor design is the submersion of the reactor in water in case of the accident and crash of the launch vehicle carrying the power unit into the ocean. The reactor core of the current design will be supercritical if surrounded with water.

Case 21 in Tables 4.2.2-1 and 4.2.2-2 demonstrates the potential feasibility of the reference core control by the direct leakage. All BOL core reactivity can be suppressed for the reactor with 6 cm axial reflectors and the radial reflector with 50% of its nominal density.

Environmental Safety Assessment

The major disadvantage of using Pu fuel in space power systems is the general public concerns over the potential environmental hazard in case of an accident. If an accident occurs during the launch, the space power system may lose its structural integrity and this, in turn, may lead to the introduction of some radioactive material into the environment. The launch of the “Cassini” [11] spaceprobe in 1997 was accompanied by fierce public opposition because the spacecraft used three Pu radioisotope powered thermo-electric generators (RTG). Considerable effort by the NASA to prepare a detailed environmental safety report and the last minute intervention of high government officials enabled the Cassini launch as scheduled.

The RTGs are powered by the energy released in natural radioactive decay of Pu-238 isotope which has a half life of about 87 years. The Cassini spacecraft power system utilizes about 30 kg of Pu with over 80% of which is Pu-238. The total output of the Cassini power system is about 1 kW electric. In comparison, the power system proposed in this study (molten salt cooled fast reactor – MSFR) uses about 50 kg of Pu but generates considerably higher power (~ 4 MWe). The MSFR fuel is of a reactor grade Pu quality and it is much easier to obtain and therefore cheaper than Pu with high Pu-238 content. The reference RG Pu composition used for the MSFR design corresponds to a typical commercial pressurized water reactor (PWR) spent fuel with 50 MWd/kg burnup after 10 years of cooling. The RG Pu and RTG Pu isotopic compositions are summarized in Table 4.2.2-3.

A number of calculations were performed to evaluate the environmental impact of the Pu release in case of an accident during the launch of MSFR system and compare it with the corresponding Cassini numbers. The calculations were performed using the data from the ORIGEN2 [9] radioactive decay data libraries and ICRP recommended dose coefficients [12].

The results of this evaluation are reported in Tables 4.2.2-4 and 4.2.2-5. The results confirm that the MSFR and Cassini RTGs have comparable chemical and radiological hazard indices even in the absolute comparison. If the numbers are normalized per unit of power generated by each system (Table 4.2.2-5), the MSFR has clear advantage over RTGs.

Table 4.2.2 – 3 Pu Isotopic Composition

| | Cassini | MSFR |
|--------|---------|-------|
| Pu-238 | 84.1 | 3.18 |
| Pu-239 | 13.5 | 56.35 |
| Pu-240 | 1.9 | 26.62 |
| Pu-241 | 0.4 | 8.02 |
| Pu-242 | 0.1 | 5.83 |

Table 4.2.2 - 4 Environmental Hazard Characteristics Comparison

| | Cassini | MSFR |
|--|----------|----------|
| Total Pu mass, kg | 28.8 | 50 |
| Pu238, kg | 24.2 | 1.6 |
| Pu239, kg | 3.9 | 28.2 |
| Pu240, kg | 0.5 | 13.3 |
| Pu241, kg | 0.1 | 4.0 |
| Pu242, kg | 0.0 | 2.9 |
| Activity, Ci | 4.26E+05 | 4.45E+05 |
| Radioactive Ingestion Hazard Index, Sv | 3.07E+09 | 3.31E+08 |
| Chemical Ingestion Hazard Index, m ³ H ₂ O | 3.59E+07 | 6.25E+07 |

Table 4.2.2 - 5 Environmental Hazard Characteristics per Unit of Power Output

| | Cassini | MSFR |
|---|----------|----------|
| Activity, Ci/kWe | 5.32E+05 | 1.11E+02 |
| Ingestion Radiotoxicity Hazard Index, Sv/kWe | 3.84E+09 | 8.28E+04 |
| Chemical Ingestion Toxicity Hazard Index, m ³ H ₂ O/kWe | 4.49E+07 | 1.56E+04 |

Summary and Conclusions

An evaluation and preliminary design of 11 MW_{th} space reactor have been performed. The reactor is a part of high electric power supply for the spacecraft propulsion system that is capable of fast transfer of large payloads from Earth orbit to Mars orbit.

Thermal and fast reactor options were evaluated.

The thermal system with Am-242m based fuel was found to be feasible. Am-242m fuel can achieve high burnup (30 a/o and higher) while maintaining the total HM mass in the reactor on the order of 20 kg. However, relatively high enrichment of Am-242m in Am-241 are required implying the isotopic rather than chemical separation technologies have to be used. This greatly decreases the attractiveness of this fuel and increases its costs. In addition, very large mass of moderator (a number of MT) is required for feasible reactor design. Lastly, the BOL reactivity of the core with Am-242m fuel is very high which will require sophisticated reactor control mechanisms.

As a result, fast spectrum reactor was found to be more attractive because of the much smaller core mass and control flexibility.

The preliminary reactor design description is summarized in Table 4.2.2-6. Figure 4.2.2-9 shows schematic view of the reactor core and honeycomb fuel elements.

Table 4.2.2 – 6 MSFR Core Description

| | |
|-------------------------|------------------------------------|
| Power | 11 MWth |
| Core Dimensions | 20×20×20cm |
| Total mass | 185 kg |
| Reflector thickness | 6 cm |
| Reflector material | Zr3Si2 |
| Coolant | (50:50 NaF-ZrF4) molten salt |
| Coolant volume fraction | 40v/o |
| Fuel | RG Pu carbide |
| Fuel volume fraction | 55 v/o |
| Fuel element geometry | plates, arranged in honeycomb grid |
| Cladding | Nb based refractory alloy |
| k-eff BOL | 1.10 |
| EOL fuel burnup | 12 a/o |
| Core lifetime | 570 EFPD |

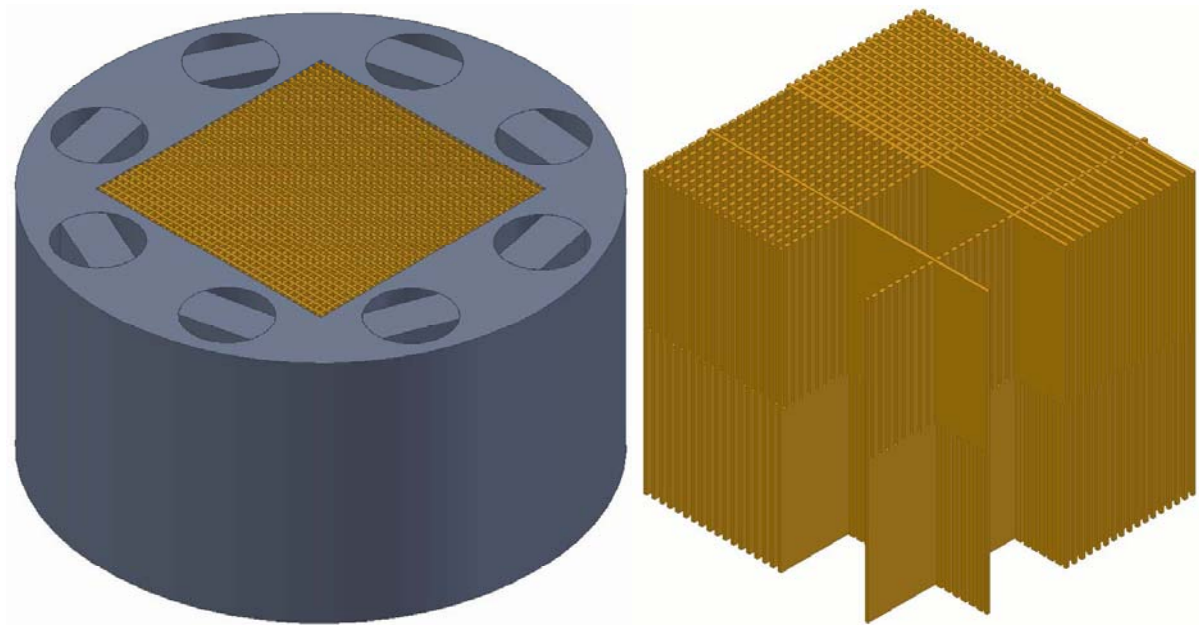


Figure 4.2.2 - 9 MSFR and Honeycomb Fuel Elements Grid.

The proposed reactor is a molten salt cooled fast reactor (MSFR) design is very compact and has very small mass. It can be controlled entirely by direct leakage. The reactor has negative coolant void coefficient. The fuel temperature coefficient is slightly positive but it is expected that fuel thermal expansion will override the Doppler effect and bring the total prompt fuel temperature coefficient to the negative value.

Relatively small delayed neutron fraction and prompt neutrons lifetime were estimated implying fast reactivity transients. Addition of some U-238 to the fuel can improve Doppler coefficient and β -eff.

Reactor criticality in the case of a water submergence accident is another open issue that will have to be addressed in the future.

The impact on the environment of the Pu release from MSFR in case of an accident was found to be comparable to one of the Cassini [12] RTG power system.

4.2.3 References

- [1] *CRC Handbook of Chemistry and Physics*, (3rd Electronic Edition), D.R. Lide, Ed., CRC Press, 2000.
- [2] D.I. Poston, "Nuclear Design of the SAFE-400 Space Fission Reactor," *Nuclear News*, ANS, December 2002.
- [3] "Table of Nuclides," <http://www2.bnl.gov/ton/>, Nuclear Data Evaluation Lab, 2002.
- [4] Y. Ronen, M. Aboudy, D. Regev, "A Novel Method for Energy Production Using ^{242m}Am as a Nuclear Fuel," *Nucl. Technol.*, 129, 3, 2000.
- [5] Y. Ronen, E. Shwageraus, "Ultra-Thin Am-242m Fuel Elements in Nuclear Reactors," *Nuclear Instruments and Methods in Physics Research A*, 455, 442-451, 2000.
- [6] M.Edenius, K.Ekberg, F B.H.orssen, D.Knott,"CASMO-4, A Fuel Assembly Burnup Program: User's Manual," STUDSVIK/SOA-95/1, Studsvik of America, Inc., 1995.
- [7] J. F. Briesmeister Ed., "MCNP - A General Monte Carlo N-Particle Code, Version 4C," Los Alamos National Laboratory, LA-13709-M, March 2000.
- [8] Xu Z., Hejzlar P., Driscoll M.J., and Kazimi M.S., "An Improved MCNP-ORIGEN Depletion Program (MCODE) and Its Verification for High burnup Applications," PHYSOR 2002, Seoul, Korea, October 7-10, 2002.
- [9] "RSICC Computer Code Collection – ORIGEN 2.1, Isotope Generation and Depletion Code Matrix Exponential Method," CCC-371, Oak Ridge National Laboratory, Oak Ridge, Tennessee, Revised version, May 2002.
- [10] R. R. Gouw, "Nuclear Design Analysis of Square-Lattice Honeycomb Space Nuclear Rocket Engine," M. Eng. Thesis, University of Florida, Gainesville, FL, 2000.
- [11] <http://saturn.jpl.nasa.gov/>
- [12] "ICRP Publication 68: Dose Coefficients for Intakes of Radionuclides by Workers: A report of a Task Group of Committee 2 of the International Commission on Radiological Protection," Edited by ICRP, 0-08-042651-4, 1995.

4.3 THERMO PHOTOVOLTAIC (TPV) PRIMER

4.3.1 Overview

The power conversion unit for the space reactor has been designed to use thermo photovoltaic (TPV) cells. TPV cells offer several advantages, including the following items.

1. Generate DC electricity, which is needed by electric propulsion technologies.
2. High power generation density ($2 \text{ W}_e/\text{cm}^2$).
3. High efficiency (40%).
4. No moving parts. This feature improves the system reliability and lowers the maintenance needed.
5. Simplicity.
6. Lightweight.

In this section, TPV technology is introduced. The reason for choosing TPV conversion is explained. The design parameters will be justified. At the end of this section, the dimensions of the TPV collector in our design will be presented, as well as the calculation of armor weight.

4.3.2 Introduction of TPV

Before introducing thermophotovoltaic cells, we should describe photovoltaic cells and their working principle. An everyday application of photovoltaic cells is solar cells, which are used to convert incident sun light into electricity. TPV cells are similar to solar cells. They convert thermal radiation from a heat source into electricity.

Operation principle of solar cells

The basic structure of a typical solar cell is shown in Figure 4.3.2-1. Light enters the device through a layer of material called the antireflection layer. The function of this layer is to trap the light falling on the solar cell and to promote the transmission of this light into the energy-conversion layers below. The photovoltaic effect, which causes the cell to convert light directly into electrical energy, occurs in the three energy-conversion layers below the antireflection layer. The first layer is the top junction layer in Figure 4.3.2-1. The next layer is the core of the device; which is the absorber layer. The last of the energy-conversion layers is the back junction layer.

There are two additional layers that must be present in a solar cell. They are the electrical contact layers. There must be two such layers to allow electric current to flow out of and into the cell. The electrical contact layer on the face of the cell where light enters is generally present in a grid pattern and is composed of a good conductor such as a metal. The grid pattern does not cover the entire face of the cell since grid materials are generally not transparent to light. The back electrical contact layer has no such restrictions. It need simply function as an electrical contact and thus covers the entire back surface of the cell.

The conversion of light to electricity (photovoltaic effect) depends on the electronic structure of solar cells, with two or more layers of semiconductor material in the absorber layer that can absorb photons. The photons raise the energy level of the electrons in the semiconductor, exciting some to jump from the lower-energy valence band to the higher-energy conduction

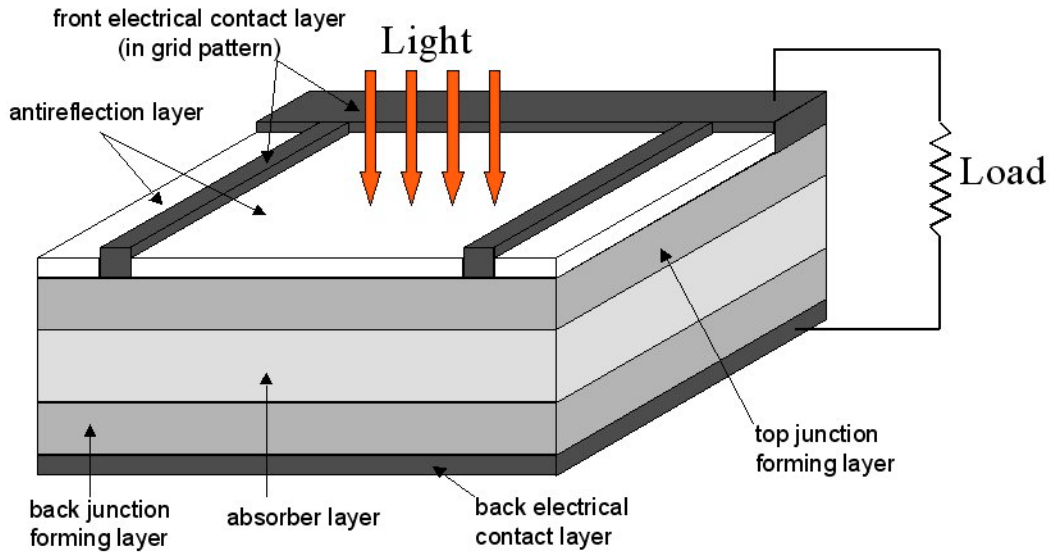


Figure 4.3.2 - 1 A Typical Solar Cell Structure.

band. The electrons in the conduction band and the holes they have left behind in the valence band are both mobile and can be induced to move by a voltage. The electron motion, and the movement of holes in the opposite direction, constitutes an electric current. The force that drives electrons and holes through a circuit is created by the junction layers of two dissimilar semiconducting materials, one of which has a tendency to give up electrons and acquire holes (p-type) while the other accepts electrons (n-type). For an n-type semiconductor, the Fermi level* is near conduction band; but for p-type, the fermi level is near valance band. Once they are put together to form a p-n junction, there is a potential difference at the junction because two fermi levels have to align at the same level. The potential difference is the photovoltaic effect, which is the key point to form solar cell. The electronic structure that permits this is the band gap (E_g); which is equivalent to the energy difference between valence band and conduction band.

The magnitude of this gap is important. Only photons with energy greater than that of the band gap can excite electrons from the valence band to the conduction band; therefore, the smaller the gap, the more efficiently light will be converted to electricity. The gap cannot be too small, because the electrons and holes then find it easy to recombine, and a sizable current cannot be maintained. Therefore, the band gap defines the theoretical maximum efficiency of a solar cell.

These energetic, free electrons move in the direction forced on them by the built-in electric field. They are collected by the electrical contact layers for use in an external circuit where they can do useful work. This is the basic operating principle of solar cells.

Semiconductors can absorb all incident visible light in thicknesses of about one-hundredth of a centimeter or less; consequently, the thickness of a solar cell can be of this size.

* Fermi level is a concept of probability, it is the energy level where the probability is 50% to find an electron at this level.

Operation principle of TPV cells

The working principle of TPV cells is similar to that of solar cells. Rather than converting visible light to electricity as in a solar cell, TPV converts conventional source of radiant energy, such as a nuclear fission power in our design, to electricity in low bandgap cells that surround the heat source. In the case of 1000°K to 2000°K radiator operating temperature, the incoming radiation is in the infrared (IR) part of the spectrum, while in a solar cell, the radiation is receiving from the sun at a temperature of about 6000°K and the incident radiation is shorter-wavelength visible light. Therefore, the base material of TPV cells should be an infrared-sensitive material, whose bandgap is smaller than that of solar cells.

TPV was originally intended to improve the conversion efficiency of sunlight in photovoltaic cells because of insufficient photon energy ($h\nu < E_g$) of the long-wavelength range of the solar spectrum. The idea of TPV consists in generating a spectrum adapted to the band gap of the cell material. The radiation is emitted by a radiator, and the energy loss in the long-wavelength range is minimized either by optical filtering or by selective emission (Figure. 4.3.2-2). When the filtered thermal radiation hits the TPV cells, the photovoltaic effect occurs as in solar cells, and direct current electricity is generated. The residual radiation heat can be either dissipated from the surface of the back contact layer of TPV cells or bounced back to the radiator, which can enhance the thermal power of the radiator and improve the energy conversion efficiency.

The function of the filter is to shape the incoming radiation spectrum with a cut-off wavelength adapted to the bandgap of the TPV cell material. Without filtering, the natural radiation spectrum is a blackbody or grey-body spectrum, and the TPV efficiency turns poor. Matching the radiative emission spectrum to the conversion bandgap of the TPV device is the key to achieving the desired power density and efficiency. [2, 10] After filtering, the radiation towards TPV cells is that with energy higher than the bandgap of the TPV material ($h\nu > E_g$). This spectral-shaping is also generally employed to recycle unusable energy back to the radiator, thus improving conversion efficiency. In addition, the absence of low-energy photons prevents heating of the TPV cell through thermalization of excited carriers (i.e. free electrons), which needs more cooling power. The layer of filter could be positioned anywhere between the radiator and the TPV cells.

The most obvious difference between thermophotovoltaics and conventional photovoltaics is that in TPV one has access to, and control over, the source.

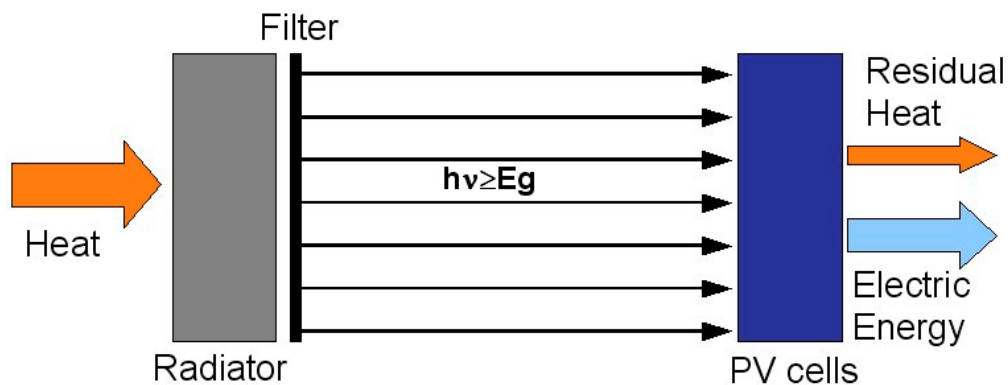


Figure 4.3.2 – 2 TPV Energy Conversion.

4.3.3 The Chosen Material for TPV Cells

Gallium antimonide (GaSb) TPV cells are believed to be the most suitable choice for modern low-bandgap TPV generators, both in terms of efficiency and simplicity of the diffusion technology used (refs. 2 and 9). GaSb is a member of the III-V family, a new material that was developed in the early 1990s. These III-V compounds and alloys are high-quality, low-bandgap semiconductor converters for TPV cells. The availability of the III-V material created a re-emergence of interest in TPV technology in 1990s (ref. 10).

GaSb has an excellent low bandgap energy (0.72 eV). Many papers have been published [2, 3, 5, 7 and 9] devoted to research on GaSb as a base material of TPV cells. Its performance as a TPV converter will be presented in the following section.

4.3.4 Structure of TPV Cells

A TPV cell has the same structure as the solar cell shown in Figure 4.3.2-1. Figure 4.3.4-1 is a cross section of a heterostructure monolithic tandem TPV cell based on GaSb, which is reported in ref. 3. It could be regarded as a typical configuration of a GaSb TPV cell. From Figure 4.3.4-1, one can learn that the antireflection layer is made of $ZrS+MgF_2$. Different materials are used in front and back electrical contact layers, but they are based on gold, which is one of the best electrical conductors.

From the dimensions denoted on Figure 4.3.4-1, one knows that TPV cells are very thin, on the order of a micrometer. Therefore, in our design, the thickness and weight of the TPV collect can be ignored compared to the armor necessary to support and protect the collector.

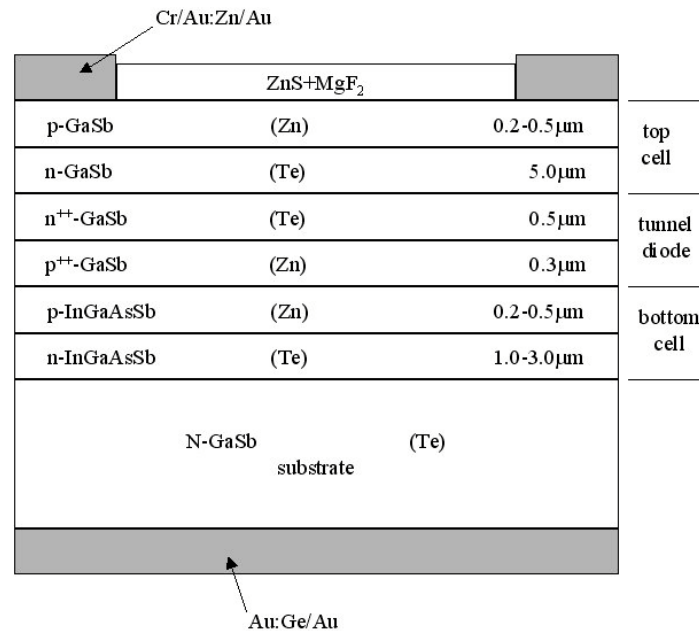


Figure 4.3.4 – 1 Cross Section of the Monolithic Two-Junction Two-Terminal TPV Cell.

4.3.5 Filter and Spectral Shaping

Some materials radiate in relatively narrow wavelength bands. Their emissivities are low outside the band and high within the band. If the incident spectrum could be represented by a delta function, the conversion efficiency should be high.

Special material suitable as a filter for GaSb TPV cells, cobalt-doped MgAl_2O_3 , has been reported. [12]. The emission band corresponds well to the region of spectral response of GaSb. The attraction of this material is that the power radiated is much more than that radiated by the highly selective rare-earth oxides (such as Yb_2O_3), which are general filter materials for low-bandgap TPV applications. In other words, using cobalt-doped MgAl_2O_3 , the energy loss in spectral-shaping filter is lower than other general filter material for GaSb TPVs.

4.3.6 Layers

Even with the perfect spectral control of incident photons with cut-off at the energy of the specific bandgap, the TPV cell still only has an inherent conversion efficiency at about 40% or less. Most photons with high energy are lost. TPV cell absorption is more sensitive to radiation with energy at about its bandgap. Consequently, the radiation penetrating TPV cells are those with higher energy and are treated as waste heat. To improve the system efficiency, a concept has been proposed to utilize these photons. A layer of TPV cell array made of different material, with higher bandgap, can be installed behind and parallel to the main TPV collector to convert the higher-energy waste radiations. Low-cost silicon (with bandgap of 1.16eV) solar cell would be a good choice for this purpose.

4.3.7 Photon Recirculation

The need to return the sub-bandgap photons after filtering to the radiator to maximize the efficiency of the system is important. Without recirculation, efficiencies are low because the sub-bandgap photons simply cause heating of the TPV cells and the support structure. It has been shown that the power density is unaffected by the presence or absence of recirculation. However, the efficiency of the converter is affected. [10]

One may view photon recirculation as offering the opportunity to use the same amount of fuel to heat the radiant surface to a higher temperature, or to use less fuel to heat the surface to the same temperature.

The most successful design developed for photon recirculation to date uses a concept known as back-surface reflection (BSR). [13] The principle is that the sub-bandgap photons pass through the device layers with only minimal absorption, through the substrate to the back contact layer (see Figure 4.2.2-1), by which they are reflected back along the same path to the radiator. A typical structure might consist of an InGaAs device, with a bandgap of about 0.6 eV, grown mismatched on an InP substrate. That is the reason that a typical TPV cell design uses multi-layer hetero-structure design as shown in Figure 4.3.4-1.

4.3.8 Performance of TPV -- Efficiency and Power Density

In Ref. 5, a realistic estimation of conversion efficiency and power density of a GaSb TPV system have been given. Besides thermodynamic limitation, the mechanism of radiation recombination, Auger (free electron) recombination and bandgap narrowing are considered. Under the spectrum of a 1500°K blackbody radiator being shaped by a perfect edge filter, having a cut-off frequency at E_g/h , the ideal GaSb TPV cell has the following performance:

1. Energy conversion efficiency = 44.0%
2. Power generation density = $2.27 \text{ W}_e/\text{cm}^2$.

These values are quite close to our design values, which are 40% efficiency and $2.0 \text{ W}_e/\text{cm}^2$ power density. The authors of ref. 5 estimated that the resulting performance values are realistically attainable within the next few years if a sufficient development effort is undertaken.

In other research papers [2, 10, 11], more or less the same prediction and conclusion as above have been reported.

4.3.9 Space Power TPV Energy Conversion System

To sum up, the base semiconductor material of TPV collector is chosen to be gallium antimonide (GaSb), the spectral-shaping filter is cobalt-doped MgAl_2O_3 , and the energy conversion efficiency and power generation density are 40% and $2 \text{ W}_e/\text{cm}^2$, respectively.

In our design, the TPV collector array is attached to the rocket armor receiving the thermal radiation emitted from the central internal radiator. The spectral-shaping filter is basically covered on the TPV collector with tiny clearance, which is separated by supporting material.

Heat rejection to an available heat sink is required to maintain the TPV cells at temperature low enough for adequate energy conversion performance. As described above, the principle of the solar cell and TPV is based on the semiconductor p-n junction. In the other words, once the junction is not a p-n junction anymore, it cannot be a solar cell or TPV. However, the material is metallized (become conductor) when the temperature is too high. The fermi level of p-type semiconductor is almost the same with the fermi level of n-type and the potential difference at junction disappears. This effect makes the solar cell and TPV failed. The limit of TPV cell temperature is about room temperature, because the TPV is used to absorb IR, which the wavelength is longer than visible light. Therefore, the energy gap of either the p-type or n-type semiconductor (i.e. bandgap) has to be small. Once the temperature increases beyond room temperature range, the TPV cell is metallized. For solar cell, the temperature limit is higher.

An important potential heat loss mechanism is direct parasitic heat transfer from the radiator surface to the TPV cells. Convective or conductive heat transfer through the medium filling the space between the radiator and the TPV cells may cause a significant efficiency, because this heat only heat up the TPV cells. To minimize this heat loss, vacuum, low-thermal conductivity gases or transmissive shields should be used in the gap.

The diameter of TPV collect is 4.24 meters. According to the designed power density ($2 \text{ W}_e/\text{cm}^2$), and rated electric power (4 MW_e). The length of TPV collector is 15 m.

For a conservative estimation of the armor mass, 18 meters of total armor length is assumed to cover TPV collector (15 m), reactor and shielding. 7 kg/m^2 of armor density is assumed (ref. 8). The diameter of rocket armor is assumed as 4.3 m (a little bigger than TPV diameter, 4.24 m). Thus, including the top and bottom cover, the conservative estimated armor weight is calculated to be approximately 2 MT.

4.3.10 References

- [1] Nelson, R.E., "A Brief History of Thermophotovoltaic Development," *Semiconductor Science and Technology*, 18 (2003), S141-S143.
- [2] Bett, A.W. and O.V. Sulima, "GaSb Photovoltaic Cells for Applications in TPV Generators," *Semiconductor Science and Technology*, 18 (2003), S184-S190.
- [3] Mauk, M.G. and V.M. Andreev, "GaSb-related Material for TPV Cells," *Semiconductor Science and Technology*, 18 (2003), S191-S201.
- [4] Fraas, L.M. et al., "Thermophotovoltaic System Configurations and Spectral Control," *Semiconductor Science and Technology*, 18 (2003), S165-S173.
- [5] Luther, J., et al., "Efficiency and Power Density Potential of Thermophotovoltaic Energy Conversion Systems Using Low Bandgap Photovoltaic Cells," Proceedings of the 10th Workshop on Quantum Solar Energy Conversion (QUANTSOL'98), March, 1998.
- [6] Gabler, H., "Thermophotovoltaic Generation of Electricity," Proceeding of EuroSun'96, 1996.
- [7] Andreev, V.M., et al., "Tandem GaSb/InGaAsSb Thermophotovoltaic Cells," Proceedings of the 26th Photovoltaic Specialists Conference, Anaheim (USA), September 1997.
- [8] Personal communication with Professor Mohamed S. El-Genk, Chemical and Nuclear Engineering, Director, Institute for Space and Nuclear Power Studies, University of New Mexico.
- [9] Sulima, O.V., et al., "GaSb-, InGaAsSb-, InGaSb-, InAsSbP-, and Ge-TPV Cells with Diffused Emitters," 29th IEEE Photovoltaic Specialists Conference, 2002.
- [10] Coutts, T.J., "A Review of Progress in Thermophotovoltaic Generation of Electricity," Nat. Renewable Energy Lab., USA, *Renewable & Sustainable Energy Reviews*, Vol. 3, No. 2-3; June-Sept., p. 77-184, 1999.
- [11] Baldasaro, P.F., "Thermodynamic Analysis of Thermophotovoltaic Efficiency and Power Density Tradeoffs," *Journal of Applied Physics*, Vol. 89, No. 6, 2001.
- [12] Ferguson, L, and L. Fraas, "Matched Infrared Emitters for Use with GaSb TPV Cells," Proceeding of Third NREL Conference on the Thermophotovoltaic Generation of Electricity, 1997.
- [13] Ward J.S., et al, "A Novel Design for Interconnects in a TPV Converter," Proceeding of Third NREL Conference on the Thermophotovoltaic Generation of Electricity, 1997.

4.4 MSFR THERMAL HYDRAULICS

4.4.1 Introduction

The main goal of the thermal hydraulic analysis is to prove the feasibility of the core with respect to the thermal margins. The target is to keep the fuel centerline temperature below 2000K. The core inlet temperature is 1550K and outlet temperature is 1600K.

The detailed geometry of the core is mainly determined by the thermal hydraulic considerations. As the MSFR is a fast reactor the only parameters given by the reactor physics analysis are the volume fraction of fuel, coolant and cladding. The thermal power for the core is defined by the requirement of 4 MW_e of DC from the TPV collect. Given the efficiency of the TPV collector of 40% (electric power from radiant power) and assumed thermal losses of the system on the order of 1 MW translates to 11 MW of core thermal power. This power was used in the following analysis.

4.4.2 Analysis

The coolant is a molten salt NaF and ZrF₄ mixed 50 to 50 atomic percent. The specific heat of this particular salt is 880.65 J/kgK. From the thermal power, inlet and outlet temperature and specific heat the mass flow rate is determined to be 249.81 kg/s.

The total mass of fuel is defined by the total energy requirement on the space trip and was estimated to 50 kg. The fuel density is 13550 kg/m³ and thus the required fuel volume is 36.9 cm³. It is immediately apparent that the core will have a very high power density. The fuel volumetric heat generation in the fuel is 271 kW/cm³. With such high power density the choice of plate type fuel is obvious because of the very large surface to volume ratio. In addition the plates are arranged in a honeycomb array in order to increase the heat transfer surface area. In order to simplify the manufacturing process and due to small effect on the neutronic performance the core has a cubical shape instead of the standard cylindrical shape. The basic cell for the thermal hydraulic analysis is depicted Figure 4.4.2-1. An investigation of honeycomb cores for nuclear thermal rockets was conducted at the university of Florida which indicates that the plate thickness can be as low as 1 mm without significant manufacturing problems [1]. The core dimensions are given from the mass of fuel and the fractions of coolant, fuel and cladding. The side of the cube a is given from:

$$a = \sqrt[3]{\frac{m_f}{\rho_f f_f}} = 195 \text{ mm}$$

where m_f is the mass of fuel, ρ_f is the fuel density and f_f is the volumetric fraction of fuel.

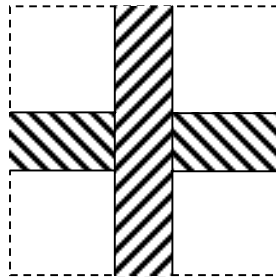


Figure 4.4.2 – 1 Unit Cell.

The number of plates used in the core is 70. There are 35 plates in each direction. The pitch of the plates is 5.5 mm. The plate thickness is given from the fraction of coolant, fuel and cladding, which is preserved within the basic cell. The plate thickness t can be calculated from:

$$t = \frac{\frac{4a}{n_{pl}} - \sqrt{\left(\frac{4a}{n_{pl}}\right)^2 - 4\left(\frac{2a}{n_{pl}}\right)^2(1-f_c)}}{2} = 2.05 \text{ mm}$$

where n_{pl} is the number of plates, f_c is the coolant fraction.

The other properties of the molten salt at the medium core temperature of 1575K are:

| | |
|----------------|----------------------------|
| Density | 2579.28 kg/m ³ |
| Viscosity | 9.999·10 ⁻⁴ Pas |
| Conductivity | 2.25 W/mK |
| Prandtl number | 0.39 |

The average molten salt velocity v within the core can be calculated as:

$$v = \frac{\dot{m}}{a^2 f_c \rho_c} = 6.39 \text{ m/s}$$

where \dot{m} is the mass flow rate of the molten salt, ρ_c is the density of the molten salt.

And the equivalent hydraulic diameter d_{eq} is:

$$d_{eq} = \frac{4p^2 f_c}{4(p-t)} = 3.52 \text{ mm}$$

where p is the plate pitch.

This results in the Reynolds number of 57,972.83. The heat transfer coefficient h for molten salt is given by [2]:

$$h = 955 \frac{v^{0.28}}{d_{eq}^{0.2}} = 13032.32 \text{ W/mK}$$

The total heat transfer surface area A_h of the core is:

$$A_h = 4(p-t)n_{pl}^2 a = 13.43 \text{ m}^2$$

Thus, the average heat flux q'' is

$$q'' = \frac{P}{A_h} = 819.35 \text{ kW/m}^2$$

where P is the core thermal power.

In a detailed thermal hydraulic analysis the temperature profile within the core would be calculated based on the power profiles. The temperature of the coolant, cladding and the temperature profile within the fuel would be calculated. However, since the power profiles are not available at present a simplistic analysis was performed instead.

The power peaking in fast reactors is in general low. For this analysis we selected 1.5 as the maximum deviation from the average value of the heat flux. This is a conservative assumption as fast reactor flux peaking values are typically much smaller. In addition, the cladding temperature was calculated at the end of the core where the coolant temperature is the highest. Using this cladding temperature the fuel centerline temperature was calculated. Using this methodology the cladding temperature t_{fo} is:

$$t_{fo} = t_{c\max} + \frac{1.5q''}{h} = 1694.3 \text{ K}$$

where $t_{c\max}$ is the maximum coolant temperature, in this case 1600 K.

Solving the Fourier equation of the heat conduction in a slab with a uniform heat generation gives the following formula for the temperature at the fuel center line t_{cl}

$$t_{cl} = t_{fo} + \frac{1.5q'''(\sqrt{2}t)^2}{2k_f} = 1767.32 \text{ K}$$

where q''' is the volumetric heat generation rate, k_f is the fuel thermal conductivity, in this case 16 W/mK

In the fuel centerline temperature the effect of cladding was neglected as the cladding thickness is very small and does not significantly affect the result. As can be seen from the above feasibility calculations the fuel center line temperature can easily be maintained below 2000 K, which was set as our current thermal margin. This was based on the melting temperature of UC, which is 2673 K. The margin of more than 600 K was left for the transient and accident situations, which were not analyzed in this work.

Our calculations show that the margin left for these transient is, in fact, even higher. This also indicates the possibility of increasing the thermal power that can be extracted from this core. This can be achieved by reducing the safety margin or by reducing the plate thickness, which would result in higher heat transfer area and thus lower temperatures within the core.

Another important part of the thermal hydraulic design is evaluation of pressure drop and pumping power. To evaluate the pressure one must calculate the friction factor. The flow regime is turbulent therefore the Colebrook equation, which also incorporates the wall roughness, was used. The friction factor f can be iteratively obtained from:

$$\frac{1}{\sqrt{f}} = -2 \log \left(\frac{\lambda / d_{eq}}{3.7} + \frac{2.51}{\text{Re} \sqrt{f}} \right)$$

where λ is the depth of surface protrusions, for commercial steels it is 0.0045 cm, this number was used in the analysis even though it can be expected that it will be less.

The value of friction factor that satisfies the above equation for our conditions is 0.042. The pressure drop Δp can now be calculated by the usual means as:

$$\Delta p = f \frac{a}{d_{eq}} \frac{\rho_c v^2}{2} = 122.73 \text{ kPa}$$

And the pumping power P_p is:

$$P_p = \Delta p f_c a^2 v = 11.89 \text{ kW}$$

Both, the pressure drop and the pumping power have reasonable values. The core hydraulic performance is good. The system is evaluated at full scale power of 4000 kW_e as well as the required power for the first precursor mission (200 kW_e). The results of these calculations are summarized in Table 4.4.2-1.

Table 4.4.2 - 1 Space Power System Characteristics

| | Cargo and Manned Missions | Precursor Mission |
|--|---------------------------|-------------------|
| Electric power (kW _{th}) | 4000 | 200 |
| Thermal power (kW _e) | 11000 | 1928.57 |
| TPV efficiency (%) | 40 | 14 |
| Core mass flow rate (kg/s) | 249.81 | 37.96 |
| Core inlet temperature (K) | 1550 | 1250 |
| Core outlet temperature (K) | 1600 | 1300 |
| Fuel outer temperature (K) | 1694.31 | 1381.04 |
| Fuel centerline temperature (K) | 1767.32 | 1389.16 |
| Pressure drop (kPa) | 122.73 | 3.04 |
| Pumping power (kW) | 11.89 | 0.04 |
| Electric pumping power (kW _e) | 39.62 | 0.13 |
| Core width (mm) | 194.69 | 194.69 |
| Core height (mm) | 194.69 | 194.69 |
| Core length (mm) | 194.69 | 194.69 |
| Coolant volume fraction | 0.4 | 0.4 |
| Fuel volume fraction | 0.5 | 0.5 |
| Cladding volume fraction | 0.1 | 0.1 |
| Thermal losses (kW _{th}) | 1000 | 500 |
| Power density (kW _{th} /l) | 1490.50 | 261.32 |
| Volumetric heat generation rate (kW/m ³) | 2,981,000.00 | 523,000.00 |
| Average heat flux (kW/m ²) | 819.35 | 143.65 |
| Molten salt velocity (m/s) | 6.39 | 0.88 |
| Heat transfer area (m ²) | 13.43 | 13.43 |
| Number of plates (both directions) | 70 | 70 |
| Plate spacing (mm) | 5.56 | 5.56 |
| Plate thickness (mm) | 2.04 | 2.04 |
| Heat transfer coefficient (W/m ² K) | 13,032.32 | 2658.79 |

The overall performance of the investigated core is very promising. The core is also scaleable for the precursor satellite mission. Table 4.4.2-1 summarizes the main core characteristics for the full power 4 MW_e design as well as for the precursor mission 200 kW_e design. The margin left for the transient and accident situation is currently more than 900K. The core pumping power is small compare to the total power produced by the reactor, thus the power consumed by pumps does not significantly reduce the overall power delivered by the system.

4.4.3 Power Conversion System

The power conversion system consists of the nuclear core, pumps, radiator and the TPV collector. For the high power space systems the mass of the radiator usually dominates the total mass of the system. Since the radiator mass is dictated by the gray-body radiation, the radiator mass will decrease with the fourth power of the temperature. The only way to keep the mass of the radiator small is to radiate the heat at very high temperature.

This is difficult with most of the systems as the temperature of the heat rejection is low in order to keep high efficiency of the power conversion cycle. In our case the transfer medium from reactor power to radiant energy requires the rejection of heat at high temperature. The use of TPV conversion approach requires that the reactor system be used only to create the thermal radiation field for the TPV collector. Therefore, the reactor loop serves only to produce and radiate the heat. Thus, the heat is radiated at a very high temperature.

In our case the mid-temperature of the radiator is 1575K and the radiated heat rate is 10 MW. The emissivity for the radiators are in the range of 0.85 to 0.93. In our conservative analysis 0.85 is used. The area of the radiator A_R can be estimated from the black body radiation law as:

$$A_R = \frac{\dot{Q}}{\varepsilon\sigma T^4} = 37.09 \text{ m}^2$$

where \dot{Q} is the total radiated power, ε is the emissivity, σ is the Stefan-Boltzman constant and T is the medium temperature at which the radiator operates.

As we would like the whole space nuclear power system to fit within a cylinder with a 4.5 m diameter and 18 m height, the maximum height of the radiator is 15 m. Because of the very high temperature of the system, the radiant heat losses are considerable. Therefore we want to keep the piping as short as possible. Thus, it was decided to employ the radiator in a form of a annular U-tube. The reason why the U-tube is annular is to minimize the mass of molten salt in the loop. The outer diameter of the U-tube is 39.35 cm, the inner tube diameter is 35.00 cm. The pressure drop and pumping power across the radiator were calculated in the same manner as for the core. The resulting pressure drop is 22.59 kPa and the pumping power required is 2.19 kW. This sets the requirement of 7.29 kW_e for the pump. The radiator is made of titanium, which has a density of 4510 kg/m³. Thus, the weight of radiator can be estimated as:

$$w_R = \pi(d_{out} + d_{in})Ht\rho_{Ti} = 2967.28 \text{ kg}$$

where d_{out} is the outer radiator tube diameter, d_{in} is the inner radiator tube diameter, H is the length of the radiator, t is the wall thickness (in our case 1 cm) and ρ_{Ti} is the density of titanium.

The weight of the molten salt in the radiator is

$$w_{MS} = \frac{\pi(d_{out}^2 - d_{in}^2)}{4} H \rho_{MS} = 1975.42 \text{ kg}$$

The heat radiated from the internal radiator is converted to DC electricity in the TPV collector. The TPV cells are located on the inner surface of armor that protects the whole power system.

The TPV cell principle of operation and performance is described in the TPV Primer chapter. Here only the design calculations are present. The used TPV cells have an efficiency of 40% (i.e., 40% of incident radiant energy will be converted to DC electricity). The TPV cells can safely produce 2 W/cm² of electric power. Therefore it is necessary to keep their active surface large enough and at a safe distance from the internal radiator so that the cells will not get damaged.

For 4 MW_e it is necessary to have 200 m² of the TPV cells. Considering the same height of the TPV cell as the radiator height the necessary TPV cell diameter is 4.24 m. This is still within the envelope of 4.5 m diameter and 18 m height cargo for the known launch vehicle.

Considering that the whole system will be enclosed in armor and using 7 kg/m² as the armor weight the total weight of armor can be estimated from:

$$w_A = 7\pi D \left(\frac{D}{2} + H \right) = 2003.94 \text{ kg}$$

The total mass of the armor and the TPV cells together was taken as 2100 kg. Figure 4.4.3-1 shows the overall layout of the space power conversion system. The flow of the Molten Salt is illustrated with blue arrows.

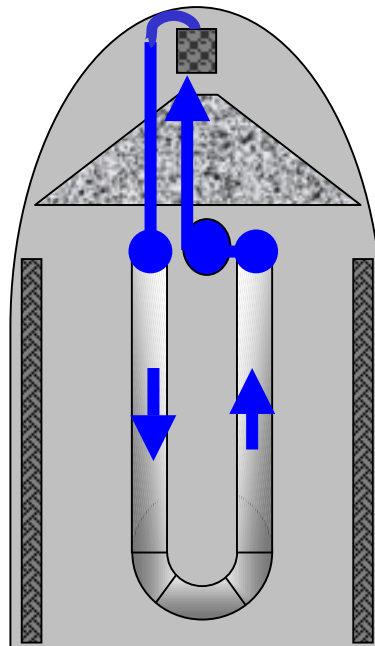


Figure 4.4.3 – 1 Space Power Conversion System.

4.4.4 References

[1] T. Knight, S. Anghaie, J. Plancher and R. Gouw, "Square Lattice Honeycomb Tri-Carbide Fueled Reactor Design for Space Power and Propulsion," Proceedings of ICAPP 03, Cordoba, Spain, 2003

[2] J. Singh, *Heat Transfer Fluids and Systems for Process and Energy Applications*, Marcel Dekker, Inc., New York and Basel, 1985

4.5 PUMP SELECTION FOR MSFR

4.5.1 Introduction

The very high operating temperature of the space nuclear power system imposes severe requirements on pumps. The pumps must be able to operate at high temperatures for an extensive period of time. They should be reliable even though several pumps will be used in parallel to pump the molten salt through the primary system. Extensive thought should be given to the pump powering and control. The high temperatures at which the pumps operate make their design very difficult.

It was decided to use pumps with no moving parts, therefore all mechanical pumps were ruled out. The electromagnetic pumps are the most promising candidates as molten salt is highly conductive they should operate with higher efficiency than, for example, liquid metals. Another possibility is the use of annular linear induction pump.

4.5.2 Comparison

The purpose of this section is not to design the pump or explain the operating principles of electromagnetic or induction pump, but rather survey the pumps used currently in the space program and screen them for use with our space nuclear power system.

Probably the best pump currently available is the thermoelectric electromagnetic pump (TEM) used in the SP-100 system. One of the main advantages of this pump is that it generates its own power from the temperature difference between the hot coolant and the cold radiator. Every TEM pump has its own small radiator. Another big advantage is that this pump is a self-starting pump and self-regulating pump. Its operation is regulated by the temperature of the coolant. Therefore, this pump does not require any additional power and control cabling. The projected lifetime of this pump is 10 years, which is sufficient for our current mission requirements. In SP-100 this pump operates at temperatures 1310 to 1350 K. This is about 300 K below the nominal temperature in our space nuclear power system. However, the precursor mission will use lower temperatures in order to demonstrate the feasibility of this pump. For the subsequent missions the pump will have to be upgraded for higher operating temperature.

The current TEM used for SP-100 has been already tested, thus certain operating experience with this type of pump is available. SP-100 uses lithium as a coolant and for lithium the pump efficiency is on the order of 30%. Figure 4.5.2-1 shows the TEM pump.

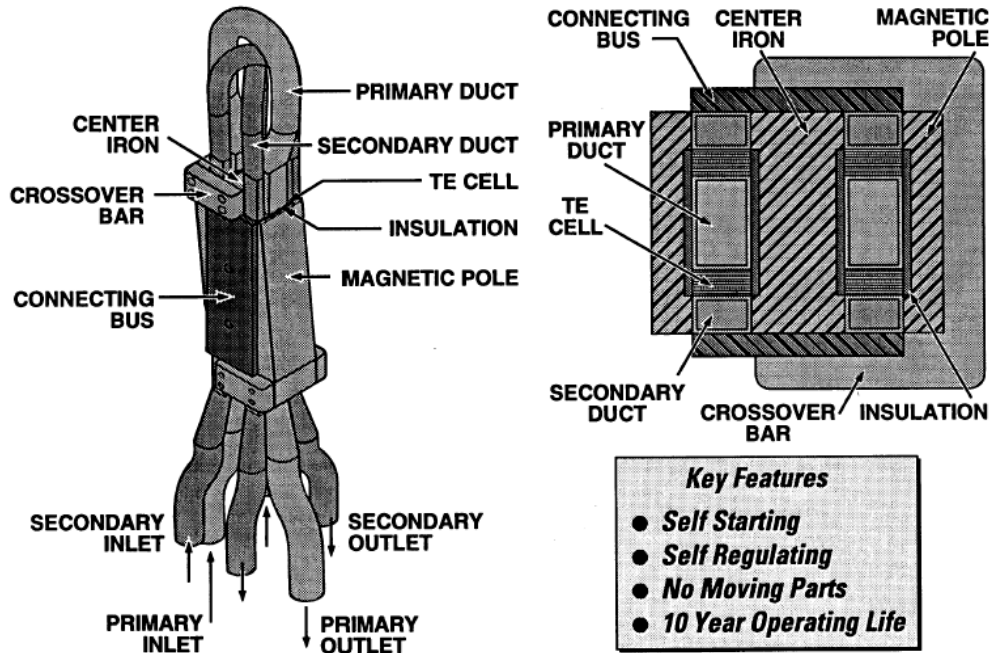


Figure 4.5.2 - 1 TEM Pump [1].

The annular linear induction (ALI) pump has been already tested as well, however their maximum operating temperatures are only ~1100K. They were used to pump lithium, sodium and magnesium. With lithium the pump efficiency was 34%. Figure 4.5.2-2 shows the ALI pump.

ANNULAR LINEAR INDUCTION PUMP EXPERIMENTAL LITHIUM SYSTEM (ELS)

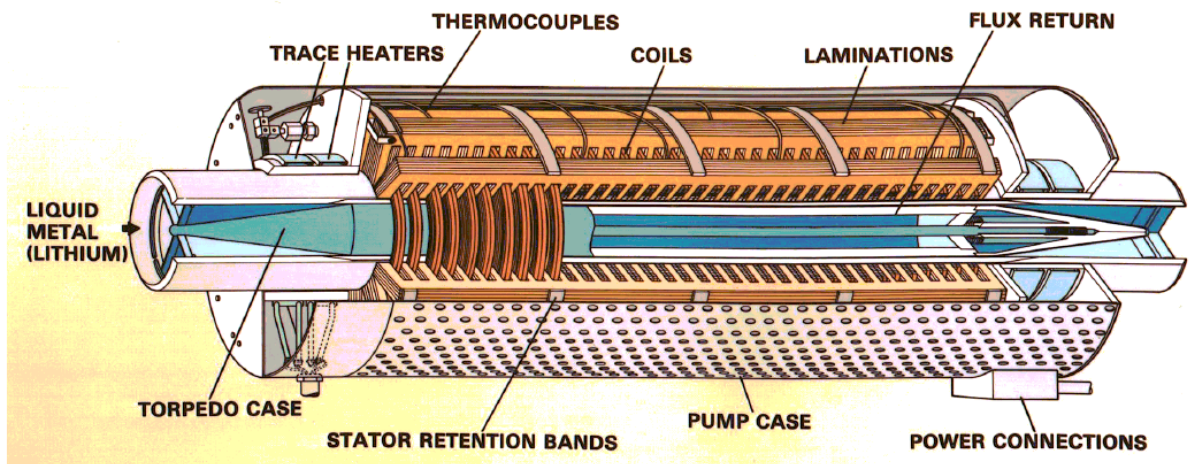


Figure 4.5.2 - 2 ALI Pump [1].

For our system the primary choice is the TEM pump. Efficiency of 30% will be used in order to estimate the electrical pumping power. This section points out the existence of high temperature pumps. The temperatures at which the pumps operate is somewhat lower than the temperatures used in our system, however it is reasonable to expect an improvement of the pump technology in the future, thus the use of high temperature in our system is not unreasonable.

4.5.3 References

[1] Weitzenberg, “LMR Concept Design, Analysis, Technology,” DOE Forrestal, November 21, 2002.

4.6 SHIELDING OF THE MSFR

4.6.1 Introduction

The magnetic belts and the atmosphere surrounding the Earth efficiently protect the planet and its inhabitants against cosmic radiation. Having evolved on the surface, humans are generally not considered to be at an immediate risk due to the penetrating cosmic radiation. However, in space there are no protecting atmospheric or magnetic layers and therefore the intergalactic radiation has become a major issue of concern for human exploration of Mars.

The reason behind the radiation concern during manned missions to Mars is the galactic cosmic rays (GCR). This radiation can be highly energetic and is omnipresent in space. Naturally, NASA spends vast resources on designing space vehicles whose material and interior layout minimizes the radiation exposure for astronauts and radiation-sensitive hardware. Due to the time constraint and lack of expertise, this project does not aim at re-designing the space vehicle’s shield against GCR. Instead of re-inventing the wheel, this mission will simply take for granted that the spacecraft is shielded by the standard mechanisms NASA uses in all space exploration missions. More concisely, these materials include Nextel, Kevlar, beta cloth and aluminum honeycomb [1]. The hydrogen feedstock as well as the water resources on board will naturally be placed in the periphery of the space vehicle in order to maximize the shielding capabilities of these materials.

Since this mission concentrates on the utilization of nuclear technology in space, the space shielding will be directly related to the nuclear power source. In other words, by powering the spacecraft with a nuclear reactor, another hazardous radiation source is added in the direct vicinity of the astronauts. Thus, extra shielding is required to minimize the crew’s radiation exposure.

4.6.2 Key Parameters

There are certain material properties that are characteristic of highly efficient shielding materials. Empirically, it has been found that high electron density per unit mass (gammas shielding) and large neutron cross section per unit mass (neutron shielding) are two desirable attributes [2]. The materials chosen must have cross sections that permit effective neutron moderation and gamma attenuation.

4.6.3 Design Options

There are two types of radiation from a nuclear reactor that is of concern from a human perspective. First, the neutron leakage from the reactor produces a steady current in all directions. As is well known, hydrogen is one of the most efficient neutron moderators [3]. Therefore, a couple of different neutron-stopping options involving hydrogen were evaluated.

Hydrogen Feedstock

The first option considered was to use the hydrogen feedstock for neutron shielding material. This feedstock is brought to Mars in order to enable operation of the ISRU plant since hydrogen is not easily accessible there. Although the hydrogen would provide more than sufficient shielding on the trip to Mars, the astronauts would essentially be without reactor shielding on the return trip since there is a risk that all or most of the hydrogen would have been used up by then. Since one of the mission objectives is to have the astronauts *return* safely to Earth, this option had to be ruled out.

4.6.4 Water Tank

Second, the water tanks onboard were considered for shielding purposes. In particular, the waste water was thought of to comprise a sufficient shield. The drawbacks with this alternative included uncertainty in how much waste water would be available at the beginning of the trip. Regarding the fresh water tanks as shields, there is a concern that the water will become activated by the neutron bombardment. When water is being used as the primary coolant for an operating reactor, it will contain radioactive N-16 and F-18. These products, however, decay away relatively fast, i.e., a few seconds for N-16 and fifteen minutes for F-18 [4]. However, in this case the water is only irradiated, not passed through a core. Water is not naturally radioactive, but can be activated when bombarded with neutrons. In case of an emergency when a lot of the water resources were immediately needed, it is highly undesirable to have the water being radioactive and (possibly) being forced to wait until the isotopes have decayed away. Based on this analysis, it was concluded that another alternative should be chosen.

4.6.5 Special Shield

The last option was to bring a specially designed shield from Earth. Whereas equipment and parts in a spacecraft usually have multiple functions, this solution gave an opportunity to design a shield whose only function would be to stop the radiation from the reactor. Differently put, instead of having a decent performance for many tasks, this shield would only serve one purpose but would do so flawlessly. The shield should be able to protect the crew against both gamma and neutron radiation.

Research of different material pointed in favor of a combination of lithium hydride (LiH) with a refractory metal (W) at both ends [5]. As pointed out above, the cross sections of a material ultimately decides whether it would make a good shield or not. It is known that lithium hydride and tungsten have cross sections that make them attractive for shielding purposes. However, in order to confirm this claim, the cross sections (both fast and thermal) of LiH and W were obtained using MCNP. Indeed, the results supported the hypothesis, Table 4.6.6-1 contains the results for calculations of the cross sections.

Table 4.6.6 - 1 Cross Sections for Shielding Material

| | $\Sigma_a^{n, fast} \text{ (cm}^{-1}\text{)}$ | $\Sigma_a^{n, thermal} \text{ (cm}^{-1}\text{)}$ | $\Sigma^\gamma \text{ (cm}^{-1}\text{)}$ |
|-----|---|--|--|
| LiH | 0.0551 | 6.55 | 0.023 |
| W | 0.00228 | 1.20 | 0.926 |

Thanks to its light atomic mass, the lithium hydride will thermalize the neutron current from the core. The thermalization and subsequent absorption in lithium would take care of the neutrons. The LiH has a relatively low density (0.78 g/cm^3) and can therefore be incorporated into shield in large quantity. The tungsten ($Z=74$) would be responsible for attenuating the gamma radiation [6]. Preliminary analysis showed that this type of shield should give efficient protection and therefore the tungsten and lithium-hydride shield was chosen for more detailed design.

4.6.6 Design Methodology

Location

The physical placement of the reactor in the spacecraft is also of importance when minimizing the exposure rate. Naturally, the reactor should be placed, in virtually all cases, as far away from the crew as possible in order to maximize the distance. Therefore, the reactor was placed in one end of the spacecraft and the crew area was located on the opposite side. Since the Titan IV rocket employed has a pointed tip, the reactor was placed there in order to save on the shielding.

Thickness

As a first-cut approximation, the standard $e^{-\mu x}$ -calculations were deemed sufficient. However, the problem of finding the correct attenuation coefficients remained. In order to make these calculations as accurate as possible, one had to account for the fact that the LiH absorption cross section is not constant throughout the shield. The neutrons coming from the core are fast, but approximately 10-15 cm into the shield the neutron spectrum thermalizes and hence the thermal absorption cross section should be used from there on. As thermalization distance, 10 cm was chosen. This estimate may be optimistic, but should still be reasonable.

In a typical design of a nuclear-driven spacecraft, the shield mass can be up to 50% of the total mass. Initial analysis of the shield predicted that the tungsten with its density of 19.3 g/cm^3 would cause a substantial increase in mass [6]. Considering that the tungsten mainly attenuates the gamma radiation, which the crew habitat must be shielded against anyway due to the GCR, it is possible to decrease the tungsten thickness. In practicality, this design choice means that the normal habitat shielding and, if not already included, water and food and other equipment will provide sufficient shielding against any hard gammas making it through the tungsten.

The LiH has a density of only 0.78 g/cm^3 [7]. Hence, a large amount of LiH can be used to shield against neutron radiation without adding enormous mass. Calculations showed that the mass of the LiH increased approximately with 40 kg per centimeter LiH added.

Shield Criteria

The imposed radiation limits determined when the shielding was sufficient. As a requirement for the neutron radiation, the requirement on the dose rate was set to $< 10 \text{ mrem/hr}$ at the back end of the shield. This value was determined based on two assumptions. First, the radiation levels at the MIT reactor were taken into account for comparison. The dose rate on the reactor top, i.e., outside the 5 metric ton heavy top lid, when the 5-MW MIT reactor is at full power typically

varies between 5-10 mrem/hr. Additionally, there is other shielding material between the crew compartment and the back end of the shield, which should be enough to moderate the neutrons further. For instance, the water tanks are to be placed between the penetrating neutron radiation and the habitat.

For the photon current, no specific dose limit was set. There were two reasons why this limit was not determined. Photon current tallies were calculated by MCNP, but normalization of the tallies was ambiguous, and therefore, no determination of the current could be made. Therefore, this task will be added to the list of things that need further investigation. On the other hand, the photon current is *highly unlikely* to have any major impact on the shield design. As is mentioned above, the crew will in either case need to be shielded from GCR and this shielding will also be more than enough to protect them from the additional gamma radiation coming from the core. Also, the tungsten layers on the shield should reduce the photon current significantly. One should also remember that the tungsten layers cannot be significantly increased, because the 19.3 g/cm³ density results in huge extra mass. More precisely, every added centimeter of tungsten to the back portion of the shield increases the mass by more than two metric tons!

Calculations

The neutron current was obtained by MCNP simulation totaled 8.752×10^{13} n/cm² s. The outcoming current could then be approximated from the formula [8]:

$$\hat{J}_{out} = \hat{J}_0 e^{-\Sigma x}$$

Where \hat{J} is the neutron current in #neutrons/cm² s, Σ is the total macroscopic cross section in cm⁻¹ of the shield material(s) and x is the distance traveled in cm through the material(s). The actual dose rate (for tissue) at the back of the shield could then be acquired from empirically based tables in reference literature [7].

The data of the W and LiH cross sections are presented in Table 4.6.6-1 above. In order to obtain precise fast and thermal neutron cross sections, MCNP code was used. The shield mass could readily be computed since the shield geometry and the material densities were known. The geometry of the shield is best described as a chopped off pyramid on a circular base (see Figure 4.6.6-1). Shown on Table 4.6.6-2 are the results of calculations on thickness shielding and doses on the back side of the shield.

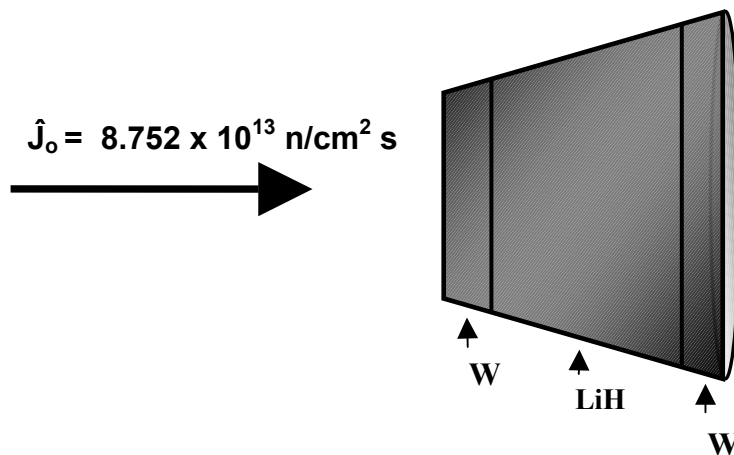


Figure 4.6.6 - 1 Cross Sectional View of the Space Reactor Shield.

Table 4.6.6 – 2 Different Shielding Thickness and Results

| Thickness (cm) | | | Shield Mass (kg) | Neutron Exposure (mrem/hr) |
|--------------------|------|-------------------|------------------|----------------------------|
| W _{front} | LiH | W _{back} | | |
| 0.5 | 15.5 | 0.5 | 3224 | 8.48 |
| 1 | 15.5 | 0.5 | 3871 | 8.47 |
| 2 | 15.5 | 0.5 | 5151 | 8.45 |
| 0.5 | 16 | 0.5 | 3243 | 1.03 |
| 0.5 | 17 | 0.5 | 3281 | <0.1 |
| 0.5 | 18 | 0.5 | 3320 | <<0.1 |
| 0.5 | 15.5 | 1 | 4513 | 4.65 |
| 0.5 | 15.5 | 2 | 7025 | 1.40 |
| 0.5 | 15.5 | 3 | 9450 | 0.42 |

4.6.7 Physical Implementation

As the space reactor plant illustration shows, the side of the shield facing the core is longer than the diameter of the core. In order to shield the collector from direct core radiation, the front diameter of the shield was calculated to 2.82 m. The length of the back diameter was limited by the diameter of the rocket (4.5 m) and therefore set to 2.12 m.

The space reactor shield will naturally be put in place during the construction of the spacecraft. Furthermore, the shield will stay in place during the entire lifetime of the vehicle or at least as long as the reactor is deployed onboard.

4.6.8 Limitations of Study

This study determines the radiation onboard due to the reactor to a good first-order approximation. However, like any other approximation, the analysis can be fine-tuned. In order to facilitate further investigation of the shielding, this section outlines the main areas that require further analysis.

The largest discrepancy on the space shielding is where the spectrum actually thermalizes. In order to determine this more precisely, an advanced computer simulation must be carried out. Also, since this is a gradual transition, more than two types of cross sections should be used. This would also require a computer program if high accuracy is desired. These simulations are, however, beyond the scope of this first-order approximation, but are mentioned as a recommendation to whoever may investigate this issue more in depth.

As already stated, the photon current should also be studied further. Although it is reasonable to assume that the crew will already have a decent gamma radiation shield system, it could prove valuable to know whether any hard gammas are expected to penetrate the reactor (neutron) shield.

4.6.9 General Comments on Radiation in Space

It is often difficult to understand the meaning of numbers if they cannot be related to anything. For the sake of comparison of what it actually means that the neutron dose rate at the shield surface is ~9 mrem/hr, the section below discusses what dose an astronaut is likely to pick up in space at different conditions. The reader is expected to be familiar with the concept of dose and have a basic understanding of what medical implications different doses may have on a human being.

Recommended radiation exposure limits vary for different professions. Clearly, the astronauts will be high up on the scale. Table 4.6.9-1 compiles some exposure limits for different groups [8,9]:

As is obvious from the table above, the astronauts' dose levels are vastly higher than for the other groups'. By studying the radiation levels in space one quickly realizes why astronauts' limits must be higher. For instance, when going through the inner radiation belt, the unshielded dose rate is about 1000 rem/hr [9]. Furthermore, the unshielded dose rate in outer space is, on average, 400 rem/year at periods of solar maximum [9]. The annual dose for astronauts behind 5 g/cm² and 35 g/cm² of shielding in free space is on average 35 and 24 rem, respectively [9].

Table 4.6.9-2 shows the estimated dose that astronauts operating on the Martian surface would pick up for different stay times. The dose estimate is based on the assumption that the only means of shielding is the CO₂ atmosphere, i.e., no extra habitat shielding has been taken into account in order to illustrate the "worst case scenario". The dose rate does not scale linearly with time because the 11-year solar cycle affects the exposure rate on Mars. In addition, solar flares may add to the total dose, but hardly more than 1 rem/year.

Table 4.6.9-3 shows the dose equivalent that astronauts would acquire en route to Mars. As expected, this dose rate also varies with the solar cycles. The estimates are conservative and assume standard minimal spacecraft shielding. More concisely, the shielding would consist of 2 g/cm² of aluminum equivalent material. Clearly, the transit time must be minimized in order to keep the astronauts' dose down. For comparison, the dose rate on the Martian surface is roughly 1-1.5 mrem/hr. Thus, the transit dose rate can be up to eight times higher during solar minima! This analysis also supports the use of VASIMR, which significantly reduces the transit time.

Table 4.6.9 – 1 Exposure Limits for Different Groups

| Astronauts Maximum Dose Limit for... | Depth – 5 cm | Eye – 0.3 cm | Skin – 0.01 cm |
|---|---------------------|---------------------|-----------------------|
| 30 days (rem) | 25 | 100 | 150 |
| Annual (rem) | 50 | 200 | 300 |
| Career (rem) | ~300 | 400 | 600 |
| Radiation Workers – | | | |
| Annual Dose Limit (rem) | 5 | 15 | 50 |
| General Public – | | | |
| Annual Dose Limit (rem) | 0.5 | n/a | n/a |

Table 4.6.9 – 2 Estimated Dose Due to GCR on Martian Surface

| Stay Time (days) | Dose Equivalent (mrem) | |
|------------------|------------------------|----------------------------|
| | Skin | Blood-Forming Organs (BFO) |
| 60 | 2 100 | 1 800 |
| 600 | 19 000 | 18 000 |

Table 4.6.9 – 3 Dose Rate (BFO) to Astronauts in Transit

| | Dose Rate (rem/year) | Dose Rate (mrem/hr) |
|----------------------|----------------------|---------------------|
| Solar maximum | 30 | 3.4 |
| Solar minimum | 75 | 8.6 |

4.6.10 References

[1] HITF – Shield Development, <http://hitf.jsc.nasa.gov/hitfpub/shielddev/materials.html>, accessed May 2, 2003.

[2] Shielding from Mars or Moon Dirt?, http://science.nasa.gov/newhome/headlines/msad20jul98_1.html, NASA, accessed on April 23, 2003.

[3] Turner, James. E., *Atoms, Radiation and Radiation Protection*, McGraw-Hill, New York, NY, 1992.

[4] Reactor Staff, *MITR-II Reactor Systems Manual*, MIT Press, Cambridge, MA, 1997.

[5] *Radiation Shielding Information Center Newsletter*, Oak Ridge National Laboratory, No. 52, March, Oak Ridge, TN, 1969.

[6] Knoll, Glenn F., *Radiation Detection and Measurement*, John Wiley & Sons, New York, NY, 1979.

[7] Tsoufanidis, N., *Measurement and Detection of Radiation*, McGraw-Hill Book Company, New York, NY, 1983.

[8] Lamarsh, John R., *Introduction to Nuclear Reactor Theory*, Addison-Wesley-Longman, Reading, MA, 1966.

[9] SIMM – MARS – Radiation and the Human Mars Mission, Version 1.0, <http://www.seds.org/pub/info/mars/RadHuman.txt>, accessed April 15, 2003.

[10] U.S. Nuclear Regulatory Commission, *Regulatory Guide 8.29*, Revision 1, February 1996.

5.0 SURFACE POWER SYSTEM

5.1 SURFACE POWER SYSTEM REACTOR (CECR)

5.1.1 Introduction

This chapter of the report discusses the design methodology applied, and the design specification for a Mars surface nuclear power reactor system. Unique approaches were taken in the system design and mathematical decision making tools were used to evaluate competing core design approaches.

There are many constraints that drive the surface core design. There is an ever-present constraint on the mass and size of the system. Coupling the mass constraint with remote operation and high system reliability creates a very challenging design problem. There is no clear cut approach that has been developed that successfully meets every design goal, and therefore tradeoffs are made to find a final system that balances the advantages and disadvantages of several proposed approaches.

System goals were defined for a long lasting core for the Martian surface application. This includes compatibility with Martian atmosphere as well as a very long-lived nuclear core with high system reliability under operating conditions without regular maintenance. Chapter 5 describes the nuclear design, power conversion system and reactor shielding for the surface application. Section 5.1 will deal primarily with the nuclear design of the core and discussion of the decision methodology.

At the end of this section the design specifications and operational reactor physics parameters for an epithermal converting core will be described. Based on importance weighting of competing design goals, this system was favored above systems with greater uranium utilization in some cases, as well as over systems with slower reactivity transients.

The Carbon-Dioxide-Cooled Epithermal Conversion Reactor (CECR) is designed to operate with ex-core control, relatively high internal conversion of fertile to fissile material, large effective delayed neutron fraction, and long life (25 years or more).

5.1.2 Design Goals

Parts of the overarching mission goals are: to develop reusable technology and to develop Martian infrastructure to support future Mars activities and reduce the cost of future endeavors. To achieve these overarching goals, the Mars surface power system must operate smoothly for long periods of time, and must also be relatively easily transported to the Martian surface.

Several surface power specific goals were developed, such that if these goals are fully met, the overall mission objective is met at the highest utility. Firstly, the reactor is designed to operate for 25 effective full power years (EFPY). This duration is assumed to support several Martian land-based missions. This is considered a priority goal for the design.

The conceptual design is evolvable, in that similar technologies could be employed with a shorter full power lifetime to demonstrate the concept. Similar or scalable applications of the CECR design will be discussed at further length in the remainder of this chapter.

The reactor must be suited for remote operation in an environment where time lags exist between control mechanism initiation and resolution. That is to say that, as the reactor must be operated for periods of time remotely from Earth, the core must have relatively slowly developing thermal and reactivity transients.

Of course, the system mass should be as small as possible while still meeting other design goals to reduce the mission cost and increase the flexibility of the mission by allowing more scientific payload to be transported to Mars. One way to achieve this goal is develop a reactor that makes very high use of the uranium fuel by reaching high atomic burnup.

Lastly, to ensure core reliability for 25 EFPY, moving control mechanisms, such as banked control rods, must be eschewed, as wear and tear on these types of systems will lead to their degradation. Also, the core materials must be chemically inert in the Martian atmosphere to avert possible chemical reactions that could fail the fuel and lead to unwanted reactivity accidents or radiological release while humans are on the surface.

5.1.3 Design Methodology

A numeric design methodology was developed to evaluate the utility of competing design alternatives. The discussion of the methodology and the results are discussed as a case study of the methodology in Chapter 3 of this report. This section of the report will discuss the development of the alternative approaches as well as the criteria by which these alternatives are measured. Several core configurations are discussed, the costs and benefits of each system are explored and ranked.

Several parameters are used to define the operating regime of the core. Before design begins, a matrix of feasible alternatives was developed based on the aim of meeting all or some of the goals proposed above. Firstly, the flux spectrum of the core is discussed. Thermal, Epithermal, and Fast flux spectrum cores have advantages and disadvantages in terms of the goals discussed.

To justify the numeric decision-making approach used, consider a typical fast spectrum and thermal spectrum reactor. Whereas the fast spectrum reactor minimizes core materials and moderator, thus reducing mass, the prompt fission lifetime is orders of magnitude smaller and large plutonium concentration yields a smaller delayed neutron fraction compared with that for a thermal reactor. Therefore, a fast reactor may have smaller mass, as well as improved fuel utilization, however, the reactivity transients may be too rapid to control. A thermal system requires less fissile material to be critical, however, because of increased radiative capture, internal conversion is worse, and therefore the reactivity swing over 25 EFPY may be too large and neutron migration area too small to avoid in-core control rod banks.

A decision methodology is necessary to evaluate the relative utility of such systems relative to one another to arrive at an ideal design approach. The following section will describe in detail the available options for core characteristics.

Component Options

Core characteristics are comprised of: spectrum hardness, fuel geometry, fuel material, matrix material, reflector, control material, and coolant. For each of these characteristics, independently, several options are available for use in the final design. The logical combination

of components for each characteristic leads to the development of a short list of potential technology approaches. Each core characteristic will be discussed separately based on the options as well as the relative strengths and weaknesses of the options.

Flux Spectrum Hardness

Thermal, Fast, and Epithermal spectrum cores are evaluated for the surface reactor. Both thermal and fast reactors have previously been proposed for space applications. The SNAP-10A reactor was a thermal reactor [1], whereas, the more advanced SAFE-400 reactor is a fast spectrum reactor [2].

Thermal reactors include moderator, typically hydrogen, graphite, or beryllium to slow fast fission neutrons to thermal energies (~ 0.05 eV) where they are preferentially absorbed by fissile uranium or plutonium nuclides. The biggest advantage of the thermal system is the time duration from neutron birth till subsequent capture in a fissile species. The neutrons must thermalize in moderator, and this process of collisions slows the neutrons down and takes some period of time. For thermal reactors the prompt fission lifetime is on the order of 100 microseconds.

The prompt fission lifetime is the average time between fission neutron birth and subsequent fission initiated by the released neutron. The asymptotic time constant for reactivity transients, and therefore power transients, is inversely proportional to this constant. Therefore, thermal reactors are attractive from the standpoint of slow power transients.

Recall, however, that moderator is required to slow the neutrons down to thermal energies. In many cases, the volume ratio of moderator to fuel must be greater than ten for the system to even be critical. If one is trying to minimize mass or size of the reactor it is difficult to carry much moderator.

Additionally, in a thermal spectrum, radiative capture is likely to occur in the fissile species. Though this alone may not seem important, if radiative capture in fissile materials is very small, then for each neutron absorbed in fissile materials, more neutrons are released. If the number of neutrons released per absorption is greater than two, then neutrons can be harvested for conversion of fertile to fissile material to flatten reactivity. Since, for thermal spectra, the number of neutrons released per absorption is on the order of 1.3 to 1.6 for uranium based fuels [3], the reactivity swing associated with these type of cores will be relatively large as excess reactivity must be loaded at the BOL to ensure criticality late in life.

Fast reactors are very different from thermal reactors. To build a fast spectrum reactor, moderator must be minimized to maximize the average neutron energy in the core. Therefore, the core may be lighter as a result. However, since there is no slowing down time, the prompt fission lifetime is much smaller, on the order of 0.5 microseconds [3]. Therefore, fast reactors are prone to much faster reactivity and power transients.

In a fast spectrum, there is an advantage in terms of neutron economy. At high neutron energies, the likelihood of fission relative to capture for fissile nuclides increases dramatically.

At high neutron energy, the fission to capture ratio decreases with increasing neutron energy. Additionally, for energies exceeding 1 MeV, fertile Uranium-238 can undergo fission. In a fast spectrum, the ratio of fission neutrons produced per absorption in fuel is much higher than in a

thermal spectrum. Recall that η^X is the number of fission neutrons released per absorption in a nuclide “X”. Symbolically, η^X can be defined as shown in Equation 1.

$$\eta^X = \frac{\nu\sigma_f^X}{\sigma_a^X} = \frac{\nu\sigma_f^X}{\sigma_\gamma^X + \sigma_f^X} = \frac{\nu}{\frac{\sigma_\gamma^X}{\sigma_f^X} + 1} = \frac{\nu}{\alpha + 1} \quad \text{Equation (1)}$$

The ratio of fission neutrons produced per absorption can be thought of as the infinite medium eigenvalue for nuclide X (k_∞^X). As k increases, the reactivity of any nuclear system increases. The infinite eigenvalue is dependent on the prompt yield and the capture to fission ratio (α). The prompt yield (ν) is only weakly dependent on incident neutron energy, and therefore, the spectral dependence of the infinite eigenvalue is tied to the spectral dependence of the capture-to-fission ratio [4].

If the infinite eigenvalue is 2 or greater, then one neutron from fission can be used to induce another fission as part of the chain reaction, and the second can be harvested to produce more fissile material by being captured in fertile material. Breeding is the state of operation where neutrons are captured in fertile material more rapidly than fissile materials are being reacted, such that the total fissile inventory increases with burnup.

Using conventional uranium fuel in a thermal reactor does not allow breeding. However, in a fast spectrum, the value of the capture-to-fission ratio for all fissile nuclides decreases. As the prompt yield for Pu-239 (2.91) is greater than that for U-235 (2.47) [1], one can imagine a reactor where Pu-239 fission is used to fuel fertile breeding in U-238 as well as continued fission in Pu-239. Fast reactors are well suited to this goal as the hard spectrum, and therefore high energy neutron population, are absorbed in a regime where capture is much less likely than fission, and more neutrons are released per absorption in fissile material. For some fast reactors η^{49} is ~ 2.4 , significantly greater than 2, allowing for breeding [3,4].

Since reactivity is added to the core via breeding while reactivity is being removed via fission, the net change in reactivity through burnup may be very small, and in fact, some fast reactors have net increases in reactivity through burnup. Therefore, in a fast spectrum reactor, it would be possible to design a system that has a flat reactivity through life. With a small reactivity swing over core life, minimal control devices are necessary for the operation of the core.

Epithermal reactors have not recently been explored in great detail for conventional power application. One example is the LWBR experiment with thorium-based fuels in Shippingport, a 60 MWe plant, however operation was complicated, as fueled seed regions were inserted and withdrawn from the core regularly [19]. Epithermal reactors have flux spectra between those of fast reactors and thermal reactors. There is some moderator present to soften the flux spectrum slightly. This pushes the neutron population into the energy regime where resonance absorption is prevalent.

The capture to fission ratio for fissile nuclides is relatively low, though not as low as in a fast spectrum. At the same time there is increased epithermal capture in fertile nuclides compared to a thermal spectrum and limited conversion is achievable.

Summary

Compared to a fast reactor, epithermal reactors have longer prompt fission times because fission occurs once the neutrons have slowed to intermediate neutron energies and are absorbed in fission resonances. Therefore, reactivity transient time for an epithermal reactor is between that for thermal and fast reactor. An epithermal reactor is a compromise of the benefits of the thermal or fast reactors.

Fuel Geometry

Several options are considered for fuel geometry: pins, plates, and blocks. From a neutronics view point, there are only small differences between the different geometries. Particularly in fast or epithermal spectra where the migration area is large, the fuel geometry has little to no impact on the core neutronic behavior. Therefore, the driver for the downselection of core geometry is the core response in thermal transients.

Block cores with fuel in matrices have much larger heat capacities than plate or pin type cores. On the other hand, pin and plate type cores have larger surface area to volume ratios than block type cores. Therefore, heat transfer surface area is larger for a pin or plate type core.

Summary

Block type core with fuel matrices are favored because of the additional heat capacity, pressure drop and heat transfer area, however, remain a concern for the thermal-hydraulic design of the power conversion system.

Fuel Material

Metallic fuels were not considered for the surface core. At 25 years of operation, fuel swelling for metallic fuel at high temperature would be egregious. Additionally, with melting temperatures on the order of 1100°C, metallic fuel alloys do not appear promising from the standpoint of system safety and reliability. Ceramic fuel forms have melting temperatures on the order of 2200°C or higher [5].

UO₂, UN, UC, and US are considered for application in the surface reactor core. These fuel forms have various advantages depending on their application. The key fuel characteristics are heavy metal density and the scattering properties of the light constituents of the fuel. High heavy metal density fuels are ideal for fast reactors, UN and UC both have very high heavy metal density. Light constituents that act as moderator are excellent for epithermal or thermal systems, UO₂ has strongly moderating light constituent, particularly because there are two light nuclei for each heavy metal nucleus.

In a hard spectrum, UC has very low parasitic absorption cross-section with a relatively large heavy metal density (13.0 g/cc). UO₂ has a lower heavy metal density (9.70 gU/cc) than UN (13.5 gU/cc) or UC (13.0 gU/cc), but the oxygen atoms contribute to moderation, and UO₂ has excellent oxidation resistance compared with the other fuels. US has a similar heavy metal density to UO₂ (9.58 gU/cc) however, sulfur will not contribute as significantly to neutron moderation as the oxygen in UO₂ [4].

Based on these parameters, each fuel form is more suited for a particular spectrum. It is difficult to operate a small fast reactor with UO_2 fuel because of the oxygen moderation, and therefore, these types of options are not explored. On the same token, operating a thermal reactor with US fuel is not beneficial when UO_2 fuel could be used.

Summary

In light of some of the advantages of the block type core, and epithermal spectrum, UO_2 is a favored fuel form. It is also relatively inert in CO_2 at low temperatures. Therefore, UO_2 is a primary candidate for the surface reactor fuel form.

Matrix Material

Inert host matrices are not necessary for each reactor type, but where moderator is needed, or in cases where block type cores are being used an inert matrix becomes indispensable. Only CERCER fuel arrangements are considered, metallic matrices are not considered. Since the fuel must potentially withstand very high temperatures under accident or transient conditions with delayed intervention, ceramics with higher melting temperatures than metals look attractive as matrices.

Many ceramic materials ranging from MgO to VC have been proposed as potential matrices for nuclear reactors. A shorter list was developed for the surface reactor. These materials were selected based on neutron transparency in thermal and fast spectra, oxidation resistance, and previous use for industrial or research application. BeO , SiC , and ZrO_2 are selected as potential matrix materials.

Summary

Of the potential matrix materials, BeO has the highest thermal conductivity (250 W/m-K) [6] and is an excellent neutron moderator [7]. SiC is a tough material and has much weaker slowing down power than BeO . Because BeO acts as a moderator, a fast reactor would not use this material as a matrix. Similarly, a thermal reactor would not use SiC as a matrix when BeO could be used.

Reflector Material

To minimize the surface power system mass, the reactor core must be small, as a consequence, the neutron leakage is large. Therefore, a reflector is essential to the neutron economy. For small cores the reflector worth is large, and a considerable amount of reactivity can be controlled via ex-core reflector control.

A host of potential ceramic reflectors have been examined. They were selected based on a plethora of slowing down powers, high melting temperature, and high albedo. Albedo is a measure of the reflection probability for neutrons incident on a slab of a given material. Beryllium compounds constitute a significant fraction of the potential reflectors based on its low mass, and hence strong slowing down power. The potential thermal reflectors include: BeO , Be_2C , Be_3N_2 , and Graphite.

For fast reactor applications reflectors with weaker slowing down power, but high albedo are preferred. PbS and Zr_3Si_2 are selected based on reflector screening done for fast reactors at MIT [8].

Calculations were done to compare reflectors for the epithermal spectrum reactor case. The results will be discussed in following sections.

Control Materials

Two control materials were identified for potential use. Natural Boron has a large neutron absorption cross section for any incident energy [9], and therefore B_4C was selected as a potential control material. Tantalum has a significant fast and epithermal absorption cross section [9], and therefore TaB_2 is also considered for core control. Both of these ceramics have high melting temperatures ($> 2400^\circ C$) [10].

If the system reactivity is controlled via ex-core mechanisms, the control material will be placed as a “shutter” for control drums. A shutter is a thin layer of absorber on one side of a control drum. When the reactor is shut down the control drum is rotated such that the absorbing shutter is close to the reactor. Figure 7 shows the whole core model. The black colored layers on the circular drums are the control shutters. Neutronic performance of TaB_2 and B_4C are discussed in the following sections.

Coolant

Two coolants were considered, one gas and one liquid metal. For a liquid metal coolant, Lead Bismuth Eutectic (LBE) was chosen as a reference. The gas reference coolant selected was CO_2 . The Martian atmosphere is almost pure CO_2 . Therefore, selecting CO_2 as a coolant would save on system mass in that coolant would not have to be transported to Mars.

Though experience in fast reactors is predominantly with sodium cooled systems because it allows for more rapid doubling time, these economic concerns are not drivers for the Martian surface reactors. LBE has excellent heat removal capabilities and offers safety advantages compared to sodium [11]. The melting temperature of LBE is $1670^\circ C$ [11], and in thermal transients there is a smaller risk of reactor thermal explosions from internal pressure at high temperature compared with other liquid metals. LBE also has a weaker slowing down power than sodium or potassium and therefore improves fast reactor neutron economics [11]. Lead, however, has strong non-elastic cross sections at high neutron energy that may compromise neutronic behavior in some regimes.

CO_2 is a favored coolant between these two for several reasons. The core is designed already, preferably, to be chemically inert in CO_2 , and therefore, the core will be chemically inert with the coolant as well. Additionally, if a leak develops in the system, as is likely to occur after 25 EFPY, more CO_2 can be drawn in from the atmosphere during operation. This option is not available for liquid metals.

Summary

From the standpoint of operations, safety and mass; CO_2 appears a favorable candidate for the surface power system coolant.

Structural Material

For the core cladding and structural material, INCOLOY MA956 steel is proposed. MA956 is a super alloy initially developed for aerospace applications. The Fe-Cr-Al alloy combined excellent oxidation resistance with good strength. Because of the high chromium (20 w/o) and aluminum (4.5 w/o) the material is incredibly resistant to oxidation in CO₂, even up to 1300°C for prolonged exposure times [12].

The oxidation resistance of the alloy comes from the relatively high aluminum content in particular. The aluminum will oxidize to form protective alumina layers on the outer surface of the metal. If these layers are damaged for whatever reason, aluminum in the meat of the material will form alumina to repair the damaged surface [12]. This resistance to oxidation damage makes this material ideal for applications in Martian atmosphere, which is predominantly CO₂.

5.1.4 Viable Alternatives

A few viable options were drawn up from the potential list of different core characteristics. Each one of the options is logical in that none of the aforementioned preclusive characteristics are matched. Trying to maximize one or two of the goals exclusively led to the development of the different options.

The first option is one identified as a compromising alternative. A UO₂ fuel in BeO matrix block type core, CO₂ cooled, with an Epithermal Spectrum. Control and Reflector are addressed after a core concept is more mature. This core attempts to balance neutron economics with slow reactivity transients. Additionally, the core is comprised of oxidation resistant materials.

The second option is Fast Spectrum, US fuel in SiC matrix block type core, CO₂ cooled. This core aims for slow thermal transients and decent neutron economics. Oxidation resistance in Martian atmosphere is somewhat compromised by the presence of the US, however, oxidation of US will not lead to propagating fuel failure because of the similarity in density between US and UO₂ [13].

The third option is a Fast Spectrum, UC fuel, LBE cooled, tightly packed pin type core. This core maximizes neutron economy and minimizes the core mass (not including the coolant mass). The expense of doing so is poor oxidation resistance and rapid thermal and reactivity transients.

The fourth and last option is a Thermal Spectrum, UO₂ fuel, BeO Matrix, CO₂ cooled block type core. The thermal and reactivity transients will be very slow, however, the volume of matrix relative to fuel required to operate the core will be very large. Additionally, breeding ratio in a thermal spectrum is lower than in an epithermal or fast spectrum, so reactivity swing for the same burnup will be greater than for any of the other options.

Additional Alternatives Not Considered

Given time constraints for the project, some concepts were not fully considered because they were outside of the self-imposed design envelope. These include highly enriched uranium fueled cores where conversion is not considered because small reactivity swing can be attained by limiting the fuel burnup.

Downselection of Viable Alternatives

A decision methodology based on Multi-Attribute Utility Theory was applied to the four alternatives to downselect the best option based on limited information. The operation time of 25 EFPY was assumed, and the extent to which a system with the characteristics of each option was expected to meet the remainder of the goals was ranked.

The study confirms that the first alternative, which balances neutron economics against transient time, is in fact the best approach given our goals. The concept is named the CO₂ cooled, Epithermal Conversion Reactor (CECR).

5.1.5 Assumptions

To converge on a final design, several assumptions about core parameters were made to facilitate the design process. These assumed parameters are areas for potential optimization in future work in this area.

For ex-core control, the radial leakage must be significant, at least as large as the desired reactivity swing of the core over the effective full power lifetime. With a black reflector shutter (100% absorbing) and an albedo of unity (100% mirror), the reactivity swing can be as large as the radial leakage and the core can be controlled use ex-core reflector control exclusively. The desired core geometry could then be iterated. As a first step, an L/D for the core is assumed to be large (approximately 4). The cycle efficiency for converting thermal to electrical energy is assumed to be 20%.

The volume fractions are also set a priori. The volume fraction of matrix should be as large as reasonably achievable to reduce the core size and therefore the necessary reflector volume for a given reflector thickness. At a thermal power of 1 MW_{th} with CO₂ coolant, 30% volume of coolant is reasonable based on thermal hydraulic calculations. The coolant fraction is set, and 5% of the volume is assumed to be cladding / structure. The matrix fills the remaining 65% of the active core volume. Lastly, the blocks are assumed to be in a hexagonal array.

5.1.6 Core Design

The power system is being designed to supply 200 kWe power. The NASA reference ISRU plant requires 160 kWe of power [14]. The system is designed to provide enough power for the operation of the plant as well as extra power for conducting experiments and recharging equipment and/or battery power rovers. At 20% cycle efficiency, the thermal power of the core must be 1 MW.

Preliminary Studies

Preliminary screening calculations were carried out in MCNP to calculate infinite cell eigenvalue and conversion ratio for different volume fractions of fuel in the matrix. The effective H/HM ratio was adjusted between 0.1 and 3.0. It was found in general that for appreciable conversion (> 0.40) that the effective H/HM must be less than 0.5. Also, for very small fuel fractions of fuel in matrix the core mass increases dramatically.

To achieve very hard spectrum ($H/HM \sim 0.1$) the volume fraction of fuel in matrix was increased above 30 % of the volume and SiC/PyC coatings were added to the fuel particles to increase the fission product retention capabilities of the fuel [15].

In cases above 30% volume, the addition of the SiC coatings makes the system look more like ceramic fuel in a SiC matrix. These systems look unattractive until very high fuel volume fractions are achieved and the spectrum approaches a fast reactor spectrum. Therefore, going above 30% volume fuel in matrix is not advisable. A plot of BOL keff vs. H/HM equivalent is shown below in Figure 5.1.6-1.

An epithermal spectrum is proposed for conversion and this would correspond to an effective H/HM of approximately 0.5 to extend the core average burnup [16]. From Figure 5.1.6-1, the reactivity is fairly insensitive to changing H/HM equivalent in this range. Taking the moderating elements in the matrix and normalizing the number densities to the average lethargy gain and scattering cross section of hydrogen gives the effective H/HM ratio.

The matrix has Be and O as strong moderating agents. The thermal scattering cross sections and average lethargy gains for Be, O, and H are tabulated and the following equation gives the effective H/HM ratio for the matrix

$$\frac{H}{HM_{eff}} = \frac{N^o \left(\frac{2}{\frac{2}{3} + 16} \right) \left(\frac{\sigma_s^o}{\sigma_s^H} \right) + N^{Be} \left(\frac{2}{\frac{2}{3} + 9} \right) \left(\frac{\sigma_s^{Be}}{\sigma_s^H} \right)}{N^{25} + N^{28}} \quad \text{Equation (2)}$$

Substituting in the numbers for typical cross sections [3], we find that the expression can be written as shown in Equation (3).

Keff vs. H/HM from initial scoping study

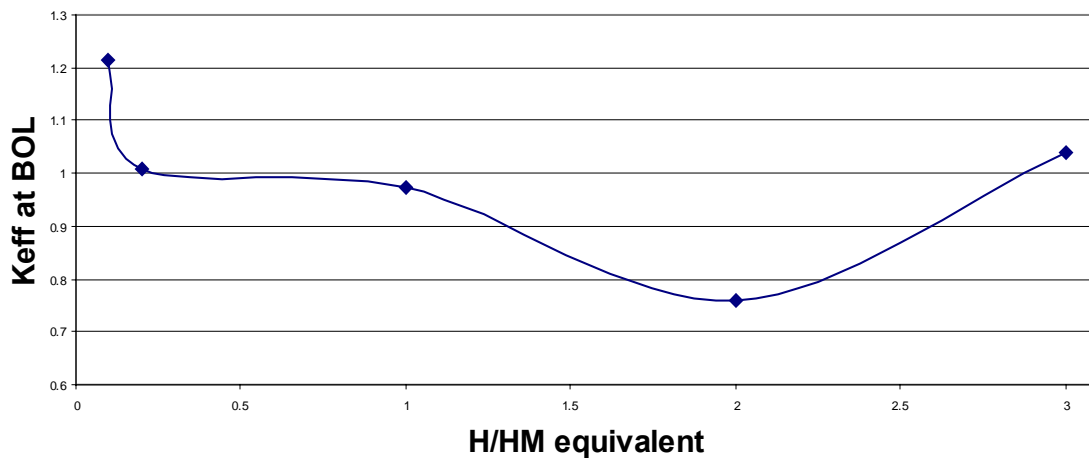


Figure 5.1.6 - 1 Study of H/HM_{eff} Dependence.

$$\frac{H}{HM_{eff}} = \frac{N^o(0.013) + N^{Be}(0.038)}{N^{25} + N^{28}} \quad \text{Equation (3)}$$

The scattering cross section for H is on the order of 40 barns, and the average lethargy gain is significantly higher than for the heavier elements. The scattering cross sections for the heavier moderators is 10% - 20% as large as the hydrogen scattering cross section at thermal energies.

For volume fractions of fuel lower than 30% fuel in matrix, the BeO will provide sufficient fission product retention and fuel particle coating is not required, therefore, volume fractions lower than or equal to 30% of fuel are preferable [17]. At 30% UO₂ by volume in the matrix, the effective H/HM ratio is 0.40.

The enrichment is also a factor that can be changed. Since the ratio of thermal to epithermal flux is related (asymptotically) to the H/HM and the enrichment, changing these two parameters have significant impact on the spectrum as well as the reactivity.

In the limit of infinite medium the ratio of thermal to epithermal flux goes linearly with the ratio of H/HM to enrichment. Increasing H/HM and decreasing the enrichment will soften the spectrum.

To more accurately fix the value of X, the BOL conversion ratio is set. The conversion ratio (CR) is set such that the rate of reactivity lost to fission is equal to the rate of reactivity gained from fertile capture. The reactivity worth of each fissile nuclide lost is assigned the value of η^{25} and the reactivity worth of each fissile nuclide produced via fertile capture is assigned the value of η^{49} . Equation (4) shows the relationship between these parameters, the cross sections and the conversion ratio.

$$\frac{\eta^{49}}{\eta^{25}} CR = \frac{\frac{\nu^{49} \sigma_f^{49}}{\sigma_a^{49}}}{\frac{\nu^{25} \sigma_f^{25}}{\sigma_a^{25}}} CR = 1 \quad \text{Equation (4)}$$

After some manipulation it can be shown that the conversion ratio is given by Equation (5).

$$\frac{1}{CR} = \frac{\nu^{49}}{\nu^{25}} \left(\frac{1 + \alpha^{25}}{1 + \alpha^{49}} \right) \quad \text{Equation (5)}$$

Equation (5) is the condition that is imposed to balance the fissile inventory of the reactor core at BOL. The second condition is the definition of the conversion ratio, which is the rate of fertile capture divided by the rate of fissile absorption. This treatment ignores the yield of fissile material from fertile absorptions assuming a value of unity. The definition is shown in Equation (6). X is the enrichment.

$$CR = \frac{(1 - X)HM\sigma_\gamma^{28}}{(X)HM(\sigma_f^{25} + \sigma_\gamma^{25})} = \left(\frac{1}{X} - 1 \right) \frac{\sigma_\gamma^{28}}{\sigma_f^{25} + \sigma_\gamma^{25}} \quad \text{Equation (6)}$$

Solving Equations (5) and (6) simultaneously gives enrichment and BOL conversion ratio. At this conversion ratio and enrichment the reactivity will decline through burnup because of fission product poisoning. The targeted enrichment is shown in Equation (7).

$$X = \frac{1 + \frac{\sigma_{\gamma}^{49}}{\sigma_f^{49}}}{1 + \frac{\sigma_{\gamma}^{49}}{\sigma_f^{49}} + \frac{v^{25}}{v^{49}} \frac{\sigma_f^{25}}{\sigma_{\gamma}^{28}}} \quad \text{Equation (7)}$$

An infinite, homogenous, unit cell was run for the composition laid out in the assumptions and for 10% enrichment. The corresponding cross sections were used in Equation (7) to calculate the ideal enrichment. The ideal enrichment was found to be approximately 20%. This is also the limit for what is considered Low Enriched Uranium (LEU), making it easier to handle and the fuel easier to manufacture.

Given the enrichment and the one group cross sections calculated from MCNP, the conversion ratio was calculated to be 0.38. If one is to operate the reactor in this regime, the decline in reactivity is due to the buildup of fission products and the much slower rate of loss of fertile uranium. However, if the conversion ratio is increased slightly from this value, then the slope of reactivity decline with burnup will be decreased. Very large conversion ratios are unattractive because as the Pu-239 inventory increases the delayed neutron fraction decreases.

Unit Cell Modeling and Blankets

At an enrichment of 20%, the BOL reactivity will be relatively large, so the use of internal and external blankets to suppress the BOL reactivity and improve conversion ratio slightly will be beneficial to overall neutronic performance. Blankets are regions in the core where the fuel contains very little (or no) fissile inventory at BOL. The blanket may include U-238 and Th-232, either of which will absorb neutrons and decay to fissile species (Pu-239 and U-233 respectively). Blankets reduce the reactivity swing and increase the reactivity-limited burnup.

A refined unit cell model is created for a triangular pitch hexagonal block with a central coolant channel. A diagram of the radial profile of the unit cell is shown in Figure 5.1.6-2.

The block pitch (or flat-to-flat length) is 6.3 cm based on an inner coolant channel diameter of 2.9 cm. External and internal blankets are included. The block is capped axially with 10 cm thick blankets and the core center is also a blanket. The blanket material is modeled as U²³⁸O₂. Th²³²O₂ was not considered based on the exceptional neutronic performance of Pu-239. In a real application either depleted or natural uranium would be used. In terms of manufacturing the fuel cell, blocks can be manufactured in 10 cm segments and stacked in the core, or the fuel matrix can be packed in the blocks in stages so that the different enrichment zones are layered in this fashion. A total of ~40 cm of the 160 cm of core height is blanket material. The axial profile of the model is shown in Figure 5.1.6-3.

The whole core is a series of 148 unit cells. The core is comprised of 37 radial blocks. The core is roughly cylindrical with an average radius of 37 cm. Given the fuel height of 160 cm, the approximate L/D for the whole core is approximately the assumed value of 4.

The unit cell burnup analysis is done with MCODE. MCODE is a depletion code developed at MIT that couples MCNP and ORIGEN. MCNP is used to calculate the reactivity of the unit cell as well as a plethora of one group average cross sections. The cross sections are written to a file

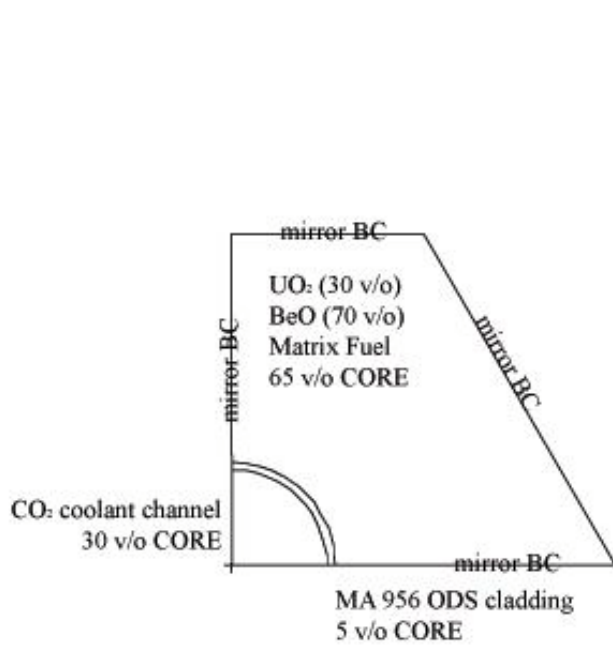


Figure 5.1.6 - 2 Radial Unit Cell Diagram.

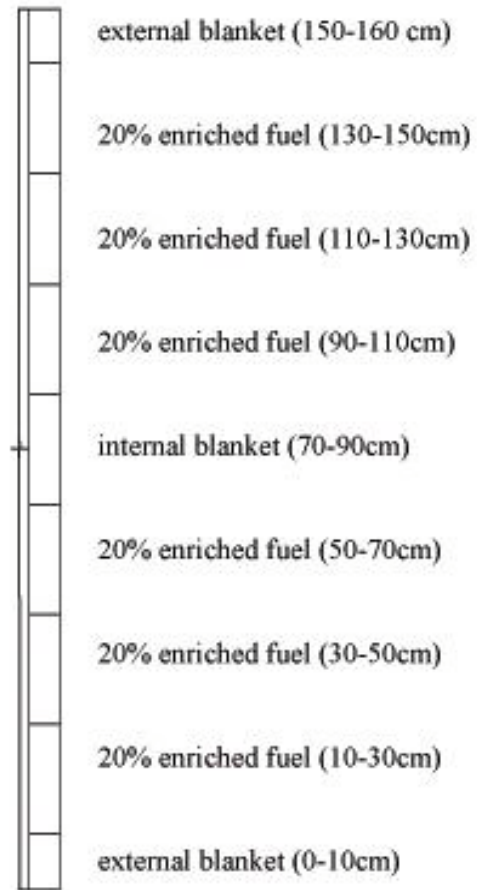


Figure 5.1.6 - 3 Axial Unit Cell Diagram.

for use with ORIGEN and the new core compositions are calculated based on the power density and cross sections. MCODE writes the new composition to an updated MCNP input file and iterates the process [18].

The results of the MCODE calculation yield the unit cell reactivity as a function of burnup. Figure 5.1.6-4 shows the evolution of the unit cell eigenvalue through a burnup of 40 MWD/kgHM. The initial dip in reactivity after a short burnup is a result of immediate fission product poisoning from strongly absorbing nuclides that quickly reach saturation.

The reactivity decreases in an almost linear fashion with burnup. Pu-239 is bred into the core during burnup; however, the fissile inventory decreases because the internal conversion ratio is less than unity. In an epithermal spectrum, Pu-239 capture is significant, and therefore, the reactivity worth of Pu-239 versus U-235 is very similar. The core average conversion ratio is 0.55 at the BOL and 0.65 by the EOL.

The axial regions tend towards an asymptotic Pu-239 concentration of 0.0002 #/b-cm. This is true of every region, and by the EOL, the fissile inventory of the core is approximately 30% Pu-239. Even at this percentage the delayed neutron fraction is considerably smaller than the BOL case, though larger than a fast reactor case where the EOL plutonium fraction of fissile inventory would be much higher due to improved conversion.

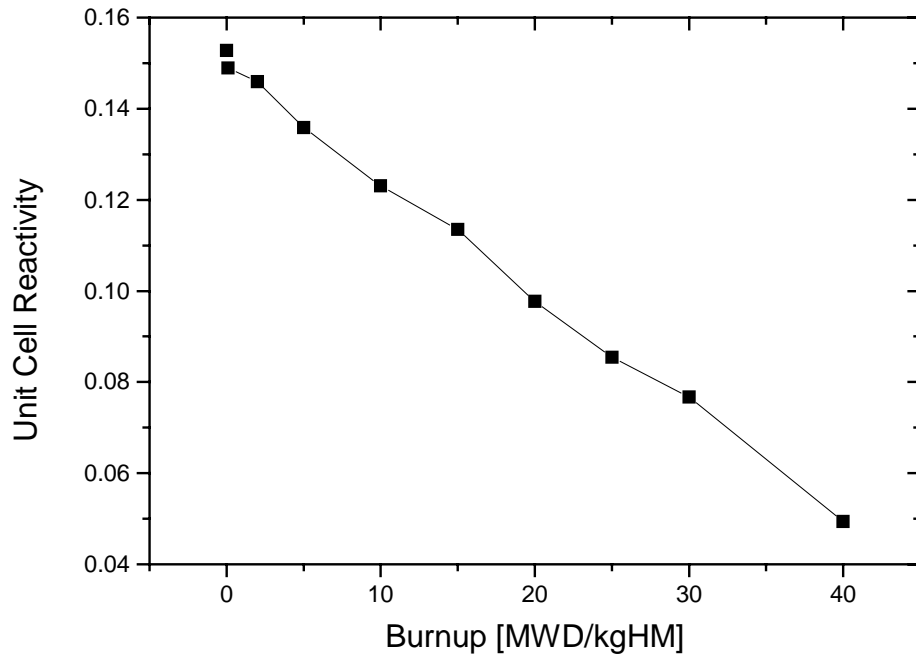


Figure 5.1.6 – 4 Unit Cell Reactivity History.

The unit cell eigenvalue is plotted in Figure 5.1.6-5 as a function of the effective full power life of the core. This graph is analogous to the reactivity vs. burnup curve, but shows the trend in core excess reactivity as the reactor approaches the end of full power life.

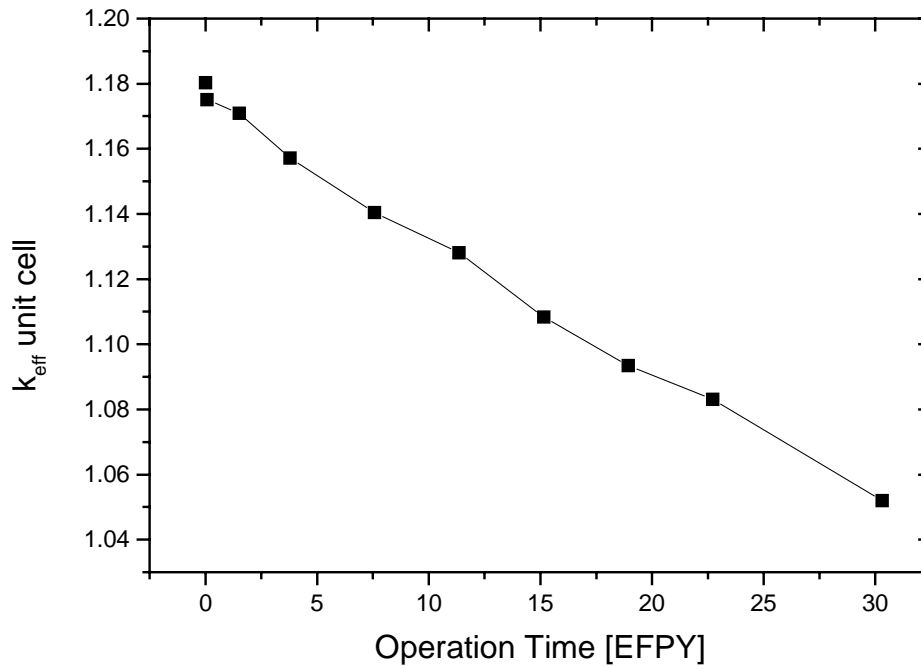


Figure 5.1.6 - 5 Evolution of K_{eff} vs. EFPY.

The total η for fissile species is approximately 1.8 throughout life. Recall that η must be greater than 2.0 to achieve breeding gain. The conversion ratio is significant (~ 0.6) during operation; however, there are several neutronic disadvantages to operating in the epithermal regime. First, the capture-to-fission ratio is relatively large in the epithermal regime compared to the fast regime, and therefore, higher plutonium isotopes buildup in the core during burnup. Also, the flux spectrum is in the resonance capture regime, leading to excess neutron capture and therefore large uneventful capture and fission product poisoning.

Breeding gains are not achievable in the epithermal spectrum, however, effective use of Pu-239 generation and fission is helpful in extending the reactivity limited burnup relative to a thermal core. An effective full power life of 25 years appears achievable using LEU fuel and little moderator.

Effective Delayed Neutron Fraction Calculation

The effective delayed neutron fraction is an important measure for determining the controllability of a nuclear reactor. Reactivity insertions less than the delayed neutron fraction result in reactor kinetics that are slower than prompt critical transients. These insertions, and the ensuing transients, are much easier to control because of the time it takes for delayed neutron precursors to decay. If the reactivity insertion is less than the delayed neutron fraction, the core multiplication is hampered by the fact that the core must wait on the decay. If the insertion is greater than the delayed neutron fraction, the core is said to be super prompt critical, where the transients occur on time scales comparable to the prompt fission time (typically on the order of milliseconds to microseconds) [3].

For ease of control, and system reliability, large delayed neutron fraction is desirable. Fissile Uranium 235 has a relative delayed neutron yield more than three times that for fissile plutonium isotopes [3]. Therefore, at very high conversion ratios the effective delayed neutron fraction will decrease dramatically by the EOL. This safety concern is another argument against fast reactors for surface applications.

The delayed neutron fraction is calculated by finding the nuclide specified delayed neutron fractions and finding the average weighted by the total fission macroscopic cross section. The equation for the effective delayed neutron fraction is shown in Equation (8).

$$\beta_{eff} = \frac{\sum_i \sigma_f^i N^i \beta^i}{\Sigma_f} \quad \text{Equation (8)}$$

A potential concern with a converting core is that the buildup of plutonium will reduce the delayed neutron fraction. This is the case. The BOL delayed neutron fraction is 0.0068, by 40 MWD/kgHM of burnup, the delayed neutron fraction is reduced to 0.0054. With a conversion ratio of 0.60 on average, the inventory of fissile plutonium doesn't exceed the fissile uranium, and therefore, the effective delayed neutron fraction doesn't drop dramatically. In a fast breeder reactor, where aggressive Pu-239 breeding occurs, the delayed neutron fraction would be much smaller towards the EOL (~ 0.003).

To achieve slow transients, and maintain safe operation of the plant, large effective delayed neutron fraction is desirable. Taking advantage of plutonium conversion here does not significantly hamper the safe operation of the reactor because the EOL delayed neutron fraction is relatively large compared to fast reactor alternatives.

Energy Dependence of the Flux

The epithermal flux spectrum is plotted in Figure 5.1.6-6. The normalized flux per unit lethargy is plotted against neutron energy. For a standard LWR, the flux in the energy regime between 1 eV and 100 keV would be approximately a flat linear curve, because the epithermal flux adheres to the 1/E spectrum [7]. However, the internal moderator present in the core is a weaker slowing down agent than light water, and the flux spectrum is hard relative to that of a LWR. This is apparent with the peak in flux between 1 and 100 keV.

There is a thermal peak between 1 and 0.1 eV. This type of peak is characteristic of most thermal reactors, however, it is greater for thermal systems. Most nuclides have resonant structure in this regime. This will enhance Doppler temperature feedback for the surface core, however, during normal operation parasitic absorption via radiative capture in fissile species and fission products reduces system reactivity.

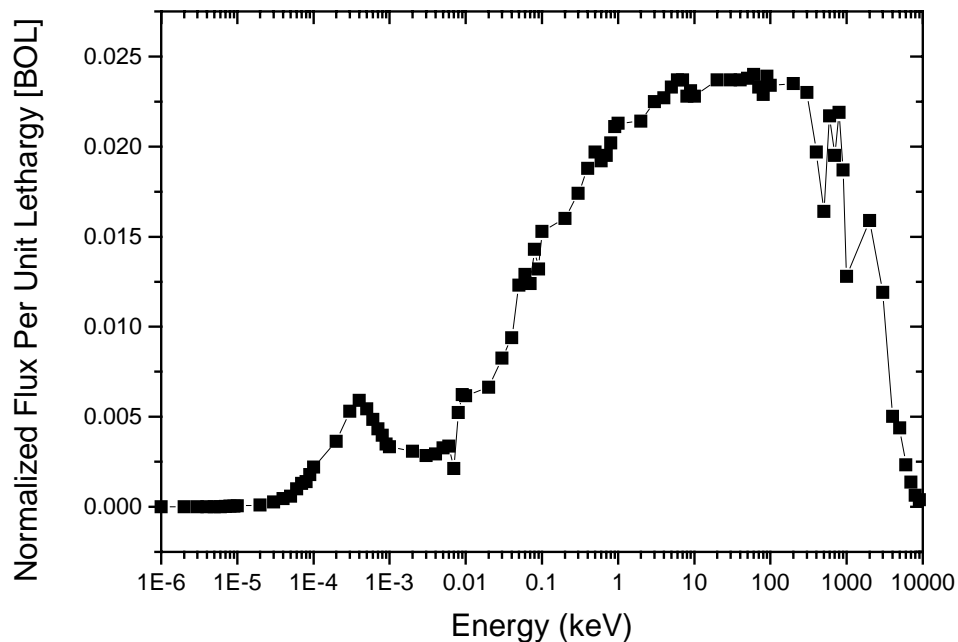


Figure 5.1.6 - 6 Normalized Flux Energy Spectrum.

Axial Power Shape

The evolution of the axial power shape and the power peaking factor for the axial distribution are also calculated. The core contains three axial blanket regions to improve conversion. The internal blanket is 20 cm tall. At the BOL, little to no power is generated in the central region of the core. However, Figure 5.1.6-7 illustrates the change in local power fraction with core burnup.

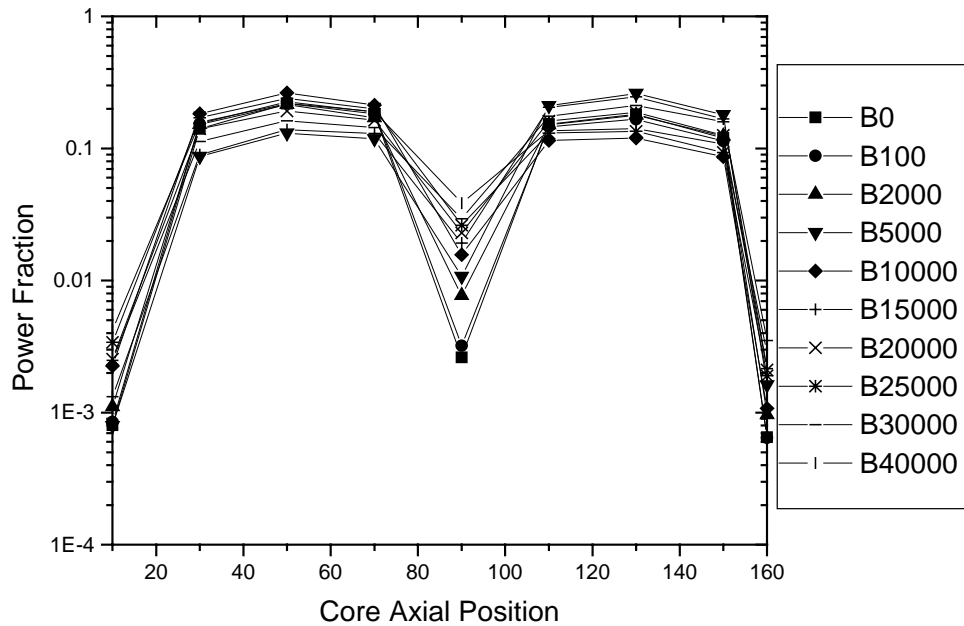


Figure 5.1.6 - 7 Axial Power Shape during Burnup.

The curves are labeled in units of MWD/MTHM for each burnup point. As is evident from the plot the power generated in the center of the core increases dramatically. As the power shifts towards the center of the core with burnup, by flattening axial power the neutron economy is improved because axial leakage is reduced. The BOL power peaking factor was calculated to be 1.53 (excluding the axial external blanket regions).

5.1.7 Reflector Design

The unit cell results are optimistic calculations in that they do not include radial leakage, and the whole core is relatively narrow based on the assumed L/D, therefore, an excellent radial reflector with high albedo is necessary for the design to be feasible. By varying the reflector worth, the core reactivity can be controlled, so the impinging neutron current (or bare core leakage) must be large to ensure that the neutron economy is heavily dependent on the reflector.

The radial reflector is a cylindrical region surrounding the blocks. The reflector has six control drums, or rotating cylinders. To control reactivity the cylinders can be rotated such that a “shutter” is exposed to the core. On one face of the cylinder there is a 1 cm thick layer of a shutter material. The shutter acts as an absorber that will effectively reduce the reflector worth, thereby reducing the core reactivity when the shutter is rotated in.

If the shutter is a completely black neutron absorber, the shutter-in-reflector configuration inserts negative reactivity equal to the radial bare leakage. This type of control system is simple. Only six rotating drums are used because of the hexagonal block geometry.

Also, the moving parts of the system are ex-core, and therefore there is no risk of wear and tear on vital structures inside the core from alternative systems such as control rod banks. Lastly, the reflector worth for a tall narrow core is large, and a relatively large reactivity swing can be controlled, so the system is redundant in that only a few of the drums should be able to suppress the BOL reactivity.

Reflector Material

Reflector worth for different materials were calculated based on BOL MCNP models. As expected high beryllium content reflectors showed the best performance because of the moderation of neutrons in the reflector. BeO and Be₃N₂ are promising from a neutronics standpoint. Though Be₃N₂ has a slightly lower density than BeO (and consequently a lower total mass), and a slightly higher beryllium number density, the oxidation resistance of BeO motivates its use as the external reflector.

Graphite and Be₂C yielded mediocre results. For the reference case run, the keff was only ~0.8 for both materials.

BeO will be inert in the CO₂ atmosphere whereas the improved neutronics performance of the Be₃N₂ comes at the expense of increased operational hazard. The fast reactor reflectors had the worst overall performance. PbS and Zr₃Si₂ have relatively low albedos compared to BeO and are much heavier. Table 5.1.7-1 compares these three reflectors. [8]. Based on acceptable neutronic performance and excellent oxidation resistance, BeO is selected as the core reflector material.

Table 5.1.7 - 1 Comparison of Potential Reflectors.

| Reflector | albedo | Density [g/cc] | keff |
|---------------------------------|---------------|---------------------------|-------------|
| BeO | 93.50% | 3.01 | ~1.05 |
| PbS | 85.63% | 7.50 | ~0.40 |
| Zr ₃ Si ₂ | 85.25% | 5.88 | ~0.45 |

Shutter Material

The neutron current impinging on the reflector is relatively hard because of the epithermal flux spectrum in the core. Therefore, the shutter material must have a large absorption cross section for epithermal neutrons. TaB₂ was selected as a potential shutter material because tantalum has a large resonance integral, and therefore large epithermal absorption cross section [9]. Natural Boron is a strong neutron absorber at any energy of incident neutrons [9].

TaB₂ is relatively dense (12.38 g/cc [10]) because of the heavy tantalum. However, the shutter thickness is only 1 cm, and this heavier shutter material does not contribute significantly to the mass of the system compared to the mass of heavy metal in the core. The control material must be manufactured with high porosity to accommodate for helium production from neutron absorption in boron. Therefore, the density is taken at 90% theoretical density.

Drum Worth and Control

The reactivity worth of the drums is determined by the reactivity worth of the total reflector. The core is tall and narrow, and therefore radial leakage is very large, on the order of 25% unreflected. The BeO reflector thickness is set to 30 cm. This is on the same order as the core dimension.

MCNP is used to model a homogenous core. The core is encased with two cylinders. The innermost cylinder is 1 cm thick and can be set to the reflector material or the shutter material. The remainder of the ex-core region (~30 cm thickness) is BeO reflector.

The difference between the effective eigenvalue of the core for the cases where the shutter is TaB₂ and BeO was calculated and the reactivity worth of the entire control drum array was computed. Rotating all six drums so that the shutter is inward reduces the reactivity by 0.4085 (3.6% error). Each drum, therefore contributes -68.1 pcm of reactivity.

Recall that the BOL effective delayed neutron fraction is 0.0068, therefore, each drum alone can be used to control \$10 of reactivity at BOL. Only three of the six drums are needed to fully suppress the BOL reactivity, therefore, as many as three drums can fail and the reactor can still be operated safely. Also, during transport all of the drums are rotated inward so that there is a lot of negative reactivity in the core to prevent reactivity accidents during transport.

5.1.8 Reactivity Feedback and Transients

The core is designed to have negative reactivity feedback once deployed on Mars. The core reactivity increases as CO₂ density increases. The gas is incredibly rare, and this coolant density coefficient is practically zero, but positive in nature. At BOL, there is a lot of fertile material in the core and these contribute to negative Doppler temperature feedback at the BOL. During burnup, fission products act as resonant absorbers and negative temperature feedback is assured throughout burnup.

The whole core model was also used to estimate the fission generation time. The reflector is a lion's share of the reactor package volume (84%). The reflector contributes to some neutron slowing down, but as the core is very leaky, a large number of neutrons impinge on the reflector and will transport through the reflector for a long time before eventually diffusing back into the core to initiate fission. The effective fission generation time is therefore much larger in the whole core calculation than was indicated in the unit cell calculation.

The unit cell calculation yields a fission generation time of 6 microseconds. This is relatively short, but more than 10 times the value for a conventional small fast reactor system (i.e., SAFE 400) [2]. In the whole core model, the fission generation time is calculated to be 700 microseconds. This is an incredible increase and very promising from the standpoint of reactor safety. The value increases because of the large radial leakage into the reflector.

Two parameters are used to gauge the reactor safety under reactivity transients are the delayed neutron fraction and the prompt fission time. Any reactivity insertion less than the delayed neutron fraction can be controlled in principle. The delayed neutron fraction for the CECR is relatively large at every point in life. The time constant for reactivity transients is proportional to the product of the fission generation time and the delayed neutron fraction for a given worth of reactivity change.

Therefore, to ensure slow reactivity transients the product of these two parameters must be large. The BOL value for the product is 5.1 microseconds, and it remains large through burnup, reaching a minimum value of 3.8 microseconds by the EOL.

H₂O Immersion Accident

Since the core is undermoderated, the reactivity will increase if there is a water immersion accident. The whole core model is used to calculate the worth of immersion of the core in H₂O. This situation can occur if there is an accident during liftoff of the surface power package. If the core lands in the ocean and is flooded with light water, the reactivity increases by 0.124 or roughly \$2. However, each control drum shutter contributes -\$10 of reactivity.

A potential safety system was considered where the reflector breaks away from the core during a launch accident. However, if the reflector and therefore control drums are severed from the core during a liftoff accident and the core lands in the ocean, the water will also acts as an external reflector and the core will be critical. Therefore, no reflector severing safety systems are considered.

5.1.9 Total Size and Mass

A brief description of the total system is given in Table 5.1.9-1. The reactor core is somewhat large compared to fast systems because of the moderator present in the fuel matrix. The total mass is less than 4 MT. The BOL k-eff includes fission product poisoning. Figure 5.1.9-1 illustrates the final core design with the reflector, core, and control drums.

Table 5.1.9 - 1 CECR Core Description

| | |
|-------------------------------------|--|
| Power | 1 MWth |
| Core Dimensions (Height / Diameter) | 160 cm / 40 cm |
| Total mass | 3800 kg |
| Reflector thickness | 30 cm |
| Reflector material | BeO |
| Coolant | Martian Atmosphere (+95% CO ₂) |
| Coolant volume fraction | 30 v/o |
| Fuel | 20% enriched UO ₂ |
| Fuel volume fraction | 30 v/o Matrix (19.5 v/o Core) |
| Fuel element geometry | Triangular Pitch Blocks |
| Cladding | MA956 ODS |
| k-eff BOL | 1.17 |
| EOL fuel burnup | 35 MWD/kgHM |
| Core lifetime | 25 EFPY |



Figure 5.1.9 - 1 Whole Core and Reflector.

The reactor system package consists of an active core region, two external blankets and a reflector. The total height of the reactor package is 160 cm. The equivalent active core diameter is a little less than 40 cm. The outer diameter of the reflector is 100 cm. The reflector constitutes more than 80% of the total volume. The total of these masses is 3800 kg.

5.1.10 Integration and Operational Issues

One potential operational concern during the integration of the turbo machinery and the reactor package is the axial neutron leakage from streaming. The block coolant channels are relatively wide (2.9 cm ID), and with a gas coolant, neutrons easily stream through the coolant channels and axial leakage is large. A calculation of the axial exit current in the unit cell model reveals that the reactivity penalty from axial leakage is roughly 6.5%.

This means that the equipment in close proximity to the core outlet will be irradiated with a hard neutron current (because the flux spectrum is epithermal). As part of the shielding design, a beam block is being developed to reduce neutron irradiation of the turbo machinery so maintenance can be performed. An area of future work will be to find methods for reducing axial leakage by perhaps going to smaller coolant channels, or incorporating a lightweight beam block or axial reflector that is nestled between the core and the turbo machinery.

There is additional need for iteration between thermal-hydraulic and nuclear design with respect to core height and coolant channel dimensions. To improve the neutron economy long narrow fuel channels are desired. The narrow channels reduce axial neutron streaming, and therefore increase the core reactivity. On the same token, large L/D is desirable to increase the reactivity worth of radial leakage. Unfortunately, both of these approaches are unfavorable from a thermal-hydraulic standpoint because each increases the pressure drop of the coolant flowing through the reactor. The tradeoffs and importance of these issues are discussed at more length in the following section of this report.

5.1.11 Future Work and Design Evolution

This conceptual design is certainly evolvable. Several of the assumed parameters may be optimized to increase the reactor performance. The L/D for the active core is assumed to be 4, and it was found that there is sufficient reactivity control margin using the TaB₂ shutter material in the control drums to reduce the radial leakage fraction and still control the core. In fact, the reflector control appears to work so well that L/D of 2 or smaller can probably be employed with large reactivity swing.

Also, neutron economy can be improved through more careful consideration of axial enrichment zoning. The H/HM ratio is chosen to be in the epithermal regime, and a conversion ratio of 0.6 was achieved, however, the capture to fission ratio of plutonium is incredibly sensitive to the neutron energy [4], and therefore spectrum hardening may improve the plutonium breeding and reactivity gain through burnup. However, increasing the plutonium concentration will reduce the effective delayed neutron fraction. Future work will have to examine more carefully the tradeoffs between conversion ratio and effective delayed neutron fraction.

Lastly, the 37 blocks contain relatively large coolant channels (2.9 cm ID). Axial neutron streaming reduces the reactivity considerably at every point in life and also introduces an incident neutron current on the turbo machinery near the core inlet or outlet. Going to smaller

coolant channels if possible will reduce the axial leakage, and, in general, techniques for reducing axial neutron leakage are an additional area of recommended future work.

5.1.12 References

- [1] Deickamp, H., *Nuclear Space Power Systems*, Atomics International. Canoga Park, CA, 1967.
- [2] Poston, D.I., “Nuclear Design of the SAFE-400 Space Fission Reactor,” *Nuclear News* December 2002, pp. 28 – 35.
- [3] Stacey, W., *Nuclear Reactor Physics*, John Wiley and Sons, Inc., New York, 2001.
- [4] Yarsky, P., “Neutronic Evaluation of GFR Breed and Burn Fuels,” MIT-GFR-005, May 2003.
- [5] Hofman, G.L., *A Short Note on High Density Dispersion Fuel*, Argonne National Lab, June 1996.
- [6] Ceradyne’s Ceralloy Particulate Composite Properties, CERADYNE, 2003.
< <http://www.ceradyne.com/dtpc.htm>>
- [7] Duderstadt J., Hamilton L., *Nuclear Reactor Analysis*, John Wiley and Sons, Inc., New York, 1976.
- [8] Yu, K., “Neutronic Evaluation of GCFR Core Diluents and Reflectors,” MIT-ANP-TR-084, 2003.
- [9] Online plotter for MCNP and ENDF cross section data, KAERI. 2003,
<<http://atom.kaeri.re.kr/endlplot.shtml>>
- [10] Hodgman, C., ed., *Handbook of Chemistry and Physics*, Chemical Rubber Publishing Company, 44th ed., Cleveland, OH, 1962.
- [11] Subbotin, V.I., Matveev, V.I., Toshinsky, G.I., “Lead-Bismuth Cooled Fast Reactors in Nuclear Power of the Future,” International Topical Meeting on Advanced Reactors Safety, April 1994.
- [12] *INCOLOY alloy MA956*, Special Metals Corporation SMC-008, 1999.
- [13] Thon, S., “Selection of Materials for a Supercritical CO₂ Cooled GCFR,” MIT-GCFR-001, 2002.
- [14] *The Reference Mission of the NASA Mars Exploration Study Team*, eds. Stephen J. Hoffman, David L. Kaplan, NASA, Lyndon B. Johnson Space Center, Houston, TX. July 1997.
- [15] Johnson, J.R., Lebenhaft, J.R., Driscoll, M.J., “Burnup Reactivity and Isotopics of an HTGR and Fuel Pebble,” *Trans. Am. Nucl. Soc.* vol 85 Reno November 2001
- [16] Zhiwen Xu, Michael Driscoll, Mujid Kazimi, “Effect of Moderator-to-Fuel Ratio on High Burnup Potential in UO₂-Fueled Water/Steam-Cooled Lattices,” *Trans. of Am. Nucl. Soc.*, Vol. 84, 43-44, Washington, DC, November 2000.

[17] Hejzlar, P., “Evaluation of the Block-based Core with Heat Pipes,” in Wei, T.C. and Rouaualt, J., “Development of GEN-IV Advanced Gas-Cooled Reactor with Hardened/Fast Neutron Spectrum,” I-NERI Annual Progress Report, Argonne National Lab., March 2002.

[18] Xu, Z., Hejzlar, P., Driscoll, M.J., Kazimi, M.S., “An Improved MCNP-ORIGEN Depletion Program (MCODE) and Its Verification For High Burnup Applications,” PHYSOR, Seoul, Korea, 2002.

[19] Knief, R.: *Nuclear Engineering: Theory and Technology of Commercial Nuclear Power*, 2nd ed., Taylor and Francis, Inc., Bristol, PA, 1992.

5.2 CECR CO₂ BRAYTON CYCLE

5.2.1 Introduction

The conversion of the thermal power to the electric power on Mars is investigated in this section. The Brayton cycle or Stirling engine are the prime candidates for Mars surface power generation. In our design we decided to investigate the possibility of using the Martian as a working fluid for the Brayton cycle.

Operation for long period of time without a leak from the system or Martian atmosphere ingress into the system is difficult. The easiest way to prevent this problem is to design the system to operate with the Martian atmosphere. In order to extend this protection to the reactor system as well we decided to use a gas cooled reactor connected directly with the Brayton cycle.

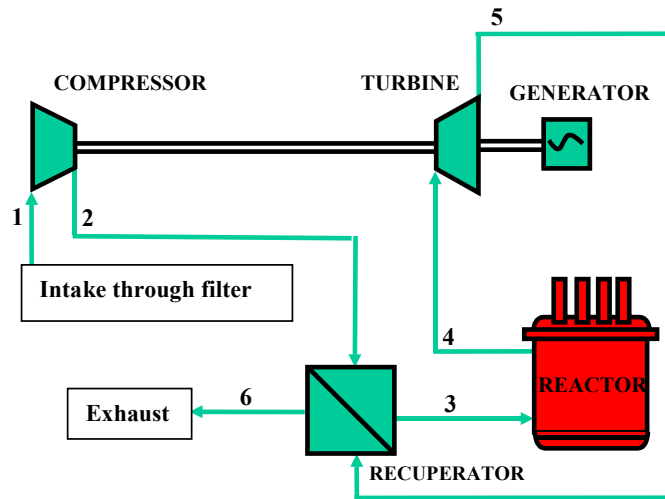
5.2.2 Analysis

For the first cut it was decided to approximate the Martian atmosphere by pure CO₂ (as CO₂ constitutes 95% of Martian atmosphere). The maximum operating temperature of the system was selected as 600°C because there is an experience in the British AGR units with low pressure CO₂ up to 650°C and the corrosion behavior is well understood [1]. The minimum operating temperature for the cycle depends on the overall design since the Martian atmosphere will be used for heat rejection purposes as well. The environmental temperature on Mars varies significantly. For this study Marsian atmosphere temperature of -40°C was. This temperature was used for intake temperature for the cooling medium to the heat rejection heat exchanger in the case of closed cycle and as the compressor inlet temperature in the case of the open cycle. The main objective is to design the cycle such that achieves efficiency around 20% and is as simple as possible in order to improve the system reliability.

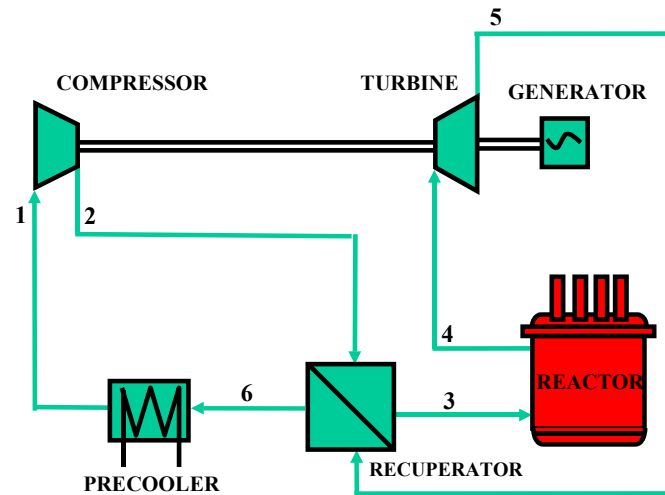
Three different types of cycles were investigated. The regenerative closed Brayton cycle is used in this study as the base option. This type of cycle is currently investigated for the terrestrial application with nuclear reactors as well. The second concept is the regenerative open Brayton cycle. The last concept investigated is the non-regenerative open Brayton cycle. Figure 5.2.2-1 shows the cycle schematics of all three concepts. Since simplicity is more important in this case than the efficiency the effect of inter-cooling was not investigated.

This analysis focuses on the feasibility study and does not attempt to design the whole system. Therefore, the cycle is investigated as a single loop, even though it is likely that the final design will be multiple loops with component cross linking in order to be able to operate at partial capacity if some components get damaged.

a) Open Cycle



b) Closed Cycle



c) Non-regenerative open Brayton cycle

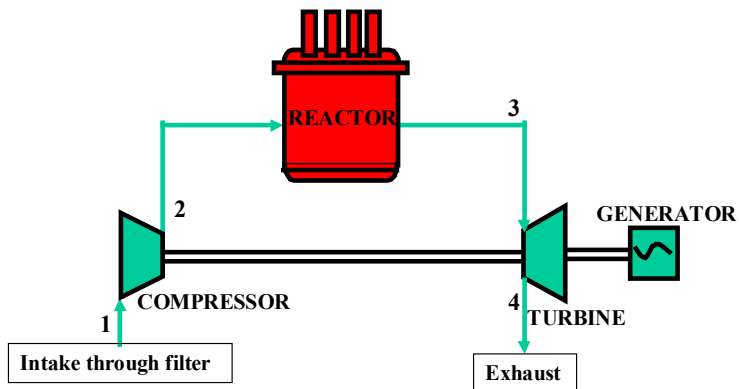


Figure 5.2.2 - 1 Brayton Cycle Layout.

Before the start of the analysis let us give some thoughts to each component within the cycle. These insights will be useful in the subsequent analysis. Probably the most vulnerable components are the compressor and turbine followed by the generator. The reason for this is that all of these components involve moving parts that are running at high rotational speed under heavy load. Since the cycle power is quite low, it is reasonable to assume that both, the compressor and the turbine will be centrifugal machines.

Centrifugal machines have the advantage of higher reliability and wider operating characteristics. Since these components will likely run for an extensive period of time without careful maintenance they should be designed with large safety margins. As turbomachinery design is not a part of this study the only suggestion that can be given is on the value of the rotational speed. The rotational speed is a free parameter. It is advisable to reduce the rotational speed as much as possible in order to reduce the stress within the blades and the bearing load.

In this analysis the turbine efficiency used is 85% and compressor efficiency is 80%. These numbers are quite low considering the current practice, however due to an extensive period of operation without maintenance they should be reasonable. Confirmation is necessary in the future when the detail design and testing is performed.

As for the heat exchangers, they will be some form of compact heat exchangers. The recuperator is of main importance as it affects the cycle efficiency in two ways: effectiveness and pressure drop. The trade-off here is that one would like to keep the system compact. That means having a small recuperator. A small recuperator reduces the cycle efficiency. Another difficulty is that the recuperator effectiveness does not solely depend upon the recuperator volume, but upon the arrangement as well. The face area versus the length are important parameters to be optimized. Usually, the small face area and long recuperator will have higher effectiveness, but also higher pressure drop. This is one of the reasons why compact heat exchangers have large face area and are short, since the trade-off between the pressure drop and effectiveness dictates the design.

The design of the recuperator significantly affects the total cycle efficiency. Another important thing to notice is that the higher pressure drop of the components the higher the optimum pressure ratio. Since we would like the optimum pressure ratio to be small we should strive for low pressure drop within the system. However, this might result in very large, and therefore massive, components. The effectiveness of the recuperator used in the study is 95%.

A precooler is used for cycle heat rejection. The design of this heat exchanger is usually not challenging, on Earth cooling by water is employed. However, on Mars the situation is different and the Martian atmosphere will likely be the only available heat sink. This may impose certain difficulties as the low atmospheric pressure on Mars reduces the cooling capabilities. It is possible to design the precooler in such a way that it will satisfy requirements on the hot side pressure drop and cold pressure drop or pumping power. The volume can be than calculated by adjusting the mass flow rate and the outlet temperature of the cooling medium. However, this sometimes results in a large precooler. Thus, it might be necessary to compromise here as well.

There are two different heat exchangers considered for the use. The plate-and-fin compact heat exchangers [2] (see Figure 5.2.2-2 for detailed view) and printed circuit heat exchangers (PCHE) manufactured by HEATRIC [3]. Figure 5.2.2-3 shows the older design of PCHE. There is a new design which is a pure counter-current flow. For simplicity, only the counter current parts of the heat exchangers were considered. This will introduce a discrepancy mainly in the case of plate-and-fin heat exchangers, because their distribution heads introduce another portion of pressure drop, which is not modeled in this analysis, thus worsening the performance of the cycle. Table 5.2.2-1 presents the geometrical characteristics as defined in [2]. Table 5.2.2-2 contains the

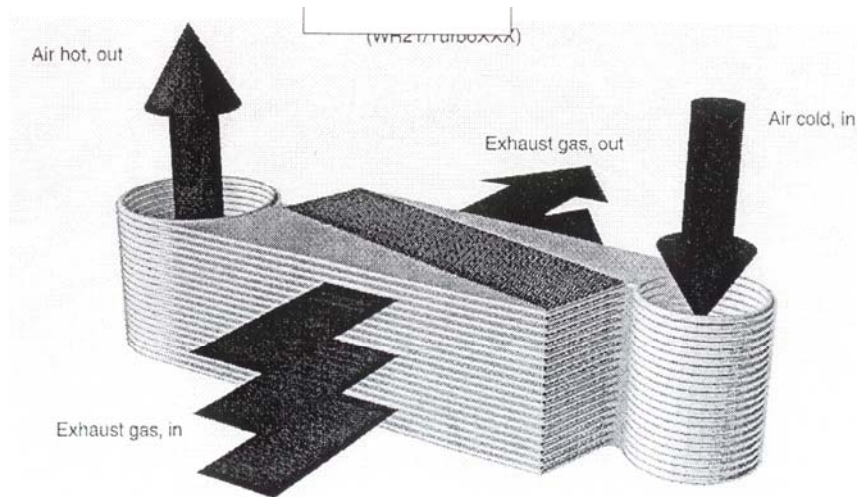


Figure 5.2.2 - 2 Plate-and-Fin Heat Exchanger.



Figure 5.2.2 - 3 Printed Circuit Heat Exchanger.

Table 5.2.2 - 1 Surface Characteristics

| Geometrical Data | Hot Side | Cold Side | |
|---|-----------------|------------------|--------------------------------|
| Ratio of free flow to face area per side | 0.852 | 0.828 | |
| Heat transfer area per unit volume per side | 4143.7 | 4721.1 | m ² /m ³ |
| Ratio of fin area to total area per side | 0.911 | 0.777 | |
| Plate spacing | 5.08 | 1.78 | mm |
| Fin material thickness | 0.08 | 0.08 | mm |
| Axial wave height of material | 1.97 | 1.97 | mm |
| Axial wave length of material | 4.76 | 4.76 | mm |
| Total fin length | 5.08 | 1.78 | mm |
| Effective fin length | 2.54 | 0.89 | mm |
| Fin material conductivity | 20.77 | 20.77 | W/m-K |
| Wall metal thickness | 0.152 | 0.152 | mm |
| Wall material conductivity | 20.77 | 20.77 | W/m-K |

heat transfer and friction data for this particular surface. A logarithmic interpolation was used to obtain the points in between those presented in Table 5.2.2-2. j factors were used in the typical manner for the compact heat exchangers as presented in [2]. In the case of PCHE the Gnielinski heat transfer correlation [1] was used.

The generator was not extensively investigated in this study. The efficiency of the generator was assumed to be 98% in all cycle calculations. In addition the mechanical efficiency of the clutches was taken as 99%.

Table 5.2.2 - 2 Heat Transfer and Friction Data

| Wavy Fin Matrix #2503 | | |
|-----------------------|--------|--------|
| | Hot | Cold |
| Re1 | 60 | 60 |
| Re2 | 2000 | 2000 |
| f1 | 0.214 | 0.214 |
| f2 | 0.0416 | 0.0416 |
| j1 | 0.039 | 0.039 |
| j2 | 0.0099 | 0.0099 |

5.2.3 Core Thermal Hydraulics

Due to the high melting point of the fuel used for the surface reactor and low operating temperature of the core as well as low power density, the temperature within the fuel was not of primary interest. The main concern was to access the pressure drop across the core, because it strongly affects the cycle efficiency.

Figure 5.2.3-1 depicts the results of core analysis for different number of hexagonal blocks in the core. It shows how the fractional pressure drop across the core decreases with the increasing core operating pressure. The value of fractional pressure drop across the core should be on the order of 5% to 10% in order to assure high efficiency. From the figure we can see that in order to achieve this goal the core has to operate at about 100 kPa. This shows the difficulty of operating in the open cycle mode since this would require a high pressure ratio across the compressor (the pressure on Mars is 6.1 kPa).

The film temperature rise for 1 block is around 100°C, for 7 blocks around 11°C, for 19 blocks around 4°C and for 37 blocks 2°C. The current reference design uses 37 blocks. The results show that there is a margin for increasing the core power density if necessary. However, considering that the core has to run 25 years low power density is one of the requirements.

Figure 5.2.3-2 shows the importance of the core fractional pressure drop on the cycle efficiency. For the reference design the 5% pressure drop across the reactor is selected. All other efficiencies are normalized with respect to this value. Thus the plot shows to what fraction the cycle efficiency will be reduced if the fractional pressure drop is increased. Figure 5.2.3-2 clearly indicates the importance of the pressure drops on the cycle efficiency.

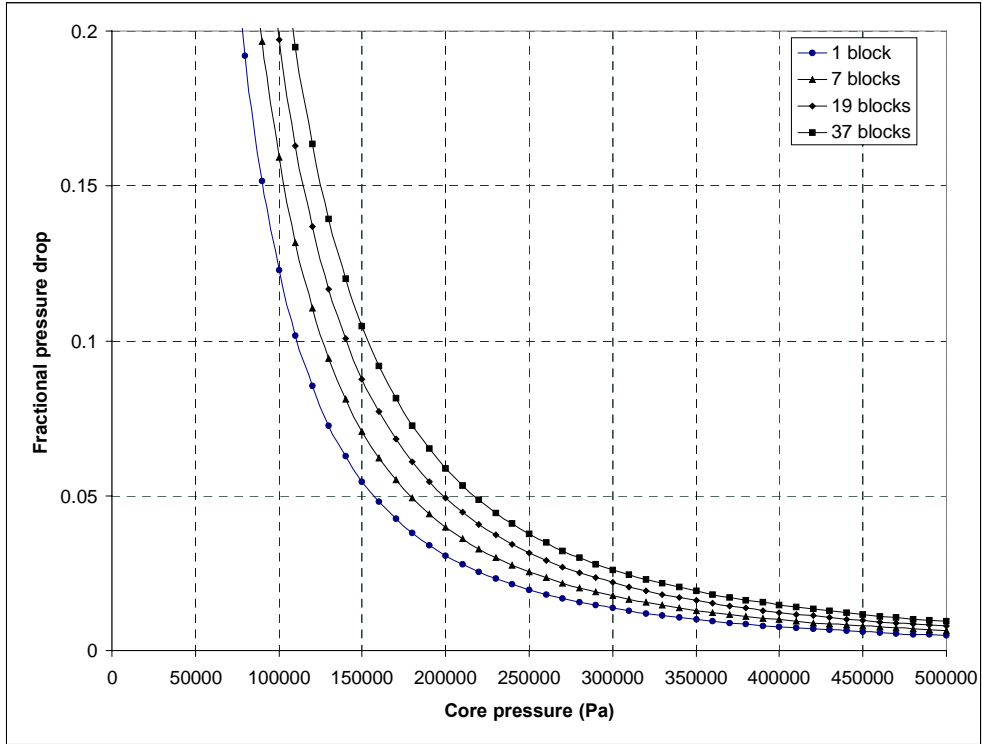


Figure 5.2.3 - 1 Effect of Core Pressure on the Fractional Pressure Drop.

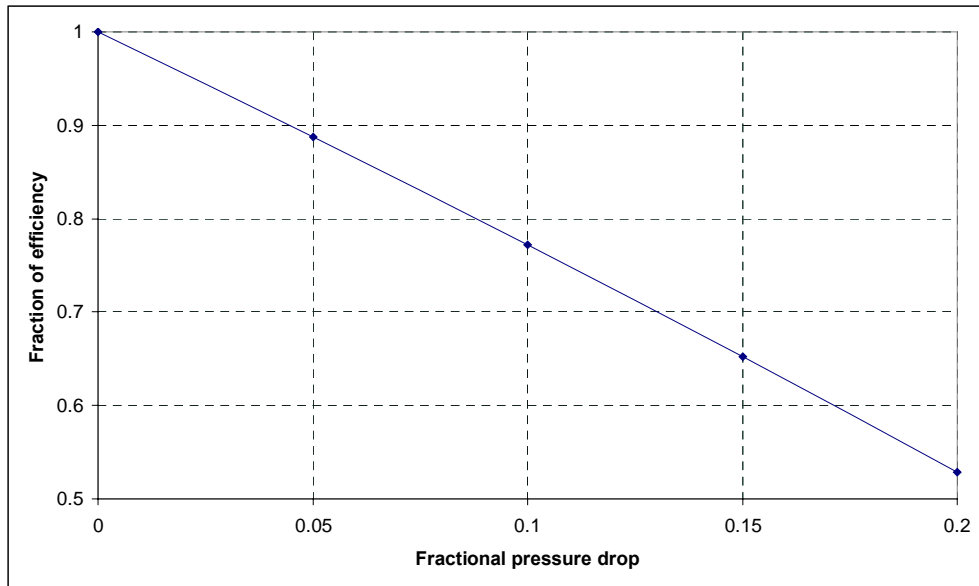


Figure 5.2.3 - 2 Effect of Core Fractional Pressure Drop on the Cycle Efficiency.

5.2.4 Investigated Concepts - Results

Regenerative Open Brayton Cycle

In this work, we focused on several different designs. We started with the simplest option, which is a regenerative open cycle. The compressor intake is directly from the Martian atmosphere, after compression the fluid is heated in the recuperator and reactor, then it generates power in the turbine. The gas from the turbine preheats the reactor inlet in the recuperator and after leaving the recuperator, the gas is discharged back into the atmosphere.

This simple idea will eliminate any possible problems with leakage relative to the closed system since it already operates as an open system. Another advantage is that this system does not require a precooler. Elimination of another component reduces the overall mass of the system and since the precooler pressure drop is not present the pressure drops in the core and in the recuperator can be increased.

The disadvantage of this concept comes from the low atmospheric pressure on Mars. The pressure on Mars is about 6.1 kPa. Even when pressure ratios of around 5.0 were used the pressure drop across the core and the recuperator was very high. The reason is that the cycle efficiency is sensitive to the fractional pressure drop, i.e. the pressure drop divided by the maximum pressure in the component. For such low pressures as those on the surface on Mars even the pressure drop of 5 kPa, which is in general very low, results in a very high fractional pressure drop of about 16% on the high pressure side and more than 90% on the low pressure side. This is unacceptable for any gas cycle.

It was possible to reduce the fractional pressure drops in the recuperator to reasonable values, however that resulted in unreasonable increase in the face area of the heat recuperator. On the other hand those heat exchangers will be only about 2 cm long with the temperature rise of about 500°C across them. Even though it was possible to theoretically design a recuperator that would satisfy the requirements on the pressure drop their practical application and compactness were significantly compromised. Moreover, when it comes to the reactor it was not possible to reduce the pressure with the currently used L/d parameter. To reduce the pressure to a reasonable value the reactor would consist of a single hexagonal block with all coolant going through one channel. The film temperature difference is around 100°C.

All the factors mentioned above makes the use of an open cycle extremely difficult and less attractive compared to other options. With the open cycle an efficiency of 20% is achievable, however the reactor design will have to follow the requirements of the power cycle. Additionally, heat exchangers that are capable of operating with temperature gradients of 500°C over just a few centimeters needs to be developed. Even then the whole plant layout is difficult as virtually any system pressure drop dramatically compromises the cycle efficiency. Therefore a reference design of this cycle was not established.

The possible way of making the core design acceptable is to increase the pressure ratio of the compressor. This would result in a larger and more difficult compressor design, however it is likely the only way how to make the cycle attractive. However, even if the cycle operated at high pressure ratio the design of the hot side of the recuperator is still very difficult.

Closed Cycle – Heat Rejected by Natural Convection

Since the efforts on the regenerative open Brayton cycle were not satisfactory, we directed our efforts to the closed cycle operating at higher pressure. In this case a feed compressor and storage tank needs to be added to the cycle. It is also necessary to add a precooler into this system. The feed compressor pumps the Martian atmosphere to a storage tank and keeps it at the compressor inlet pressure. In the beginning of operation the Martian atmosphere is pumped to the whole system through this feed compressor. If a leak occurs in the system the pressure in the tank starts to decrease and the feed compressor starts adding gas into the storage tank.

The maximum available leak is defined by the maximum flow rate through the feed compressor. This value is up to the designer. However, the higher the allowable leak the more power is consumed by the feed compressor.

The analysis in this case focused on increasing the cycle operating pressure to an extent when the component pressure drops will be sufficiently low. For the compressor outlet pressure of 500 kPa the pressure drops were very small, thus the 25% was achieved at the pressure ratio of 1.7. The efficiency improvement of 5% over the regenerative open cycle seems a bit small considering the pressure drop reduction. The reason is that for the open cycle the intake was directly from the atmosphere, thus at significantly lower temperature (-40°C vs. 40°C for the closed cycle). The reason for such increase of compressor inlet efficiency is that a large temperature difference is required for the precooler.

The recuperator size is 1.5 by 1.5 m the face are and 0.32 m long, which is reasonable. The fractional pressure drops are 1.75% on the hot side and 3.15% on the cold side. Fractional pressure drop in the reactor is less than 1%. The fluid flow rate for the 1 MW reactor thermal power is 7.7 kg/s. The results of the cycle looks promising; however, a problem arises once the design of the precooler is attempted.

The finned tube precooler was investigated. It was discovered that in order to reject the heat about 17,000 finned tubes with a tube diameter of 9.65 mm, fin diameter of 23.4 mm, and length of 1 m would have to be used. This results in an array of tubes of about 3 by 3 m. This is unacceptably large since the mass of the precooler even when aluminum is used is around 7 MT.

The closed cycle achieves 5% higher efficiency at significantly lower pressure ratio. However, the cycle gets more complex since the closed cycle uses a precooler. Precooler design in particular is very difficult. In order to take advantage of the higher efficiency it is necessary to reduce the mass of the precooler. Therefore the forced circulation cooling will be investigating next.

Closed Cycle – Heat Rejected by Forced Convection

In order to overcome the problems with the precooler described above and to reduce its volume and mass the use of an additional fan for the precooler was investigated. The plate and fin compact heat exchanger described in Table 5.2.2-1 was used. The hot side geometry was used on the cold side as well since its hydraulic resistance is less. In this case we assumed the same cycle design only the finned tube precooler was replaced by the plate-and-fin precooler and the flow on the cold side was forced by a fan. The analysis focused on evaluating the pumping power requirements. The reactor is designed to run for the desired lifetime at 1 MW thermal power, thus with the efficiency of 25% there is about 50 kWe that can be used for the fan and still meet the design goal of 200 kWe net generation.

The intake was directly from the atmosphere at -40°C and 6.1 kPa. The analysis showed that with the currently used precooler design the required fan power was more than 50kW. The best result was on the order of 135 kW_e, which is not acceptable. The problem here is that the temperature drop on the hot and cold side of the recuperator are similar as well as the specific heat. Thus high mass flow rate is necessary on the cold side of the precooler. The mass flow rate on the cold side is about 1.62 times less than on the hot side. At 6.1 kPa this results in high velocity and thus high volumetric flow rate. Regardless of the pressure drop and face area this constitutes high pumping power requirements. It was attempted to reduce the cooling flow rate by increasing the cycle compressor inlet temperature, and thus extending the available temperature rise of the cooling flow; however this did not have a significant effect on the reduction of the cooling mass flow rate and the cycle efficiency was significantly compromised.

In order to overcome this problem it is necessary to introduce the combination of natural convection and forced convection. The resulting precooler will be made of finned tubes with the fan forcing the flow around it. This should significantly reduce the fan pumping power as well as reduce the volume of the precooler compared to the pure natural convection case. The analysis of this type of precooler is more difficult than those for the pure natural and pure forced convection cases. It was not possible to complete this analysis as a part of this work and if there is interest in the CO₂ cycle in the future this option should be explored in more detail, since it is likely be the only feasible design.

Table 5.2.4-1 shows the current reference design. It depicts the cycle state points and other major characteristics. The cycle efficiency is 25% at the pressure ratio of 2.6 and mass flow rate 7.47 kg/s for 1000 kW_{th} of the core power. In Table 5.2.4-1, thermal efficiency reflects the reference state points, efficiency is the thermal efficiency corrected by generator efficiency and mechanical efficiency, net efficiency is the efficiency corrected by the loads required to run the precooler fan and the feed compressor. The relatively low value of the net efficiency is due to the high power consumption of the precooler fan, however if the fan power is reduced with the introduction of mixed natural and forced convection the efficiency may reach 20%.

Table 5.2.4 - 1 Brayton Cycle Reference Design (see Figure 5.2.2 –1 for Ref. Points)

| Ref. Pts. | p(kPa) | T(°C) | h(kJ/kg) | s(kJ/kg/K) |
|---------------------------|---------------|------------------|-----------------|-------------------|
| 1 | 192.31 | 40.00 | 517.95 | 2.656 |
| 2 | 500.00 | 127.31 | 595.70 | 2.695 |
| 3 | 484.25 | 486.18 | 977.32 | 3.375 |
| 4 | 480.38 | 600.00 | 1111.22 | 3.541 |
| 5 | 203.91 | 504.53 | 998.91 | 3.566 |
| 6 | 200.34 | 148.39 | 617.29 | 2.920 |
| Compressor work | | 77.75 | kJ/kg | |
| Turbine work | | 112.31 | kJ/kg | |
| Added heat | | 133.9 | kJ/kg | |
| Rejected heat | | 99.34 | kJ/kg | |
| Thermal Efficiency | | 25.81 | % | |
| Efficiency | | 25.04 | % | |
| Net Efficiency | | 11.3 (20) | % | |

Non-regenerative Open Brayton Cycle

Since both regenerative cycles were difficult to employ it was necessary to find another option. The heat rejection from the cycle is really difficult therefore the precooler should be avoided. In the regenerative open Brayton cycle the fractional pressure drops are the problem. In order to reduce the fractional pressure drops it is necessary to increase the operating pressure. This is impossible on the hot side of the recuperator as this part of the cycle operates at the Martian atmospheric pressure. Therefore, it is necessary to remove the precooler from the system to avoid the heat rejection related problems to remove recuperator to avoid the hot side recuperator fractional pressure drop and increase the pressure ratio in order to minimize the reactor fractional pressure drop. The non-regenerative open Brayton cycle is the option how to achieve these goals. The question is if its efficiency is going to be high enough. Figure 5.2.4-1 shows the efficiency of the non-regenerative Brayton cycle as a function of cycle pressure ratio for different fractional pressure drops. Table 5.2.4-2 lists the parameters of the reference design for open cycle.

From the core thermal hydraulic analysis we know that fractional core pressure drops of 10% are achievable at about 100 kPa, which is about 18 times the pressure on Mars. Thus, with the compressor capable of handling a pressure ratio of 18 or more, the direct cycle that uses only a compressor, turbine and the reactor is possible. The reactor must be able to take the temperature rise of about 400°C, which is normal for the gas cooled reactor, such as for example PBMR. At the small length of this reactor it might however present a difficulty. This cycle can achieve the target efficiency of 20% and is very simple. This design is the best option for the open cycle.

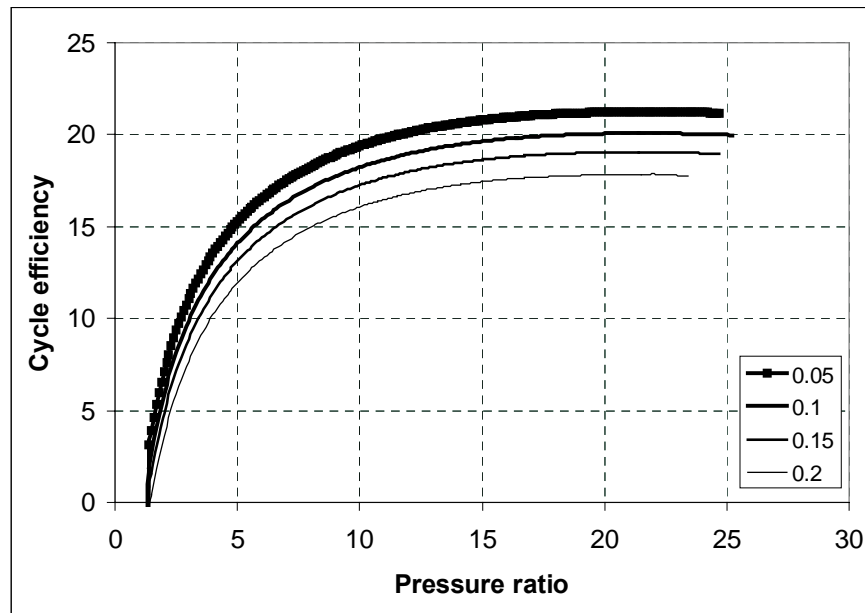


Figure 5.2.4 – 1 Efficiency of Non-Regenerative Brayton Cycle (different fractional core pressure drop).

**Table 5.2.4 – 2 Non-Regenerative Open Brayton Cycle Reference Design
(see Figure 5.2.2 - 1 for Ref. Points)**

| Ref. Pts. | p(kPa) | T(°C) | h(kJ/kg) | s(kJ/kg/K) |
|---------------------------|--------|---------------|--------------|------------|
| 1 | 6.11 | -40 | 454.11 | 3.070721 |
| 2 | 110 | 210.01 | 678.21 | 3.168107 |
| 3 | 97.9 | 600 | 1111.54 | 3.842062 |
| 4 | 6.11 | 326 | 799.22 | 3.938269 |
| Compressor work | | 224.10 | kJ/kg | |
| Turbine work | | 312.32 | kJ/kg | |
| Added heat | | 433.33 | kJ/kg | |
| Rejected heat | | 345.11 | kJ/kg | |
| Thermal Efficiency | | 20.36 | % | |
| Efficiency | | 19.75 | % | |

5.2.5 Conclusion

The possible use of the Brayton cycle using the Martian atmosphere as a working fluid was investigated in this section. The reason for this investigation was our philosophy to utilize as many Mars resources for our surface nuclear power system as possible. If the Martian atmosphere is used, the whole reactor system will be sent dry and we will save on the mass of coolant.

The use of the open cycle with direct intake from the Martian atmosphere is possible only if high pressure ratio (18) compressor is used and the cycle is non-regenerative. Nevertheless, careful design with respect to minimizing the pressure drops is necessary. The current reference non-regenerative open Brayton cycle design achieves a net efficiency of 19.75%. This is very close to our target efficiency of 20%. In addition the cycle is very simple. It uses only one compressor, one turbine and the reactor. The reference conditions are -40°C compressor inlet temperature and 600°C reactor outlet temperature. Given the difficulties with designing the precooler for the closed cycle this might be the only attractive option. Careful design of turbomachinery has to be performed in the future. Especially the design of the compressor with intake at -40°C might require special materials.

For the closed cycle the efficiency achievable at 600°C reactor outlet temperature and 40°C compressor inlet temperature is 25%. It was necessary to use a closed slightly pressurized cycle in order to reduce the fractional components pressure drop. The current operating pressure is 500 kPa. The main difficulty is to design the precooler.

In all closed cycles the most difficult part was the design of the precooler. The reason is that if the low pressure Martian atmosphere is used for heat rejection then the precooler volume is large in the case of natural convection or the pumping power of the fan is large in the case of forced convection. There are two more possible solutions that should be investigated in the future and that is use of heat conduction to the ground and the use of finned tubes and fan configuration. The use of the heat conduction might be difficult as the potential for getting the precooler in the

direct contact with the soil might be difficult. There is also a possibility of deploying a heat pipe in order to provide precooler cooling. However, this complicates the whole system and the benefit is questionable. Use of the fan over the finned tube surface will definitively have smaller pumping power requirements than in the case of plate-and-fin heat exchanger. Its feasibility would have to be confirmed, but the use of mixed forced and natural convection might be the only solution to the precooler design. The current volume of precooler (3 by 3 by 1m) is unacceptable.

For the open cycle some thoughts are given to the non-regenerative Brayton cycle. The main reason for using regenerated Brayton cycle was to reduce the temperature rise across the reactor core and improve the cycle efficiency. If no regeneration is used this temperature rise can be as high as 500°C, which may not be acceptable. Nevertheless, as will be shown later if high pressure ratio (18) compressor and 390°C temperature rise across the core could be used than the non-regenerative Brayton cycle can achieve the same efficiency as regenerative with a significantly simpler cycle.

5.2.6 References

- [1] V. Dostal, M. J. Driscoll, P. Hejzlar, and N. E. Todreas, "CO₂ Brayton Cycle Design and Optimization," Massachusetts Institute of Technology, MIT-ANP-TR-090, November, 2002.
- [2] W. M. Kays, A. L. London, *Compact Heat Exchangers*, 3rd edition, McGraw-Hill, 1984.
- [3] S. J. Dewson, B. Thonon, "The Development of High Efficiency Heat Exchangers for Helium Gas Cooled Reactors," Proceedings of ICAPP'03, Cordoba, Spain, May, 2003.

5.3 SHIELDING OF THE CECR

5.3.1 Introduction

Being an astronaut on a mission to Mars project means receiving a large dose of radiation. In order to enable manned missions, this dose must naturally be kept down. Usually, the most significant radiation sources in space for this mission are the galactic cosmic radiation (GCR) and possible solar flares. However, this mission utilizes nuclear reactors that make up a third source. The classic approach to limit dose from radiation is to minimize exposure *time*, maximize *distance* and use *shielding*.

5.3.2 Time - Distance - Shielding for Mars Explorers

Time

In the case of a Mars mission it is difficult to limit the time after the mission plan has been established. Limiting the traveling time in space is a priority in each space mission. A faster transit time does not only reduce the astronauts' dose, but also leads to an overall lighter payload since less support material, e.g., food, fuel etc., is needed. In most cases, the technology dictates what the fastest possible type of interplanetary transport is. Once the spacecraft has been determined, there is not much else that can be done in order to change the time in space for the mission's human explorers.

Another time when astronauts are exposed to radiation is during space walks. However, these short excursions are inevitable in case there is an immediate need to repair or replace a component. Lastly, excursions on the Martian surface may lead to higher doses. On the other hand, these exploration trips are also strongly regulated by the mission's objective. Since most of the parameters mentioned above are beyond the control of the astronauts, one should analyze the possibilities offered by the two remaining concepts (distance and shielding) in order to reduce the dose further.

Distance

Slashing the dose by moving further away from the source works fine if the source can be considered a point source. However, that is clearly not the case for the galactic background radiation reaching the Martian surface. Thus, distance hardly contributes to lowering the GCR dose. On the other hand, in the case of the reactor it would help to stay away from it. Since radiation falls off as r^{-2} , doubling the distance to the reactor would reduce the picked up dose to a quarter of its original value. This approach would be most effective in the case of an unshielded reactor. However, practically speaking, it is a technical necessity to have the turbomachinery in the immediate vicinity of the reactor. Moreover, if a (repairable) accident would occur with the reactor or with the turbomachinery, it is highly desirable to have the crew near enough that they might repair the damage and restore the operation of the system. Any repair, or maintenance, work of that type is only possible if the reactor is shielded. Otherwise, the skyhigh radiation levels in the local reactor area will prevent any human beings from coming close. Therefore, distance does not provide the ultimate solution for protecting the astronauts from the extra radiation source the reactors comprise.

Shielding

The limited applicability of time and distance in this mission increases the importance of shielding. The effectiveness of a shield largely depends on the material selection and the thickness. The material selection is related to what type of radiation one is concerned about whereas the thickness depends on how energetic the particles (photons) to be stopped are. As far as the material is concerned, it is well known that high Z materials, e.g., lead, stop high energy gamma rays most efficiently. However, many of these materials have a high density ($\rho_{Pb} = 11.4 \text{ g/cm}^3$). Since one of the key requirements is to minimize the payload, bringing complete shielding material from Earth can be ruled out. Consequently, the shielding material must be found elsewhere; namely, on the Martian surface.

5.3.3 Comparison with MITR

For comparison, the mass of the shielding material of the MIT nuclear reactor (MITR) was estimated. This comparison is valid because the power level of the MITR (5 MW) is similar to that of the surface reactor ($\sim 1 \text{ MW}$) and because the enrichment is different by a factor of five approximately, the two neutron fluxes should be comparable.

Although the MITR shielding brings the radiation levels down to a lower level than what would be necessary on the Martian surface, it is still a relevant first-order approximation of the shielding mass. The comparison showed that MITR uses more than 200 metric tons of shielding material, as shown below in Table 5.3.3-1 [1].

Since the payload per rocket is set to around 60 tons, there is very little – if any – room for surface reactor shielding material onboard. Thus, one must look into other options of finding shielding material.

Table 5.3.3 – 1 Shielding Materials in MITR (excluding water tanks)

| | Ri [cm] | Ro [cm] | V [cm ³] | ρ [g/cm ³] | M [kg] |
|-------------------------------|------------|------------|-------------------------|---------------------------|------------------------|
| Steel (1 st layer) | 121.9 | 127.0 | 160 x 10 ⁶ | 7.85 | 1.26 x 10 ⁴ |
| Lead | 127.0 | 130.8 | 1.23 x 10 ⁶ | 11.4 | 1.40 x 10 ⁴ |
| Steel (2 nd layer) | 130.8 | 135.9 | 1.71 x 10 ⁶ | 7.85 | 1.34 x 10 ⁴ |
| Concrete | 135.9 | 303.6 | 9.26 x 10 ⁷ | 2.35 | 2.18 x 10 ⁵ |

Water has Ro-Ri ~0.6 m
Height ~ 400 cm

5.3.4 Martian Soil Composition

If the shielding cannot be provided by terrestrial sources, the natural choice is to use in-situ materials. Analyses of geological samples analyzed by previous Mars exploration missions have shown that the Martian soil is rich in relatively high Z elements (minerals). The approximate composition of the Martian soil is displayed in Table 5.3.4-1 below [2].

Table 5.3.4 – 1 Martian Soil Composition

| | Weight% of Soil | Elements | Z | Atomic weight (g/mol) | Weight% of Compound per Element | Total Fraction of Compound |
|--------------------------------|--------------------|----------|-----|-----------------------------|---------------------------------------|----------------------------------|
| SiO ₂ | 40 | Si | 14 | 28 | 47 | 0.19 |
| | | O | 8 | 16 | 53 | 0.21 |
| FeO | 15 | Fe | 26 | 56 | 78 | 0.12 |
| | | O | 8 | 16 | 22 | 0.03 |
| Al ₂ O ₃ | 10 | Al | 13 | 27 | 53 | 0.05 |
| | | O | 8 | 16 | 47 | 0.05 |
| MgO | 10 | Mg | 12 | 24 | 60 | 0.06 |
| | | O | 8 | 16 | 40 | 0.04 |
| Na ₂ O | 5 | Na | 11 | 23 | 74 | 0.04 |
| | | O | 8 | 16 | 26 | 0.01 |
| Other (XO) | 20 | X | ~20 | 40 | 71 | 0.14 |
| | | O | 8 | 16 | 29 | 0.06 |

X is essentially the average of the other soil constituents.

High Z materials provide good gamma shielding and if a sufficiently thick reflector or moderator is used as well, the fast neutron dose rate should be kept down too.

5.3.5 Required Thickness of Martian Soil Shield

The surface reactor that is to be deployed on Mars is expected to have a power level in the megawatt range. As is obvious from the table with the MIT reactor stats above, a significant amount of shielding is necessary for a reactor in the lower megawatts. The final thickness can only be determined if there is a constraint on the exposure. In order to set this limit to a

reasonable value considering that the environment is Mars and not a nuclear power plant on Earth, it is crucial to find out what the exposure rate due to GCR is on Mars. Setting the limit below this value would hardly be beneficial. According to the literature, the annual unsheltered dose rate on the Martian surface equals 1.1 mrem/hr [3]. Furthermore, considering that the plant would not be located closer than necessary to the surface habitat, the dose rate can be further increased thanks to the radiation falling off with distance. In order to evaluate the different options, the dose rate on the surface of the shield was calculated for different shield thickness.

The Martian soil was calculated to have a density of 1.66 g/cm³ and a macroscopic removal cross section of 0.0792 cm⁻¹ [4].

The mathematical formula behind the thickness computations uses the known parameters above and empirical constants to render a good first-order dose rate approximation [5]. The flux was given from:

$$\phi(P) = \frac{SA}{4\pi} \cdot \left(\frac{R}{R + \alpha} \right)^2 \cdot e^{-\Sigma R \alpha} \cdot (1 - e^{-2\alpha R})$$

where S is the neutron production rate in the core in neutrons/cm³-sec, A is the area in cm², R is the core radius in cm, Σ is the macroscopic removal cross section in cm⁻¹ and α is a constant involving the core metal volume fraction and the macroscopic removal cross sections of the metal and the reflector. Once the flux is known, the equivalent dose rate can be read off a table [5].

Since both the core composition and dimensions and the removal cross sections for the shielding material were known, the dose rate could be approximated. The macroscopic removal cross sections were obtained from literature [6,7].

The results of these calculations are shown on the Table 5.3.5-1 below.

Based on the values presented in the table above, a thickness of 200 cm was chosen. This choice limits the neutron escape to an initial dose rate on the shield surface of 5.6 mrem/hr. Although this value is probably lower than needed, it leaves some room for a gradual decrease in shielding. For instance, a severe storm could reduce the thickness. However, even a reduction by 20 cm to 180 cm still keeps the dose rate below 50 mrem/hr. Thus, there is some margin if something unexpected happens. However, one should keep in mind that the rovers can easily add new shielding material, if needed.

Table 5.3.5 - 1 Martian Soil Shielding Results

| | | | | | |
|--|------|------|------|-----|-----|
| Thickness (cm)¹ | 170 | 180 | 190 | 200 | 210 |
| Corresponding dose rate, shield surface (mrem/hr) | 75.5 | 31.7 | 13.3 | 5.6 | 2.4 |
| Dose rate (GCR), Martian surface (mrem/hr) | | | | | 1.1 |

¹Excluding 30 cm BeO reflector

5.3.6 Listing of Shielding Deployment Options

Once it has been shown that a reasonable thickness of Martian soil will provide sufficient shielding, one must determine where to place the reactor. Initially, four possible locations were considered:

- To bury the reactor in the ground
- To place the reactor in a cave or other natural cavity and cover the opening with rocks
- To deploy the reactor without any particular shielding behind a large rock far away from the habitat
- To keep the reactor on the surface and build a shield around it from rocks and dirt

In order to assess the proposed options, one must first address the constraints and challenges the Martian surface environment offers.

5.3.7 Environmental Constraints

Atmosphere

The composition of the Martian atmosphere is 95.3% CO₂, 2.7% N₂, 1.6% Ar, 0.15% O₂, 0.03% H₂O [7]. This composition implies that there is little water vapor present. Thus, the risk of damages due to corrosion on a surface or cave based reactor is minor.

The average pressure on Mars is 7 mbar [7]. This pressure should have no immediate impact on the choice of location.

Wind loading, on the other hand, may have to be taken into consideration. Space probes measurements have confirmed that dust storms (local and global) are a “most significant Martian meteorological phenomenon” [2]. Ground velocities of up to 100 m/s have been measured in some areas. Since the landing site will be chosen in an area with less severe natural phenomenon, it is more reasonable to assume a lower maximum value of anticipated wind velocities. Therefore, the maximum velocity will be set to 50 m/s whereas the average wind speed is estimated to 5 m/s [8]. The consequence of these storms is that the two surface options (shielded and unshielded) require the reactor and the shield to be strongly anchored to the ground in order to withstand the wind loading.

Terrain

It can be assumed that the terrain will contain rock boulders of varying diameters. Furthermore, the surface cannot be assumed to be flat, but will have a maximum inclination of ~30 degrees. These constraints have no direct impact on the location of the reactor, but it does affect operational conditions of the robotic rovers that are to deploy the reactor and shield.

Soil Hardness

Expert assessment claims that the ground on Mars does not have an “average hardness”. Instead, it is argued that the strength can vary from virtually zero (loose sand) to very hard (unweathered

basalt) [8]. Hopefully, the first mission orbiter can narrow down the choice of landing site by having its high power technology determine the quality of the soil.

5.3.8 Shield Option Selection Process

Based on the mission requirements, environmental constraints and the technological feasibility, each of the deployment options was evaluated.

Subsurface Deployment

The advantage of this option is that it safely protects the reactor and shield from the strong Martian surface winds. The hole also constitutes a mechanically stable structure that cannot be removed easily. Hence, the reactor is well shielded. There are, however, also major drawbacks with this option. The primary obstacle is digging the hole. Although methods such as scraping, scooping, drilling, digging or even blasting excavations are readily employed on Earth, none of these techniques have been tested on a large scale on other planets. Despite the small core size (0.80 m^3), the shielding thickness was determined to 200 cm. Thus, this would require a fairly large excavation. Considering that feasible designs for drilling as deep as 200 meters down in the Martian crust have been developed, it should not be impossible to create a hole in the ground [8]. However, if the reactor is placed in a hole, it will be problematic to connect the turbomachinery that is supposed to be closely connected to the core. Thus, this option appears to have advantages and disadvantages weighing about equal. Perhaps a combination with one of the other options will lead to the ultimate solution.

Cave Deployment

This option also provides adequate protection of the reactor against the wind. Another benefit is that no digging in the ground or piling of rocks is necessary since the reactor is simply put in a cave (cavity). The power could then be transferred to the habitat by means of a (long) cable. The main disadvantage is the difficulty of locating a suitable cave. Also, caves are usually not easily accessible and the reactor must somehow be transported to its final destination. An alternative approach would be to blast an excavation in a large rock or in a mountain. However, it is highly unlikely that preparing, controlling, performing and evaluating such a blast can be done remotely with a high degree of accuracy. Another problem with the cave deployment is that the reactor is unshielded once inside the cave. Consequently, the crew is unable to perform any kind of repair or maintenance of the turbomachinery or the reactor itself since the radiation levels in the vicinity of the reactor would be incredibly high. Therefore, this option does not seem to be a technologically viable alternative and also precludes direct crew repair of the power system.

Far Distance Deployment

This option essentially eliminates the need for rovers that are capable of building, or at least assembling, a shield around the reactor. By deploying the reactor far away from the habitat, for instance, behind a large rock, the radiation reaching the habitat (penetrating the rock or from “skyshine”) will be insignificant due to the r^{-2} -dependence. Although this option does not require the rovers to collect shielding materials, the rovers must still be used to anchor the reactor in the ground against the wind. As with the cave deployment option, the lack of any outer shielding inhibits the crew from directly carrying out maintenance or repair work. This deployment would

also limit the astronauts' area of action, because they would always have to worry about possibly being exposed to radiation from the "unshielded reactor behind the hill". Hence, this option is ruled out due to its constraints on repair possibilities and crew mobility.

Conclusion

Although drilling deeply is possible, there are difficulties connected with digging a two-meter deep hole. The best alternative was therefore chosen to be a combination of digging a hole and simply placing the reactor on the ground. A shallow hole, essentially a form, could be excavated specifically for the reactor. Thereafter, the reactor is placed in this relatively shallow excavation and the support structure is placed on top of it and secured to the ground. Since the reactor is lying down, it is in a stable formation. Finally, the rovers add the soil (or bricks) to the support structure and the shield is complete.

5.3.9 Assembling the Shield

The physical dimensions and the structure of the shield are directly related to the size of the core. Preliminary analysis of the core dimensions point in the direction of a tall, thin core with an L/D-ratio around 4. More specifically, the height of the core has been estimated to 1.6 m and the diameter to 0.4 m.

The challenge in this part of the mission is to construct the shield and then ensure that it withstands the Martian weather conditions. Since the reactor is supposed to operate when the crew arrives, the shield must have been assembled ahead of time.

The idea is to have robots (rovers) carry out most of the assembling work. Since the shield will be comprised of dirt and rocks from the Martian surface, the shield has to be completed on the Red Planet by default. However, by having the rovers putting the shield together, the whole construction process can easily be tested and fine-tuned on Earth. Possible trials that the shield may face on Mars, e.g., strong winds and significant temperature changes, can also be simulated without problems on Earth during the test phase. Additionally, the first mission (the satellite) can do more precise measurements on the proposed landing site. Such additional data, e.g. landscape profile, winds, surface geology, naturally contribute to enhancing the probability of success. Therefore, the reliability of building the shield on Mars should be high.

5.3.10 Support Structure

When it comes to the actual construction of the shield, it is clear that some sort of support structure is needed to keep the dirt and the rocks in place. This support structure should be manufactured on Earth and can be made of any strong and corrosion resistant metal. Stainless steel would be one alternative. Moreover, the support structure should be manufactured in such a way that it is placed on top of the core and preferably has a standard mechanism that locks it to the core. Also, the support structure can easily be anchored to the ground. It will be a task for the rovers to drill holes and secure the structure in the ground. Drilling the holes should not be a major obstacle for the rovers. Previous NASA design projects have analyzed drilling in the Martian surface in detail. In fact, meticulous designs of equipment for drilling as deep as 200 m have been developed [8]

The support structure will also have pockets or cavities whose purpose is to ensure that the shielding material stays in place. The rovers will be responsible for collected as much dirt and rocks that are needed. The dirt will be placed as a first (inner) layer and then more solid rocks will be placed on the outside. By being on the outside, the larger rocks contribute to keeping the dirt in place. Collecting dirt and rocks should not pose a major problem to the rovers. Again, the first (satellite) mission will locate an area whose geology and surface terrain seems feasible for deployment of the reactor.

There is also an alternative approach to pouring in Martian dirt inside the support structure. This option makes the shielding somewhat more compact and appears to result in the shield being more thoroughly built. In this method, the Martian dirt is mixed with polymers that have been brought from Earth. The mixture of soil and polymers is then used for casting shield bricks. When the bricks have dried, the rovers can put the building bricks in the pre-manufactured holes or compartments in the support structure. Finally, the polymers may even be produced on Mars. This production would require some slight additions or modifications to the ISRU plant, something NASA is currently investigating [9].

5.3.11 Enhanced Shielding Options

The proposed core design proves to have a small radial leakage. With the proposed shielding thickness of 200 cm, radiation in the axial direction should not be a problem. Axially, however, the neutron streaming is a concern due to the coolant channels. Since parts of the turbomachinery is to be directly connected to the ends of the reactor, they will be exposed to more intense radiation, because the short end shielding will not be perfect due to the pipe connections etcetera. Moreover, in case something would have to be repaired or replaced in the turbomachinery by the astronauts, these would in turn get dosed up. In order to enhance the short-end shielding, special shutters will be brought from Earth. These shutters can be placed on the reactor ends and easily closed in case time-consuming maintenance work of the turbomachinery is necessary. The material of the shutter could be similar to the shielding of the space reactor, i.e., W and LiH, and the estimated weight could be up to 100 kg. Additionally, a movable shield could be brought from Earth or partly constructed on Mars. This movable shield would simply be a large size brick of a shielding material placed on wheels or caterpillar treads. Thus, whenever the astronauts have to spend more time in the immediate vicinity of the reactor, they can obtain extra shielding by closing the shutter(s) and operating behind this easy-to-move block constituting an extra piece of shielding.

5.3.12 References

- [1] Reactor Staff, *MITR-II Reactor Systems Manual*, MIT Press, Cambridge, MA, 1997.
- [2] Mars Facts, <http://www.estec.esa.nl/outreach/marskite/marsfacts/marsatmosphere.htm>, accessed on April 23, 2003.
- [3] SIMM – MARS – Radiation and the Human Mars Mission, Version 1.0, <http://www.seds.org/pub/info/mars/RadHuman.txt>, accessed April 15, 2003.
- [4] Shultis, Kenneth J., et al., *Radiation Shielding*, Prentice Hall PTR, Toronto, Canada, 1996.

[5] Lamarsh. John R., *Introduction to Nuclear Engineering*, 2nd Ed., Addison-Wesley Publishing Company Inc., New York, NY, 1983.

[6] Profio, Edward A., *Radiation Shielding and Dosimetry*, John Wiley & Sons Inc., New York, NY, 1979.

[7] The Encyclopedia of Astrobiology, Astronomy, and Spaceflight,
<http://www.angelfire.com/on2/daviddarling/Marsatmos.htm>, accessed on April 23, 2003.

[8] Blacic J. D. et al, "Report on Conceptual Systems Analysis of Drilling Systems for 200-m-Depth Penetration and Sampling of the Martian Subsurface," Los Alamos National Laboratory, 2000.

[9] Shielding from Mars or Moon Dirt?,
http://science.nasa.gov/newhome/headlines/msad20jul98_1.html, NASA, accessed on April 23, 2003.

6.0 SUMMARY, CONCLUSIONS AND RECOMMENDATIONS FOR FUTURE WORK

6.1 SUMMARY

This report details not only options for a viable plan of staged missions to demonstrate technology that will eventually allow for a nuclear-powered manned mission to Mars, but also the application of a numerical decision methodology, and conceptual designs for nuclear power systems that will meet the stringent demands of space exploration.

The mission plan focuses on the use of reusable technology and developing long-term Martian infrastructure to reduce the recurring costs of future exploratory missions. The technical designs of the power systems contained in this report have met the constraints and requirements imposed by the mission plan.

The application of the numerical decision methodology was invaluable in quickly down-selecting potential design alternatives for rapid convergence in the allotted time frame. However, there is still much room for improvement in the conceptual designs presented in this report on many levels.

6.2 CONCLUSIONS

As a conclusion to this report, it is valuable to give an overview of our distinctive design features that the team feels are innovative. First, the application of molten salt in the space reactor plant is a key contribution. This option has not been explored fully in previous analyses. Molten salt can operate at extremely high temperature and is much lighter than liquid metal, with comparable heat transfer capabilities. As a design alternative, liquid lithium, with similar heat removal capabilities and modest density may also be employed.

Also, the emerging technology of thermo photovoltaics (TPV) will be invaluable to future space missions. This technology promises to be very efficient in the conversion of radiant to electrical energy. The DC output also saves on required mass, as most systems will require AC to DC converters for DC power to operate on the craft. Additionally, TPV arrays do not have any moving parts, and will be more reliable and simple than systems such as Brayton cycles for space applications.

In the end, the team had two major objectives, first was to design a space power system that provides up to 4 MWe of DC electric power for a VASIMR engine at a specific mass of less than 3 kg/kWe. We have achieved the first goal with the design of the MSFR. Secondly, the team strove to design a long life surface plant that could operate for 25 EFPY on the Martian surface with remote operation. Though there are some pieces still to be completed in future work, the conceptual design is a valid approach to attaining this goal.

6.3 RECOMMENDATIONS FOR FUTURE WORK

The team has identified and discussed many areas for further optimization and future work on design with in the scope of space applications. First, more work can be done to optimize the surface reactor plant. The CECR concept is a valuable one, and should not be discarded. However, a more integrated approach to the design of the system must be used. Neutronics and

Thermal Hydraulic parameters are closely intertwined. It was discovered that the reactor leakage control can be employed at relatively low L/D for the reactor core, and therefore, lower pressure drops are attainable for the direct CO₂ cycle. Optimization of parameters in this area is a primary target for future investigation.

At the same time as we identify an area for future investigation, the team has also, through both reasonable decision methodology and folly, discovered many design alternatives that will not work, and therefore do not warrant further investigation. For instance, the use of a highly reactive fuel (such as Am^{242m}) in a thermal space reactor will not be feasible. Also, there are several Brayton cycle options that do not appear feasible for the surface application.

There are two areas that require specific additional work. These are related to the MSFR operation and safety. First, the MSFR calls for high efficiency TPV collectors. Though 30% efficiency from radiant to electrical energy is achievable in the near term, 40% has not been demonstrated. The team feels that this technology is rapidly evolving and that 40% will be available in the near term future. However, these cells will be operating under different environmental conditions in space, particularly their operating temperature must be determined.

Simple hand calculations have shown that the TPV collector temperature may reach temperatures higher than 500 K during operation for the full power design. Therefore, research must be done to establish if there will be technologies available for both high temperature and high efficiency photovoltaic cells.

As a design alternative, layering TPV collectors in concentric rings is proposed. The outer rings will collect the radiation transmitted through or emitted from inner rings. Though the efficiency of each ring may be small (~15-20%) the total efficiency of the system may be on the order of 40%.

Using low efficiency PV cells also allows for a smaller collector as the inner radius is constrained by the upper limit of the electric power density. Therefore, packing several layers of collectors at lower individual efficiency will allow us to reach our goal of 40% efficiency from heat to DC electrical power.

In terms of launch safety, the current design for the MSFR will become critical at the BOL if immersed in water. Therefore, while the radioactivity and radiotoxicity hazards are comparable with the Cassini probe, the threat of core criticality in the event of water immersion must be explored more carefully.

Lastly, as a general body of work concerning proposed design alternatives for the surface application, those options that have similar performance indices to the CECR may be explored more closely to define the margins and give better numerical values to the advantages and disadvantages of each alternative. Particularly, a US/SiC fast block type core (CO₂-cooled Fast Breeder Reactor - CFBR) may yield an improvement in neutron economy that outweighs its disadvantages in terms of reactor kinetics. These margins cannot be established without more detailed analyses.